The Polyakov loop and its Correlators in higher Representations of SU(3) at finite Temperature

Dissertation
an der
Fakultät für Physik
Universität Bielefeld

vorgelegt von

Kay A. Hübner

September 2006

It is a capital mistake to theorize before one has data.
Insensibly one begins to twist facts to suit theories,
instead of theories to suit facts.

Sherlock Holmes

Contents

1 Introduction

The understanding of the behaviour and properties of strongly interacting matter is one of the most challenging tasks of high energy physics. Due to the non-Abelian nature of Quantum Chromo Dynamics (QCD) – the theory that describes strongly interacting matter – an analytical or perturbative treatment of many physically interesting situations is not possible. Therefore the interaction of experimental results, numerical investigations and progress in analytical methods is a cornerstone of research devoted to the understanding of strongly interacting matter.

In the vacuum and at low temperatures quarks and gluons are confined in hadronic bound states. At higher temperatures of the order of 10^{12} K it is expected that hadronic matter undergoes a transition to the Quark Gluon Plasma (QGP), in which quarks and gluons can exist in other than colour-singlet states in the thermal medium. This new form of matter is of special interest for the physics of the early universe and has been investigated in several heavy ion collision experiments, in which it is expected, that a thermally equilibrated QGP can form.

At the Relativistic Heavy Ion Collider (RHIC) at BNL collision experiments with heavy nuclei are conducted, reaching CMS-energies of up to 200 AGeV. One of the most important discoveries of this experiments was that the Quark Gluon Plasma is not a weakly coupled plasma but rather a system that interacts strongly, the so called *sQGP* [1]. Moreover, this sQGP was found to behave as a nearly perfect liquid at RHIC energies with very small viscous corrections, as measurements of the elliptic flow reveal. Future experiments at the Large Hadron Collider (LHC) at CERN and at FAIR at GSI are expected to clarify the situation further. The physical mechanisms responsible for the emergence of the sQGP are still under discussion. The survival of bound states in the deconfined phase, including colour non-singlet states like diquarks, have been proposed as a possible reason for the observed deviation from the weakly coupled gas behaviour [2]. Lattice calculations of hadronic fluctuations suggest, however, that net quark number and electric charge are predominantly carried by quasi-particles with the quantum numbers of quarks [3]. In this work we try to elucidate the question of bound states further by providing diquark and baryonic free energies of heavy quarks, which can be used for the computation of bound state energies in the deconfined phase.

Moreover, we can add knowledge to the understanding of the shape of the flux tube in the baryon at finite temperature and address whether genuine three-body forces exist on the fundamental level between the three valence quarks of the baryon.

One of the most outstanding problems of QCD is the understanding of the confinement mechanism. Unfortunately there exists no exact analytical formalism for this non-perturbative phenomenon and one has to resort to the use of models for an analytical treatment, which are derived from the QCD Lagrangian with the help of additional

assumptions. Many models have been proposed in this way, which lead to a wealth of different predictions.

Lattice calculations provide the supreme means for the theoretical investigation of the QCD vacuum and the confinement/deconfinement transition from first principles, since they are capable of exploring regions of the gauge coupling and the temperature where analytical or perturbative methods fail. Potentials and free energies in higher irreducible representations of SU(3) than the fundamental one are relatively easily accessed by lattice calculations and can provide a test for confinement models and their predictions for QCD. An especially important property is the realisation of Casimir scaling in the $Q\bar{Q}$-potential with sources in higher representations in lattice calculations of the SU(3) pure gauge vacuum [4] and in perturbative calculations up to two loop order [5]. In this work we extend the investigation of the Polyakov loop and $Q\bar{Q}$-free energies at finite temperature to higher representations and study their relation to the confinement/deconfinement transition.

A more technical point to be addressed in this work is the renormalisation of the Polyakov loop and some of its correlation functions in irreducible representations of the SU(3) gauge group. In order to obtain physically meaningful information from lattice calculations, non-perturbative renormalisation procedures have to be administered to the bare values of lattice observables. These procedures are in general not unique, but should, of course, in the end lead to the same physical results. A sound and well tested renormalisation procedure for the Polyakov loop and its correlators is an indispensible prerequisite for the investigation of the QGP and the confinement/deconfinement transition mentioned above.

This work is organised as follows. In chapter 2 we will introduce the Polyakov loop and its relation to the center symmetry of SU(N) gauge theories and the confinement/deconfinement phase transition. Moreover we will introduce Polyakov loop correlation functions and the corresponding free energies and some of their properties at finite temperature. After that, we will discuss the lattice implementation of the Polyakov loop and its correlators. We will then extend the framework to the case of higher irreducible representations of SU(3) for the Polyakov loop and the free energies and discuss the relevance of the Casimir scaling hypothesis.

In chapter 3 we will discuss the renormalisation procedure for the $Q\bar{Q}$-singlet free energies with sources in the fundamental representation and extend it to the case of adjoint sources and propose and test the N_τ-variation method as a new renormalisation procedure suitable for the Polyakov loop in arbitrary irreducible representations. Finally in this chapter, we will discuss a third renormalisation procedure starting from different assumptions and compare the results from this method with those of our methods.

In chapter 4 we will address the question of Casimir scaling in $Q\bar{Q}$-singlet and -average free energies with sources in different representations in SU(3) pure gauge theory. Moreover, we will investigate Casimir scaling for the Polyakov loop in different representations for both SU(3) pure gauge and 2-flavour QCD. Then we will perform the thermodynamic limit for Polyakov loops at strong coupling and below T_c in SU(3) pure gauge theory and obtain the renormalised adjoint Polyakov loop in the thermodynamic limit. From this observable we will estimate the binding energy of the gluelump at finite temperature

and the string breaking distance for the $Q\bar{Q}$-free energy with adjoint sources.

Chapter 5 will show results from calculations of diquark free energies in SU(3) pure gauge theory and 2-flavour QCD. We will investigate the thermodynamic limit of the QQ-anti-triplet free energy below T_c and compare its properties to that of the $Q\bar{Q}$-singlet free energy in the confined and the deconfined phase.

In chapter 6 we will examine results for the static baryonic free energies obtained in both SU(3) pure gauge theory and 2-flavour QCD. We will discuss the relation of QQQ-free energies to those of the QQ-system in the deconfined phase and discuss the shape of the flux tube of the QQQ-singlet colour state in SU(3) pure gauge theory. In 2-flavour QCD we will investigate string breaking in the QQQ-system in the confined phase. Moreover, we will discuss the ramifications of our findings concerning the diquark and baryonic free energies for the screening mass and the question of bound states in the vicinity of the phase transition in the Quark Gluon Plasma.

Finally, in chapter 7 we will conclude and give an outlook on future research.

2 The Polyakov Loop and its Correlation Functions

As we are interested in the lattice formulation of pure gauge theory and full QCD at finite temperature in thermal equilibrium, we start directly with the path integral expression of the partition function in Euclidean spacetime. For a system at temperature T and volume V in the grand canonical ensemble with vanishing chemical potential we have the partition function

$$Z(T,V) = \int \mathcal{D}A \ \exp\left(-S[A]\right), \tag{2.1}$$

where

$$S[A] = \frac{1}{2}\int_0^{1/T} \mathrm{d}x_0 \int_V \mathrm{d}^3\mathbf{x} \ \mathrm{Tr}\, F_{\mu\nu}(x)F_{\mu\nu}(x) \tag{2.2}$$

is the Euclidean gauge action and

$$F_{\mu\nu} = \partial_\mu A_\nu - \partial_\nu A_\mu - ig\left[A_\mu, A_\nu\right] \tag{2.3}$$

is the field strength tensor of the SU(N) gauge theory with the coupling constant g and $x = (x_0, \mathbf{x})$. The non-Abelian vector potential is defined by

$$A_\mu(x) = A_\mu^a(x)t^a, \tag{2.4}$$

where the $A_\mu^a(x)$ are real valued functions and t^a are the hermitian generators of the SU(N) gauge group with $a = 1, \ldots, N^2 - 1$. The theory defined through (2.2) includes only gauge fields and neglects the dynamical quark sector and is hence called *pure gauge theory*. The fields appearing in (2.1) are classical fields; the quantisation is achieved by virtue of the partition function (2.1). All thermodynamic information on the system can be deduced from $Z(T,V)$.

Expectation values of an operator $\hat{O}$ can be obtained by inserting its corresponding classical expression $O[A]$ in the path integral. More explicitly we have the expression

$$\left\langle \hat{O} \right\rangle = \frac{1}{Z(T,V)} \int \mathcal{D}A \ O[A] \exp\left(-S[A]\right). \tag{2.5}$$

The quantity $\left\langle \hat{O} \right\rangle$ contains in general infinities, which have to be cured by a suitable renormalisation procedure in order to obtain physically meaningful results.

If we also want to include dynamical quark fields Ψ and anti-quark fields $\bar{\Psi} = \Psi^\dagger \gamma_0$, we can do so by defining the action

$$S_F[\Psi, \bar{\Psi}, A] = \int_0^{1/T} \mathrm{d}x_0 \int_V \mathrm{d}^3\mathbf{x} \sum_{a,f} \bar{\Psi}_f^a(x_0, \mathbf{x}) \left(i\gamma_\mu D_\mu + m_f\right) \Psi_f^a(x_0, \mathbf{x}), \tag{2.6}$$

where $a = 1, \ldots, N$, $f = 1, \ldots, N_f$ numbers the flavours, m_f is the corresponding quark mass and $\{\gamma_\mu, \gamma_\nu\} = 2\delta_{\mu\nu}$. The *covariant* derivative D_μ is defined by

$$D_\mu = \partial_\mu + igA_\mu \tag{2.7}$$

and includes interactions with the gluons by virtue of the second term. The partition function now includes an integration over the Ψ and $\bar{\Psi}$ fields and becomes

$$Z(T, V) = \int \mathcal{D}A\mathcal{D}\Psi\mathcal{D}\bar{\Psi} \ \exp\left(-S[A] - S_F[\Psi, \bar{\Psi}, A]\right). \tag{2.8}$$

This is the partition function of *full QCD*. In nature, we have $N_f = 6$, but usually we restrict ourselves to theories with $N_f \leq 3$. This is a sound approximation for the phenomena we wish to study, since the corresponding m_f span a wide range of energies ($< 5\,\mathrm{MeV}$ for the up quark to $\sim 174\,\mathrm{GeV}$ for the top quark [6]) and effects due to the three heaviest flavours are strongly suppressed around the deconfinement phase transition, which takes place at energies $O(10^2)$ MeV.

The better part of this work is concerned with the investigation of quantities in the frame work of pure gauge theory defined by (2.1). Let us shortly discuss why studying pure gauge theory is instructive despite its negligence of the dynamical quark sector. Firstly, already pure gauge theory shows confinement, providing an opportunity to study this phenomenon in a somewhat simplified environment. Much on the confinement mechanism and the transition to the deconfined phase can be learned by investigating higher representations of the SU(3) gauge group in pure gauge theory, as we will show below. Secondly, it has turned out, that calculations in pure gauge theories get at least the order of magnitude of many interesting observables right, compared to calculations in full QCD. And, last but not least, pure gauge theory is relatively easy to handle regarding numerical simulations in contrast to full QCD, where the inclusion of dynamical quark fields causes a considerable additional numerical effort. Therefore the investigation of pure gauge theory is important and helps to obtain a deeper understanding of the phenomena observed in full QCD.

For a review on the thermodynamics of QCD consult [7], introductions to finite temperature field theory can be found in textbooks [8, 9].

2.1 The Center Symmetry and the Polyakov loop

We will now introduce the center symmetry as an important global symmetry of SU(N) gauge theories, explain its relevance for the confinement mechanism and for the phase transition to the deconfined phase and introduce the Polyakov loop as an order parameter

for the confinement/deconfinement phase transition. We will mainly follow [10, 11] in this part.

As the vector potential A_μ is a bosonic field, it obeys periodic boundary conditions

$$A_\mu(x_0 + \beta, \mathbf{x}) = A_\mu(x_0, \mathbf{x}) \tag{2.9}$$

in the Euclidean time direction, where $\beta = \frac{1}{T}$ is the length of the Euclidean time direction. The gauge action (2.2) is invariant under local gauge transformations

$${}^g A_\mu = g\,(A_\mu + \partial_\mu)\,g^\dagger, \tag{2.10}$$

where $g(x) \in \mathrm{SU}(N)$. Obviously, any gauge transformation which is periodic in the Euclidean time direction,

$$g(x_0 + \beta, \mathbf{x}) = g(x_0, \mathbf{x}) \tag{2.11}$$

fulfils the requirement (2.9). It was noticed [12, 13], however, that there are also topologically non-trivial transformations which leave the gauge action (2.2) invariant but which are periodic only up to a global twist matrix $z \in \mathrm{SU}(N)$,

$$g(x_0 + \beta, \mathbf{x}) = z g(x_0, \mathbf{x}). \tag{2.12}$$

The strictly periodic gauge potential then transforms as

$$\begin{aligned} {}^g A_\mu(x_0 + \beta, \mathbf{x}) &= g(x_0 + \beta, \mathbf{x})\,(A_\mu(x_0 + \beta, \mathbf{x}) + \partial_\mu)\,g(x_0 + \beta, \mathbf{x})^\dagger \\ &= z g(x_0, \mathbf{x})\,(A_\mu(x_0, \mathbf{x}) + \partial_\mu)\,g(x_0, \mathbf{x})^\dagger z^\dagger \\ &= z\ {}^g A_\mu(x_0, \mathbf{x}) z^\dagger. \end{aligned} \tag{2.13}$$

In order to maintain the boundary conditions (2.9) for the vector potential, we must have

$$z\ {}^g A_\mu(x_0, \mathbf{x}) z^\dagger = {}^g A_\mu(x_0, \mathbf{x}), \tag{2.14}$$

which is only possible if z commutes with ${}^g A_\mu$. Thus, z must be an element of the center $\mathbb{Z}(N)$ of the gauge group $\mathrm{SU}(N)$. The elements of the center commute with all group elements and are proportional to the unit matrix,

$$z = e^{i\phi}\mathbb{1}, \qquad \phi = \frac{2\pi n}{N}, \qquad n = 0, \ldots, N-1. \tag{2.15}$$

Although the action (2.2) is invariant under global $\mathbb{Z}(N)$ transformations, not all physical quantities must show this behaviour. As we will see below, the global $\mathbb{Z}(N)$ symmetry can break *spontaneously*, signalling a phase transition from the confined to the deconfined phase. Moreover it is easy to see that the global $\mathbb{Z}(N)$ symmetry is *explicitly* broken by the introduction of dynamical quark fields Ψ. These transform under local gauge transformations as

$${}^g\Psi = g\Psi, \tag{2.16}$$

and, being fermions, satisfy anti-periodic boundary conditions in Euclidean time,

$$\Psi(x_0+\beta,\mathbf{x}) = -\Psi(x_0,\mathbf{x}). \tag{2.17}$$

Under global gauge transformations like (2.12) we obtain for Ψ,

$$\begin{aligned} {}^g\Psi(x_0+\beta,\mathbf{x}) &= g(x_0+\beta,\mathbf{x})\Psi(x_0+\beta,\mathbf{x}) \\ &= -zg(x_0,\mathbf{x})\Psi(x_0,\mathbf{x}) \\ &= -z\ {}^g\Psi(x_0,\mathbf{x}). \end{aligned} \tag{2.18}$$

Maintaining the boundary condition for the quark fields (2.17) now is only possible if $z = \mathbb{1}$, i. e. $\phi = 0$, so that the center symmetry has vanished.

We proceed by studying pure gauge theory defined by the action (2.2), where dynamical quark fields are absent. Nevertheless it is possible to introduce *static* quark fields, i. e. infinitely heavy quarks ($m_q \to \infty$), which serve as test charges that probe the behaviour of the gauge field. We start by defining the thermal Wilson line in the fundamental representation of SU(N)

$$P(\mathbf{x}) = \mathcal{P}\exp\left(ig\int_0^\beta \mathrm{d}x_0\, A_0(x_0,\mathbf{x})\right), \tag{2.19}$$

where $\mathcal{P}$ denotes path ordering. It winds once around the Euclidean time direction and transforms like an adjoint field under SU(N) gauge transformations. The thermal Wilson line is proportional to the propagator of a infinitely heavy test quark, which does not move in space, but still interacts in colour space, thus acquiring a SU(N)-phase through the Aharonov-Bohm effect [11]. A test anti-quark is a quark moving backwards in Euclidean time, so we have to employ the conjugate thermal Wilson line $P^\dagger(\mathbf{x})$ for it.

The *Polyakov loop* in the fundamental representation is the trace in colour space of the thermal Wilson line in the fundamental representation [14, 15],

$$L(\mathbf{x}) = \mathrm{Tr}\, P(\mathbf{x}), \tag{2.20}$$

where $\mathrm{Tr}\,\mathbb{1} = 1$. Since the trace is cyclic, $L(\mathbf{x})$ is a gauge invariant quantity. It is in general a complex scalar field, though for $N = 2$ it assumes purely real values. Under global $\mathbb{Z}(N)$ transformations $L(\mathbf{x})$ behaves non-trivially,

$$\begin{aligned} {}^gL(\mathbf{x}) &= \mathrm{Tr}\ {}^gP(\mathbf{x}) \\ &= \mathrm{Tr}\left[g(x_0+\beta,\mathbf{x})P(\mathbf{x})g(x_0,\mathbf{x})^\dagger\right] \\ &= \mathrm{Tr}\left[zg(x_0,\mathbf{x})P(\mathbf{x})g(x_0,\mathbf{x})^\dagger\right] \\ &= e^{i\phi}L(\mathbf{x}), \end{aligned} \tag{2.21}$$

acquiring a $\mathbb{Z}(N)$-phase ϕ.

The importance of the Polyakov loop now derives from the fact that its expectation value, $\langle L\rangle$, can serve as an *order parameter* for the confinement-deconfinement phase transition in pure gauge theory. Let us define the expectation value of L by

$$\langle L\rangle = \lim_{h\to 0}\frac{1}{Z}\int \mathcal{D}A\ L(\mathbf{x})\exp\left(-S[A]-S_h[A]\right), \tag{2.22}$$

where we have included an additional term $S_h[A]$ in the action, which breaks the center symmetry explicitly by virtue of an external auxiliary field proportional to some parameter h. This additional term is defined by

$$S_h[A] = \frac{h}{2T} \int_V \mathrm{d}^3\mathbf{x} \ \left(L(\mathbf{x}) + L^\dagger(\mathbf{x}) \right). \tag{2.23}$$

The integrand of (2.23) acts now as an effective potential for the expectation value of the Polyakov loop. This has the effect, that the integral on the rhs of (2.22) is not continuous at $h = 0$ in the deconfinement phase and therefore its limit $h \to 0$ does not vanish for $T > T_c$ in the thermodynamic limit, although the external auxiliary field has vanished, signalling a spontaneously broken symmetry [12]. This leaves the expectation value of the Polyakov loop in the thermodynamic limit real and non-zero in the deconfinement phase.

The expectation value of the Polyakov loop is connected to a free energy [16],

$$\langle L \rangle = \exp\left(-\frac{F}{T} \right), \tag{2.24}$$

where T is the temperature and F is the *difference* in free energy due to the presence of the infinitely heavy test quark in the gluonic heat bath. We note that (2.24) still needs a proper renormalisation.

Since $\langle L \rangle > 0$ in the thermodynamic limit in the deconfinement phase, the cost in free energy for inserting a single quark into the heat bath according to (2.24) is finite, signalling deconfinement. Below the critical temperature, the expectation value of the Polyakov loop receives equal contributions from all $\mathbb{Z}(N)$-sectors, thus leading to $\langle L \rangle = 0$ in the thermodynamic limit. According to (2.24) this means that the difference of free energy due to the presence of a single test quark goes to infinity, $F \to \infty$, resulting in an infinite amount of (free) energy which is necessary to insert the quark into the heat bath, thus signalling confinement.

In lattice calculations we are dealing with systems in a finite volume without the inclusion of the symmetry breaking term (2.23). In this situation we encounter L clustered around N distinct vacua distinguishable by the N possible values of the $\mathbb{Z}(N)$-phase ϕ in the deconfinement phase. Consequently, $\langle L \rangle = 0$ in this situation above T_c. Moreover, *tunnelling* between these vacua is possible but strongly suppressed with volume [17]. We will discuss in chapter 2.2.2 how $\langle L \rangle$ can be obtained without utilising an external auxiliary field and in chapter 2.3 we give an estimator for $\langle L \rangle$ on finite volumes.

The nature of the confinement/deconfinement transition in SU(3) pure gauge theory is that of a *(weakly) first order phase transition* at $T_c = 270\,\mathrm{MeV}$, as lattice calculations show [18]. In a first order phase transition, we observe the order parameter to jump from zero in the disordered (confined) phase to a finite value in the ordered (deconfined) phase at the critical temperature. The energy associated to this discontinuous change at T_c is called *latent heat*. This is the amount of energy released due to the restructuring of the gauge fields at the critical temperature when crossing T_c from below. The correlation lengths of the system stay finite at the transition temperature, such that we observe

phase coexistence, i. e. ordered and disordered phase occur simultaneously at T_c. This is not possible in a *second order phase transition*, where correlation lengths diverge at the transition temperature and thus an universal behaviour of the bulk of the system emerges which is independent of its microscopic details. At T_c the order parameter then changes continuously, i. e. the latent heat has vanished. A *crossover* does not have a rigorous critical temperature and is therefore not a genuine phase transition. The observables employed as order parameters show a rapid but smooth change in what is then called the *transition region*. Nevertheless we can give the temperature where the susceptibility of the order parameter reaches its maximum as a typical temperature. QCD with $2+1$ flavours shows a crossover behaviour at $T_c \sim 190\,\mathrm{MeV}$, as new calculations show [19].

2.2 Correlation functions of L and Free Energies

We are interested in a state of n quarks and $\bar{n}$ anti-quarks at the spatial positions $\mathbf{x}_1, \ldots, \mathbf{x}_n$ and $\bar{\mathbf{x}}_1, \ldots, \bar{\mathbf{x}}_{\bar{n}}$. The correlator defined by

$$C_{n\bar{n}}(\mathbf{x}_1, \ldots, \mathbf{x}_n, \bar{\mathbf{x}}_1, \ldots, \bar{\mathbf{x}}_{\bar{n}}, T, V) = \left\langle \prod_{i=1}^{n} L(\mathbf{x}_i) \prod_{i=1}^{\bar{n}} L(\bar{\mathbf{x}}_i)^\dagger \right\rangle \tag{2.25}$$

is connected to the difference in the free energy due to the insertion of n quarks and $\bar{n}$ anti-quarks into the gluonic medium by

$$F_{n\bar{n}}(\mathbf{x}_1, \ldots, \mathbf{x}_n, \bar{\mathbf{x}}_1, \ldots, \bar{\mathbf{x}}_{\bar{n}}, T, V) = -T \ln\left(C_{n\bar{n}}(\mathbf{x}_1, \ldots, \mathbf{x}_n, \bar{\mathbf{x}}_1, \ldots, \bar{\mathbf{x}}_{\bar{n}}, T, V)\right). \tag{2.26}$$

For the sake of brevity we will from now on only speak of a free energy when we have the difference in free energy due to the presence of static quarks and anti-quarks in mind. Furthermore, we will wrap up the position dependence of the correlators and the free energies in the *distance measure* r with $r = f(\mathbf{x}_1, \ldots, \mathbf{x}_n, \bar{\mathbf{x}}_1, \ldots, \bar{\mathbf{x}}_{\bar{n}}, T)$, where f is a relation depending on the spatial positions of the n quarks and $\bar{n}$ anti-quarks and the temperature. For the $Q\bar{Q}$-, QQ- and QQQ-systems, the distance measure will be given explicitly below.

We note that in $F_{n\bar{n}}$, because of the traces present in the Polyakov loops, colour interactions of the quarks with an exchange of one gluon (OGE) are not included. Therefore $F_{n\bar{n}}$ is sometimes called the *average* free energy of the system. In order to study the free energies of systems composed of quarks and anti-quarks that include OGE, we have to consider quarks that are in a defined colour state.

2.2.1 Correlators for symmetry states in colour space

We will now give a general prescription how to obtain correlators for a system where the static quarks and anti-quarks are in a definite colour state, which exhibit certain symmetry properties under the pairwise interchange of quarks and anti-quarks, respectively. For a system composed of n quarks and $\bar{n}$ anti-quarks we start by defining the correlator

of the corresponding thermal Wilson lines

$$C^W_{n\bar{n}}(r,T,V) = \left\langle \prod_{i=1}^{n} P(\mathbf{x}_i) \prod_{i=1}^{\bar{n}} P(\bar{\mathbf{x}}_i)^\dagger \right\rangle . \tag{2.27}$$

The state of the system in colour space is now described by the direct product of n times the fundamental representation times $\bar{n}$ times the anti-fundamental representation,

$$\bigotimes_{i=1}^{n} N \otimes \bigotimes_{i=1}^{\bar{n}} \bar{N} = \underbrace{N \otimes N \otimes \cdots}_{n \text{ times}} \otimes \underbrace{\bar{N} \otimes \bar{N} \otimes \cdots}_{\bar{n} \text{ times}} = \bigoplus_i s_i, \tag{2.28}$$

which can be reduced out into a direct sum of irreducible representations s_i. In order to find the correlator corresponding to each irreducible representation s_i, we define projection operators $P(s_i)$ which have the general form

$$P(s_i) = A_i^1 \bigotimes_{k=1}^{n+\bar{n}} \mathbb{1} \oplus A_i^2\, t^a \otimes \bigotimes_{k=1}^{n+\bar{n}-1} \mathbb{1} \oplus \cdots \oplus A_i^m \bigotimes_{k=1}^{n} t^a \bigotimes_{k=1}^{\bar{n}} \bar{t}^a, \tag{2.29}$$

where the A_i^k with $k = 1, \ldots, m$ and $m = n\bar{n}$ have to be determined such that $P(s_i)$ projects out the symmetry state associated with s_i. The $P(s_i)$ satisfy the orthogonality and completeness relations

$$P(s_i)P(s_j) = \delta_{ij} P(s_i) \quad \text{and} \quad \sum_i P(s_i) = \mathbb{1}. \tag{2.30}$$

The correlator for the colour symmetry state is now found by applying

$$C^s_{n\bar{n}} = \frac{\text{Tr}\, \left(P(s) C^W_{n\bar{n}}\right)}{\text{Tr}\, P(s)}, \tag{2.31}$$

where we have suppressed the dependence on temperature and the spatial positions of the quarks on both sides. The free energy of the symmetry state s can now be calculated from the correlator (2.31) through

$$F^s_{n\bar{n}} = -T \ln \left(C^s_{n\bar{n}}\right), \tag{2.32}$$

where again the dependence on temperature and the spatial positions of the quarks on both sides has been omitted.

We will now apply this procedure to the cases relevant for this work, which are the $Q\bar{Q}$-, QQ- and the QQQ-system, where the correlators of the first two have been explicitly calculated in [20, 21], those of the latter one in [22]. Moreover, we will restrict ourselves to the SU(3) gauge group, since we are interested in QCD. Additionally, we drop the $n\bar{n}$ subscript from now on and give only the system name, e. g. $Q\bar{Q}$, for convenience instead.

Let us start with the $Q\bar{Q}$-system. Reducing out the direct product into a direct sum of irreducible representations according to (2.28) yields

$$3 \otimes \bar{3} = 1 \oplus 8, \tag{2.33}$$

where $3(\bar{3})$ is the (anti-)fundamental representation. Thus we obtain in the direct sum a symmetric singlet and an anti-symmetric octet, which is at the same time the adjoint representation. The corresponding projectors are then found to be

$$P_1 = \frac{1}{9}\mathbb{1}\otimes\mathbb{1} - \frac{2}{3}t^a\otimes\bar{t}^a \tag{2.34}$$

$$P_8 = \frac{8}{9}\mathbb{1}\otimes\mathbb{1} + \frac{2}{3}t^a\otimes\bar{t}^a. \tag{2.35}$$

Applying now (2.31) gives the correlators

$$C^1_{Q\bar{Q}}(r,T) = \left\langle \mathrm{Tr}\,\left(P(\mathbf{x}_1)P(\bar{\mathbf{x}}_1)^\dagger\right)\right\rangle \tag{2.36}$$

$$C^8_{Q\bar{Q}}(r,T) = \frac{9}{8}\left\langle \mathrm{Tr}\,P(\mathbf{x}_1)\mathrm{Tr}\,P(\bar{\mathbf{x}}_1)^\dagger\right\rangle - \frac{1}{8}\left\langle \mathrm{Tr}\,\left(P(\mathbf{x}_1)P(\bar{\mathbf{x}}_1)^\dagger\right)\right\rangle. \tag{2.37}$$

We can now make use of the fact that these two point correlation functions are invariant under translations and thus only depend on the separation of the quark anti-quark pair. Therefore we obtain for the distance measure of the $Q\bar{Q}$ system $r = |\mathbf{x}_1 - \bar{\mathbf{x}}_1|$. Furthermore in (2.37) we have deliberately not inserted the expression for the Polyakov loop $L(\mathbf{x}) = \mathrm{Tr}\,P(\mathbf{x})$ where it would have been possible in order to make the structure of the correlator manifest. Obviously we have for the average correlator of the $Q\bar{Q}$ system the relation

$$C_{Q\bar{Q}}(r,T) = \sum_s \frac{s}{9}C^s_{Q\bar{Q}}(r,T) \tag{2.38}$$

$$= \frac{1}{9}C^1_{Q\bar{Q}}(r,T) + \frac{8}{9}C^8_{Q\bar{Q}}(r,T), \tag{2.39}$$

which is a consequence of the completeness relation for the projectors (2.30). Inserting the correlators (2.36) and (2.37) into (2.32) will now give the singlet and octet free energies of the $Q\bar{Q}$-system.

Let us now turn to the diquark system. The colour symmetry states can be found to give

$$3\otimes 3 = 6\oplus\bar{3}, \tag{2.40}$$

that is a symmetric sextet state and an anti-symmetric state, which is – special to SU(3) – at the same time the anti-fundamental representation. The corresponding projectors are

$$P_6 = \frac{2}{3}\mathbb{1}\otimes\mathbb{1} + t^a\otimes t^a \tag{2.41}$$

$$P_{\bar{3}} = \frac{1}{3}\mathbb{1}\otimes\mathbb{1} - t^a\otimes t^a. \tag{2.42}$$

By applying (2.31) the correlators are then found to be

$$C^6_{QQ}(r,T) = \frac{3}{4}\langle \mathrm{Tr}\, P(\mathbf{x}_1)\mathrm{Tr}\, P(\mathbf{x}_2)\rangle + \frac{1}{4}\langle \mathrm{Tr}\, [P(\mathbf{x}_1)P(\mathbf{x}_2)]\rangle \tag{2.43}$$

$$C^{\bar{3}}_{QQ}(r,T) = \frac{3}{2}\langle \mathrm{Tr}\, P(\mathbf{x}_1)\mathrm{Tr}\, P(\mathbf{x}_2)\rangle - \frac{1}{2}\langle \mathrm{Tr}\, [P(\mathbf{x}_1)P(\mathbf{x}_2)]\rangle\,, \tag{2.44}$$

where the distance measure is again given by the separation of the quark pair $r = |\mathbf{x}_1 - \mathbf{x}_2|$, due to translational invariance. We note here once more, that the average free energy of the diquark system is given by

$$C_{QQ}(r,T) = \sum_s \frac{s}{9} C^s_{QQ}(r,T) \tag{2.45}$$

$$= \frac{2}{3}C^6_{QQ}(r,T) + \frac{1}{3}C^{\bar{3}}_{QQ}(r,T). \tag{2.46}$$

Again, the corresponding free energies are obtained by using (2.32).

We now study the baryonic QQQ-system. Again, reducing out the direct product of three fundamental representations leads to the colour symmetry states

$$3 \otimes 3 \otimes 3 = 1 \oplus 8 \oplus 8' \oplus 10, \tag{2.47}$$

where 1 denotes the singlet, 8 the first octet, $8'$ the second octet and 10 the decuplet state. The singlet is totally anti-symmetric, the first octet anti-symmetric in the first and second, the second octet in the second and third component and the decuplet is totally symmetric. The corresponding projectors are

$$P_1 = \frac{1}{6}\sum_{\mathrm{Perm}(l,m,n)} \epsilon^{lmn}\delta^{il}\delta^{jm}\delta^{kn}$$

$$= \frac{1}{6}\left(\delta^{il}\delta^{jm}\delta^{kn} - \delta^{il}\delta^{jn}\delta^{km} - \delta^{in}\delta^{jm}\delta^{kl} - \delta^{im}\delta^{jl}\delta^{kn} + \delta^{im}\delta^{jn}\delta^{kl} + \delta^{in}\delta^{jl}\delta^{km}\right) \tag{2.48}$$

$$P_8 = \frac{1}{3}\Big(\delta^{kn}\left(\delta^{il}\delta^{jm} - \delta^{im}\delta^{jl}\right) + \delta^{km}\left(\delta^{il}\delta^{jn} - \delta^{in}\delta^{jl}\right)\Big) \tag{2.49}$$

$$P_{8'} = \frac{1}{3}\Big(\delta^{il}\left(\delta^{kn}\delta^{jm} - \delta^{km}\delta^{jn}\right) + \delta^{im}\left(\delta^{kn}\delta^{jl} - \delta^{kl}\delta^{jn}\right)\Big) \tag{2.50}$$

$$P_{10} = \frac{1}{6}\sum_{\mathrm{Perm}(l,m,n)} \delta^{il}\delta^{jm}\delta^{kn}$$

$$= \frac{1}{6}\left(\delta^{il}\delta^{jm}\delta^{kn} + \delta^{il}\delta^{jn}\delta^{km} + \delta^{in}\delta^{jm}\delta^{kl} + \delta^{im}\delta^{jl}\delta^{kn} + \delta^{im}\delta^{jn}\delta^{kl} + \delta^{in}\delta^{jl}\delta^{km}\right). \tag{2.51}$$

Denoting the thermal Wilson line at $\mathbf{x}_i$ by P_i for convenience, we find

$$\begin{aligned} C^1_{QQQ} &= \frac{1}{6}\big\langle 27\,\mathrm{Tr}\,P_1\mathrm{Tr}\,P_2\mathrm{Tr}\,P_3 - 9\,\mathrm{Tr}\,P_1\mathrm{Tr}\,(P_2P_3) \\ &\quad - 9\,\mathrm{Tr}\,P_2\mathrm{Tr}\,(P_1P_3) - 9\,\mathrm{Tr}\,P_3\mathrm{Tr}\,(P_1P_2) \\ &\quad + 3\,\mathrm{Tr}\,(P_1P_2P_3) + 3\,\mathrm{Tr}\,(P_1P_3P_2)\big\rangle \end{aligned} \tag{2.52}$$

$$\begin{aligned} C^8_{QQQ} &= \frac{1}{24}\big\langle 27\,\mathrm{Tr}\,P_1\mathrm{Tr}\,P_2\mathrm{Tr}\,P_3 + 9\,\mathrm{Tr}\,P_1\mathrm{Tr}\,(P_2P_3) \\ &\quad - 9\,\mathrm{Tr}\,P_3\mathrm{Tr}\,(P_1P_2) - 3\,\mathrm{Tr}\,(P_1P_3P_2)\big\rangle \end{aligned} \tag{2.53}$$

$$\begin{aligned} C^{8'}_{QQQ} &= \frac{1}{24}\big\langle 27\,\mathrm{Tr}\,P_1\mathrm{Tr}\,P_2\mathrm{Tr}\,P_3 + 9\,\mathrm{Tr}\,P_3\mathrm{Tr}\,(P_1P_2) \\ &\quad - 9\,\mathrm{Tr}\,P_1\mathrm{Tr}\,(P_2P_3) - 3\,\mathrm{Tr}\,(P_1P_2P_3)\big\rangle \end{aligned} \tag{2.54}$$

$$\begin{aligned} C^{10}_{QQQ} &= \frac{1}{60}\big\langle 27\,\mathrm{Tr}\,P_1\mathrm{Tr}\,P_2\mathrm{Tr}\,P_3 + 9\,\mathrm{Tr}\,P_1\mathrm{Tr}\,(P_2P_3) \\ &\quad + 9\,\mathrm{Tr}\,P_2\mathrm{Tr}\,(P_1P_3) + 9\,\mathrm{Tr}\,P_3\mathrm{Tr}\,(P_1P_2) \\ &\quad + 3\,\mathrm{Tr}\,(P_1P_2P_3) + 3\,\mathrm{Tr}\,(P_1P_3P_2)\big\rangle. \end{aligned} \tag{2.55}$$

We have again as a consequence of the completeness relation (2.30)

$$C_{QQQ} = \frac{1}{27}C^1_{QQQ} + \frac{8}{27}C^8_{QQQ} + \frac{8}{27}C^{8'}_{QQQ} + \frac{10}{27}C^{10}_{QQQ}. \tag{2.56}$$

We have suppressed the dependence on the spatial positions of the static quarks in the correlators here. In systems composed of two quarks or a quark anti-quark pair discussed above, due to translational invariance, a simple distance measure can be given in terms of the separation of the quark pair. For a three quark system, no such simple relation holds. In chapter 6 we will discuss this topic and derive the correct distance measure for the QQQ system.

The correlators obtained by (2.31) are, except the average ones, gauge dependent quantities and thus a gauge fixing procedure has to be applied when they are calculated on the lattice. For a description of the method used in this work, see appendix A.3. Though gauge dependent, it can be shown [23], that a gauge independent definition of the colour singlet and colour octet $Q\bar{Q}$ free energies is possible in terms of dressed thermal Wilson lines $\tilde{L}(\mathbf{x}) = \Omega^\dagger(x_0,\mathbf{x})L(\mathbf{x})\Omega(x_0,\mathbf{x})$ with $\Omega(x_0,\mathbf{x}) \in \mathrm{SU}(3)$. This definition coincides with the correlators (2.36) and (2.37) for the $Q\bar{Q}$ system in Coulomb gauge. The generalisation to other heavy quark systems is possible.

We note here again, that the colour symmetry state applies here to the state the static quarks are in, which of course does not have to be a singlet state. The *whole* system, i. e. the static quarks together with the surrounding gluonic medium, will arrange such that it is in a colour singlet state.

Some further comment on the behaviour under global $\mathbb{Z}(3)$ transformations is in order. Together with (2.21), it is easy to see that the correlators of the $Q\bar{Q}$- and the QQQ-system are invariant under these transformations in SU(3) pure gauge theory, but not

those of the QQ-system. Consequently, in the confinement phase, which is $\mathbb{Z}(3)$ symmetric, all C_{QQ} average to zero. We will show in detail in chapter 5, how this problem can be dealt with. We just remark here, that we perform a global $\mathbb{Z}(3)$ transformation on each lattice configuration in pure gauge theory, such that the L, averaged over one lattice configuration, lies in the real ($\phi = 0$) sector. This leaves all C_{QQ} finite. In the deconfinement phase, where the center symmetry is spontaneously broken, also the C_{QQ} assume non-vanishing values, so that no need for such a procedure arises. In a theory that includes dynamic quark fields, the center symmetry is explicitly broken and all correlators mentioned here assume finite values.

2.2.2 Cluster property

Let us now turn to some properties of free energies at finite temperature. At large distances, the disconnected part of the average correlation function dominates, which is called the *cluster value*,

$$\lim_{r\to\infty} C_{n\bar{n}}(r,T) = \lim_{r\to\infty} \left\langle \prod_{i=1}^{n} L(\mathbf{x}_i) \prod_{i=1}^{\bar{n}} L(\bar{\mathbf{x}}_i)^\dagger \right\rangle = \left\langle L \right\rangle^n \left\langle L^\dagger \right\rangle^{\bar{n}} \tag{2.57}$$

where a suitable distance measure r for the system has to be used. For two quark systems $n + \bar{n} = 2$ this is simply the separation of the static quarks, for $n = 3$ it is easy to show [22], that (2.57) is valid if all three mutual quark separations go to infinity. The cluster value (2.57) is only different from zero in the thermodynamic limit when confinement is absent. It is known from lattice calculations [24, 25], that also correlators in specific colour symmetry states approach the same cluster value. This is physically clear, since at large separations the quarks can not interact anymore by gluon exchange. They are screened by the surrounding thermal medium, independent of their relative colour orientation. This means, that the thermal Wilson line becomes diagonal in colour space and we obtain

$$\lim_{r\to\infty} \operatorname{Tr} C^W_{n\bar{n}}(r,T) = \lim_{r\to\infty} \left\langle \operatorname{Tr} \prod_{i=1}^{n} P(\mathbf{x}_i) \prod_{i=1}^{\bar{n}} P(\bar{\mathbf{x}}_i)^\dagger \right\rangle = \left\langle \operatorname{Tr} P \right\rangle^n \left\langle \operatorname{Tr} P^\dagger \right\rangle^{\bar{n}}, \tag{2.58}$$

which agrees with the result (2.57) for the average correlator. Together with the completeness relation for the projectors on the colour symmetry states (2.30) we find in the thermodynamic limit when confinement is absent, the *cluster property* for large separations

$$\lim_{r\to\infty} C^s_{n\bar{n}}(r,T) = \lim_{r\to\infty} C_{n\bar{n}}(r,T) = \left\langle L \right\rangle^n \left\langle L^\dagger \right\rangle^{\bar{n}}. \tag{2.59}$$

Since the average correlator is gauge independent, the cluster value is also gauge independent.

By calculating the $r \to \infty$ limit of a correlator, we can define the modulus of the expectation value of the Polyakov loop in the infinite volume limit with the help of

(2.59). Usually, one uses the $Q\bar{Q}$ system, because its correlator is the easiest to obtain from the lattice. We then define

$$\langle L \rangle = \lim_{r\to\infty} \sqrt{C_{Q\bar{Q}}(r,T)}. \tag{2.60}$$

As we will see in chapter 3, the Polyakov loop can be renormalised in a multiplicative way. This allows us to define *normalised* correlators

$$\Delta C_{n\bar{n}} = \frac{C_{n\bar{n}}}{\langle L \rangle^n \overline{\langle L^\dagger \rangle^{\bar{n}}}}, \tag{2.61}$$

since the renormalisation constants of the Polyakov loops will drop out. Thus $\Delta C_{n\bar{n}}$ is independent of the renormalisation procedure applied to the Polyakov loop and contributions from the self-interaction of the Polyakov loop have been removed. While this is possible in full QCD for all temperatures, for SU(N) this can only be done when confinement is absent and hence the expectation value of the Polyakov loop is finite. In view of (2.59), $\Delta C_{n\bar{n}}$ obviously has the property

$$\lim_{r\to\infty} \Delta C_{n\bar{n}}(r,T) = 1 \tag{2.62}$$

again for a suitable distance measure r (see the remarks following (2.57)). We can again define a corresponding free energy

$$\Delta F_{n\bar{n}} = -T \ln \left(\Delta C_{n\bar{n}} \right) \tag{2.63}$$

and thus obtain

$$\lim_{r\to\infty} \Delta F_{n\bar{n}}(r,T) = 0. \tag{2.64}$$

2.2.3 Internal Energy and Entropy

Free energies in a grand canonical potential, i. e. in a system at temperature T and volume V with vanishing chemical potential, $F(T,V)$, receive contributions from the internal energy $U(T,V)$ and from the entropy $S(T,V)$,

$$F(T,V) = U(T,V) - TS(T,V). \tag{2.65}$$

Since we can only extract the *difference* in free energy due to the insertion of static quarks into the thermal medium, the same holds true for the internal energy and the entropy, i. e. we can only obtain the difference in internal energy and the difference in entropy due to the presence of the static quarks. The relation (2.65) holds for these quantities as well. Given the free energy in a colour symmetry state s, we can compute the corresponding internal energy and the entropy

$$U^s_{n\bar{n}} = -T^2 \frac{\partial F^s_{n\bar{n}}/T}{\partial T} \tag{2.66}$$

$$S^s_{n\bar{n}} = -\frac{\partial F^s_{n\bar{n}}}{\partial T}, \tag{2.67}$$

where in general both $U^s_{n\bar{n}}$ and $S^s_{n\bar{n}}$ are dependent on the temperature and the distance measure of the system.

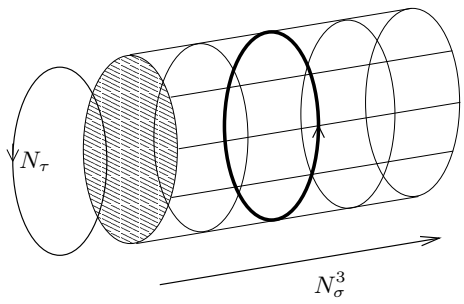

Figure 2.1: The thermal Wilson line on the lattice.

2.3 Lattice Implementation

We now turn to the lattice implementation of the Polyakov loop and the free energies. We will use the same names for observables as in the continuum for their lattice analogues where possible. For general conventions used in its implementation see appendix A.

Inspecting (2.19), the thermal Wilson line in the fundamental representation of SU(3) can be defined as the product of gauge links forming a closed path in the Euclidean time direction (see fig. 2.1). This gives

$$P(\mathbf{x}) = \prod_{x_4=0}^{N_\tau-1} U_4(x_4, \mathbf{x}). \tag{2.68}$$

The Polyakov loop in the fundamental representation is then defined by

$$L(\mathbf{x}) = \operatorname{Tr} P(\mathbf{x}), \tag{2.69}$$

where $\operatorname{Tr} \mathbb{1} = 1$. The average on one configuration is now computed through

$$L = [L(\mathbf{x})] = \frac{1}{N_\sigma^3} \sum_{\mathbf{x}} L(\mathbf{x}), \tag{2.70}$$

where $[\cdot]$ denotes the average over the spatial lattice. We now can take the average of L over all configurations now, which we denote by $\langle L \rangle$. For convenience we will also denote the *subsequent* averages over the spatial lattice and the configurations of some lattice quantity by $\langle \cdot \rangle$, when the position dependence of the enclosed observable is explicitly given, i. e. for the Polyakov loop we write $\langle L(\mathbf{x}) \rangle$ instead of $\langle [L(\mathbf{x})] \rangle$.

We will find it sometimes useful to work with a Polyakov loop, where the trace of the thermal Wilson line has *not* been normalised to unity,

$$l(\mathbf{x}) = \operatorname{tr} P(\mathbf{x}), \tag{2.71}$$

where $\operatorname{tr} \mathbb{1} = 3$. Its lattice and configuration averages can now be taken analogously to those for $L(\mathbf{x})$.

The correlators of the thermal Wilson line and the Polyakov loop and therefore the free energies of the different colour symmetry states can now be computed on the lattice in a straight forward way using the same relations as in the continuum and their averages can be obtained in the same manner as for the Polyakov loop.

Since we are ultimately interested in the physics of the continuum and lattice simulations are performed in finite volumes and with finite lattice spacings, we have to perform an thermodynamic ($V \to \infty$) and a continuum ($a \to 0$) limit for all observables O we are interested in, i. e.

$$O_{\text{cont}}(T) = \lim_{a \to 0} \lim_{V \to \infty} O_{\text{lat}}(a, N_\sigma, N_\tau). \tag{2.72}$$

The order of the limits in (2.72) is important and can not be interchanged. For the thermodynamic limit we will utilise lattices with different volumes V and then extrapolate to infinity. The continuum limit for the Polyakov loop and its correlation functions requires an additional *renormalisation procedure*, which we will explain in chapter 3.

Simulations on a lattice with a finite lattice spacing and a finite volume bring along *lattice artifacts* that might spoil a correct extrapolation to the continuum. One such lattice artifact is the violation of rotational invariance due to the presence of a finite lattice spacing. Though the tree level improved lattice gauge action employed in this work eases this problem, deviations remain at small distances. In order to correct for this, we employed *improved distances* for the distance measures of the correlators of the Polyakov loop, that are defined by the aid of the lattice Coulomb potential following [26].

As one generally does not introduce an explicit symmetry breaking term in the lattice calculations that could prohibit tunnellings between different $\mathbb{Z}(N)$ sectors in a finite volume the Polyakov loop expectation value would vanish even in the deconfined phase and therefore not assume its thermodynamic limit continuously. We therefore employ $\langle |L| \rangle$ at finite volume as an *estimator* for $\langle L \rangle$ at infinite volume, if the latter is different form zero. The calculation of $\langle L \rangle$ in (2.60) from the cluster value of the $Q\bar{Q}$ correlator, which is $\mathbb{Z}(3)$ symmetric, does not suffer from this problem.

We show in fig. 2.2 some results for the $Q\bar{Q}$ singlet and octet free energies obtained from calculation on a $32^3 \times 4$ lattice in pure gauge theory and from a $16^3 \times 4$ lattice in 2-flavour QCD below and above the phase transition.

Let us start with $F^1_{Q\bar{Q}}(r,T)$ for temperatures below T_c which is shown in the upper left corner of fig. 2.2. We see that the singlet free energies rise with growing distance, thus showing confinement over the entire distance regime studied here. For larger temperatures the steepness of the curves becomes smaller, signalling a decrease of the string tension [27], eventually assuming constant values at the critical temperature, marking the transition into the deconfined phase. In 2-flavour QCD (upper right corner) the situation is different. Though at small separations $F^1_{Q\bar{Q}}(r,T)$ rises more rapidly for smaller temperatures, at intermediate distances $rT \approx 1$ the curves become flat, assuming their asymptotic value F_∞/T, which decreases with increasing temperature. This phenomenon is called *string breaking*. Unlike in pure gauge theory, where dynamical quark fields are absent, in full QCD pair creation of a dynamical quark-anti-quark pair

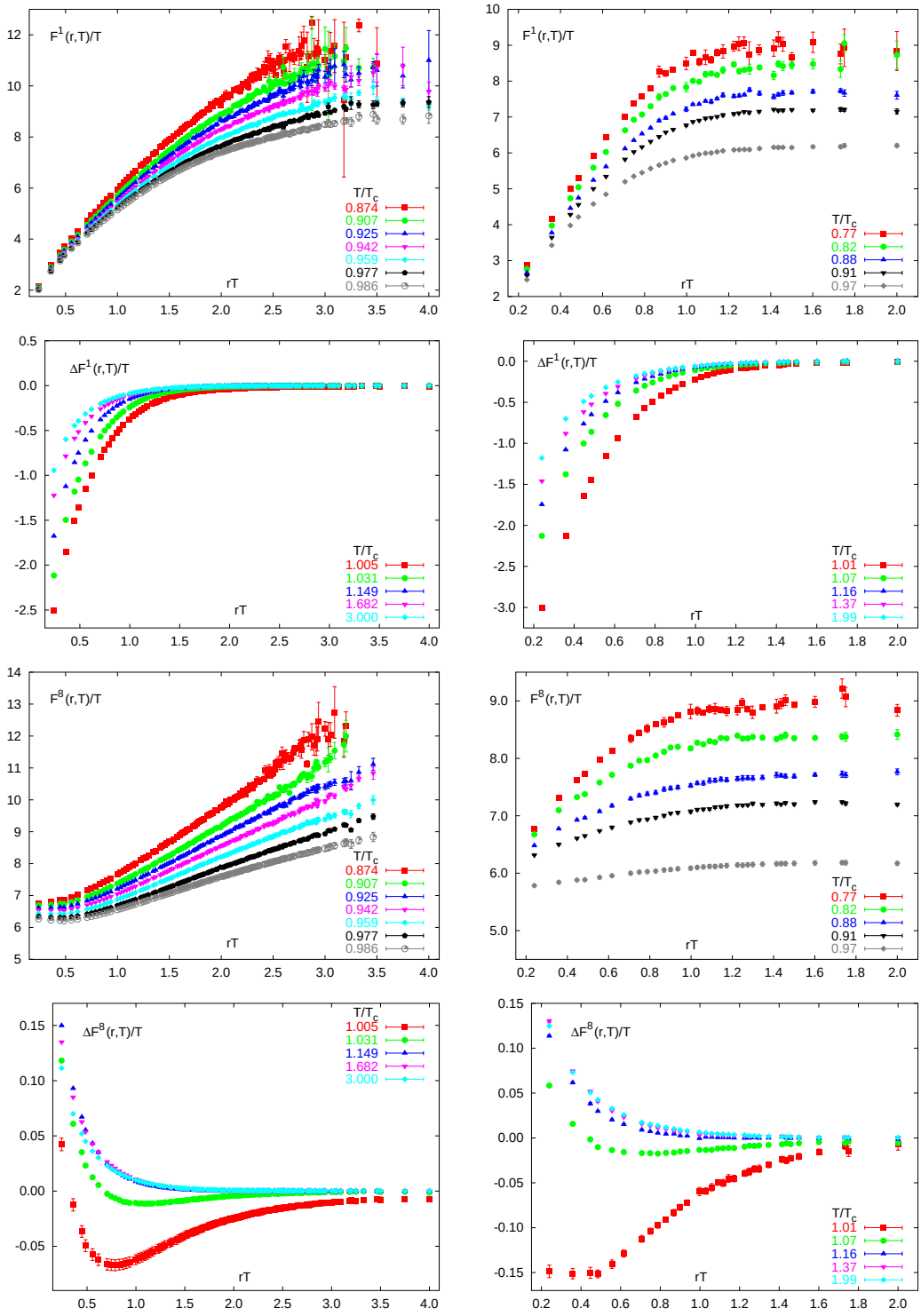

Figure 2.2: Left column: free energies from a $32^3 \times 4$ lattice in pure gauge theory. Right column: the same from a $16^3 \times 4$ lattice in 2-flavour QCD. Upper half shows $F^1_{Q\bar{Q}}(r,T)$, lower half $F^8_{Q\bar{Q}}(r,T)$ below and above T_c.

$q\bar{q}$ is possible. If the energy stored in the string is as large as the energy gap between twice the mass of the lowest heavy-light meson and the two single heavy quarks, i. e. $F(r,T) = \Delta m_{Q,q} = 2m_{Q\bar{q}} - 2m_Q$, the two heavy quarks will form bound states with the dynamical quarks and the string will break,

$$Q\bar{Q} + \Delta m_{Q,q} \quad \longrightarrow \quad Q\bar{q} + \bar{Q}q, \tag{2.73}$$

where $\Delta m_{Q,q}$ does not depend on m_Q [28]. The distance, at which F_∞ is assumed by the $T = 0$ potential, $V(r_{\text{string}}) = F_\infty$, is called the *string breaking distance* r_{string}. We note that nevertheless confinement is still realised, since all quarks in (2.73) are bound into mesons. At small separations, $F^1_{Q\bar{Q}}(r,T)$ for SU(3) as well as full QCD approach their perturbative Coulomb behaviour, which is attractive.

We turn to the second row of plots in fig. 2.2, which shows the normalised singlet free energies $\Delta F^1_{Q\bar{Q}}(r,T)/T$ above T_c, that approach zero for large distances. For SU(3) as well as full QCD, the plots qualitatively agree. At some fixed separation rT, $\Delta F^1_{Q\bar{Q}}(r,T)/T$ decreases with decreasing temperature. For the region $rT \gg 1$, the dominant effect is *screening*, i. e. the gluons acquire an effective mass through interaction with the medium, the *Debye mass* m_D. The singlet free energy than behaves as

$$\Delta F^1_{Q\bar{Q}}(r,T) = -\frac{\alpha^1_{Q\bar{Q}}(r,T)}{r}\, e^{-m_D(T)\, r} \quad rT \gg 1, \tag{2.74}$$

where $\alpha^1_{Q\bar{Q}}(r,T)$ is an effective coupling constant for the $Q\bar{Q}$-singlet system. The finite Debye mass m_D defines a *screening length* $r_D \sim m_D^{-1}$, beyond which the heavy quarks effectively do not interact any more, i. e. they are screened and can move freely in the medium. It is clear from this considerations, that the screening mass and length are important properties of the thermal medium in the deconfined phase and much work has been devoted to the extraction of m_D from lattice data [27, 29, 30].

We now come to the discussion of the octet free energies in the lower half of fig. 2.2. Below T_c we see that $F^8_{Q\bar{Q}}(r,T)/T$ in pure gauge theory is confining for distances $rT \gtrsim 0.5$ with falling steepness with growing temperature as the corresponding singlet is, but with a much smaller slope. This is due to the different Coulombic part in the free energy compared to the colour singlet case, the string tensions of both systems are the same. For small separations $rT \lesssim 0.5$ the curves bend over and eventually start to rise for $r \to 0$, thus approaching their perturbative Coulomb behaviour, that is repulsive. The octet free energy below T_c in full QCD is similar to the singlet case, i. e. attractive for small distances and showing string breaking, although the steepness of the curves for small separations is much smaller than for the singlet free energy. Again, this is due to the different Coulombic contributions compared to the colour singlet case. We expect to see a repulsive behaviour at small distances here too, which has to set in obviously at smaller distances calculated here.

Above T_c in pure gauge theory, $\Delta F^8_{Q\bar{Q}}(r,T)/T$ approaches zero for large distances, thus confirming the independence of the cluster property (2.59) from the colour symmetry state. The octet free energy is repulsive over the entire distance interval calculated

here for the highest two temperatures, whereas closer to T_c a minimum at $rT \sim (0.75-1)$ develops, which becomes more pronounced closer to T_c. For even smaller distances, the octet free energies become repulsive again also at this temperatures. $\Delta F^8_{Q\bar{Q}}(r,T)/T$ behaves qualitatively similar in full QCD, approaching zero for large distances, repulsive behaviour over the entire distance interval for the highest temperatures and the development of a minimum at smaller distances. Again, we can not see the bending back to a repulsive behaviour at even smaller separations for the distances calculated here.

2.4 Higher Representations of L

We now turn to the Polyakov loop in higher representations of the SU(3) gauge group. We will follow the custom to call a representation by its dimension D, where no ambiguity exists. In standard implementations of SU(3) pure gauge theory on the lattice, the gauge links are of course in the fundamental representation of SU(3). Consequently, the thermal Wilson line and the Polyakov loop are therefore calculated in the fundamental representation as well. In order to obtain observables in higher representations, we have to employ group theoretical relations, which allow to compute the desired observables from standard lattice quantities in the fundamental representation.

In general, two routes can now be taken. The first one utilises a property of the direct product of a group character and allows to obtain L_D and their average correlators for arbitrary irreducible representations D. Moreover, it is straight forward to implement and numerically cheap. In the second method we compute the lattice gauge links in a higher irreducible representation from their counterparts in the fundamental representation. From there, it is easy to obtain the thermal Wilson line and its correlators in the usual way from the new gauge links. In particular, this method allows us to calculate also singlet free energies in that higher representation. Unfortunately, these calculations are numerically more demanding and additionally a gauge fixing is necessary for the singlet free energies. We will now introduce both routes to higher representations of the Polyakov loop and the thermal Wilson line respectively.

Introductions to group theory and Lie-groups can be found in [31, 32, 33], a summary of facts concerning group theory and SU(3) in particular, which are relevant for this work, is offered in appendix B. For reference we list in table 2.1 the lowest irreducible representations of SU(3) up to $D = 27$ and some of their properties.

2.4.1 The Direct Product Route

This method allows to obtain the Polyakov loop in an arbitrary irreducible representation l_D from the Polyakov loop in the fundamental one, which we will call from now on l_3. We remind here, that

$$\frac{l_D(\mathbf{x})}{D} = L_D(\mathbf{x}), \tag{2.75}$$

i. e. $l_D(\mathbf{x})$ is defined with the unnormalised trace. We now use the theorem that the product of characters in the representations P and Q of a group element g is equal to

D	(p,q)	t	$C(D)$	d_D	
3	$(1,0)$	1	4/3	1	fundamental
$\overline{3}$	$(0,1)$	2	4/3	1	
6	$(2,0)$	2	10/3	5/2	
8	$(1,1)$	0	3	9/4	adjoint, real
10	$(3,0)$	0	6	9/2	
15	$(2,1)$	1	16/3	4	
$15'$	$(4,0)$	1	28/3	7	
24	$(3,1)$	2	25/3	25/4	
27	$(2,2)$	0	8	6	real

Table 2.1: Casimir $C(D)$ for the representation D of SU(3), $t = p-q \mod 3$ is the triality, d_D is defined in (2.101). (p,q) is the canonical label of the representation with dimension D.

the character of this group element in the direct product representation $P \times Q$,

$$\chi_{P\times Q}(g) = \chi_P(g)\,\chi_Q(g). \tag{2.76}$$

The Polyakov loop l_D is the character of the corresponding thermal Wilson line, which is of course an element of SU(3). The direct product can now be reduced into a direct sum of irreducible representations using the Clebsh-Gordan series to give the Polyakov loop in various representations. The identities used for this procedure are shown in appendix B. We are now in position to calculate l_D for $D \leq 27$ from l_3:

$$\begin{aligned}
l_{\bar{3}} &= l_3^* && (2.77)\\
l_6 &= l_3^2 - l_3^* && (2.78)\\
l_8 &= |l_3|^2 - 1 && (2.79)\\
l_{10} &= l_3 l_6 - l_8 && (2.80)\\
l_{15} &= l_3^* l_6 - l_3 && (2.81)\\
l_{15'} &= l_3 l_{10} - l_{15} && (2.82)\\
l_{24} &= l_3^* l_{10} - l_6 && (2.83)\\
l_{27} &= |l_6|^2 - l_8 - 1. && (2.84)
\end{aligned}$$

The relations (2.77)-(2.84) can now be employed at every spatial position on the lattice to give $L_D(\mathbf{x}) = l_D(\mathbf{x})/D$, from which the lattice and configuration averages can be calculated.

Having now Polyakov loops in different irreducible representations at our command, we can easily calculate $(n,\bar{n})$-point correlators along the lines of (2.25) to obtain the

corresponding average free energies. To be definite, we define

$$C_{n\bar{n},D}(r,T) = \left\langle \prod_{i=1}^{n} L_D(\mathbf{x}_i) \prod_{i=1}^{\bar{n}} L_D^\dagger(\bar{\mathbf{x}}_i) \right\rangle, \tag{2.85}$$

where the considerations concerning the distance measure r for the correlators built from Polyakov loops in the fundamental representation are of course still valid. The *average free energy in representation D* is then analogously to (2.26)

$$F_{n\bar{n},D}(r,T) = -T \ln \left(C_{n\bar{n},D}(r,T) \right). \tag{2.86}$$

In total, we can say that the direct product method is easy to implement on the lattice and numerically relatively cheap. First results will be given in the next section to provide a check on the employed methods and moreover from a small lattice for illustrative purposes in chapter 2.4.3.

2.4.2 The Gauge Link Route

We will now introduce a second method, which is capable of computing the thermal Wilson line and its correlators in arbitrary irreducible representations. Moreover, we will compare the results of this method for the adjoint Polyakov loop with those of the first method.

We can calculate the link variable in a higher representation U^D from those in the fundamental one U^3 for arbitrary irreducible representations. The connection to the gauge links in the fundamental representations can be found by the aid of the generators of the target representation D. This is most easily done for the adjoint representation $D = 8$. The *adjoint link variable* U^8 can be computed from its counterpart in the fundamental representation U^3 by using

$$U_{ij}^8 = \frac{1}{2} \mathrm{Tr} \left(\lambda_i U^3 \lambda_j U^{3\dagger} \right), \quad i,j = 1,\ldots,8, \tag{2.87}$$

where we have suppressed any dependence on position and direction in the link variables and λ_i are the Gell-Mann matrices. The U_{ij}^8 are real numbers, which follows from the hermiticity of the λ_i and the cyclicity of the trace. The thermal Wilson line in the adjoint representation P_8 is now obtained analogously to its definition in the fundamental representation (2.68),

$$P_8(\mathbf{x}) = \prod_{x_4=0}^{N_\tau - 1} U_4^8(x_4, \mathbf{x}), \tag{2.88}$$

and the Polyakov loop in the adjoint representation is then along the lines of (2.69) defined by

$$L_8(\mathbf{x}) = \mathrm{Tr}\, P_8(\mathbf{x}), \tag{2.89}$$

where $\mathrm{Tr}\,\mathbb{1}_{8\times 8} = 1$. It is now straightforward to define arbitrary correlators of thermal Wilson lines and Polyakov loops like we did in the fundamental representation. However, in general the symmetry states obtained from reducing out the direct product of fundamental representations will not be the same. Nevertheless, it is easy to see, that the $Q\bar{Q}$ system will always exhibit a singlet symmetry state,

$$D \otimes \bar{D} = 1 \oplus \ldots, \tag{2.90}$$

which can be obtained in the same way as in the fundamental representation. Therefore we define here the *adjoint singlet correlator* $C^1_{Q\bar{Q},8}$ to be

$$C^1_{Q\bar{Q},8}(r,T) = \left\langle \mathrm{Tr}\,\left(P_8(\mathbf{x}_1) P_8(\bar{\mathbf{x}}_1)^\dagger \right) \right\rangle \tag{2.91}$$

and the corresponding free energy

$$F^1_{Q\bar{Q},8}(r,T) = -T \ln\left(C^1_{Q\bar{Q},8}(r,T) \right). \tag{2.92}$$

Again, $C^1_{Q\bar{Q},8}$ is manifestly gauge dependent and a gauge fixing is necessary. And again, this gauge dependent correlator coincides with a gauge independent one in terms of dressed (adjoint) thermal Wilson lines [23]. We will discuss the behaviour of $F^1_{Q\bar{Q},8}(r,T)$ in chapter 3 and use it for the renormalisation of the adjoint Polyakov loop.

Moreover, we have the cluster property for general representations D,

$$\lim_{r\to\infty} C^s_{n\bar{n},D}(r,T) = \lim_{r\to\infty} C_{n\bar{n},D}(r,T) = \left\langle L_D \right\rangle^n \left\langle L_D^\dagger \right\rangle^{\bar{n}}, \tag{2.93}$$

since the dominance of the disconnected part and the diagonal thermal Wilson lines does not rely on the particular representation employed. The cluster value (2.93) is real for vanishing triality, i. e. $n - \bar{n} \bmod 3 = 0$. This can now be used to extend the definition of the normalised correlators (2.61) to some representation D,

$$\Delta C_{n\bar{n},D} = \frac{C_{n\bar{n},D}}{\left\langle L_D \right\rangle^n \left\langle L_D^\dagger \right\rangle^{\bar{n}}}. \tag{2.94}$$

An analogous definition holds for the singlet correlator. Again, this is in general only possible in the deconfinement phase, where the expectation value of the Polyakov loop is finite. We nevertheless note here, that string breaking for representations with vanishing triality ($t = 0$) results in finite values for $\langle L_D \rangle$ in the thermodynamic limit in pure gauge theory also below T_c, as will be discussed in chapter 2.4.4. We can also again define a corresponding free energy

$$\Delta F_{n\bar{n},D} = -T \ln\left(\Delta C_{n\bar{n},D} \right), \tag{2.95}$$

where the singlet free energy is defined analogously.

For the sake of completeness we just briefly mention here, that it is of course possible to calculate *cross correlators*, where the sources are in different representations

$$C^s_{Q\bar{Q},D,D'}(r,T) = A \left\langle \mathrm{Tr}\,\left(P_D(\mathbf{x}_1) P_{D'}^\dagger(\bar{\mathbf{x}}_1) \right) \right\rangle + B \left\langle L_D(\mathbf{x}_1) L_{D'}^\dagger(\bar{\mathbf{x}}_1) \right\rangle, \tag{2.96}$$

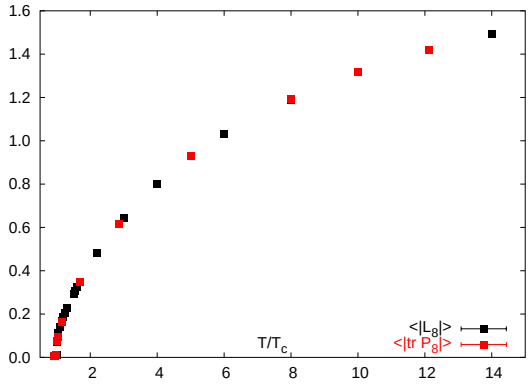

Figure 2.3: Comparison of $\langle|L_8|\rangle$ calculated with the direct product method and $\langle|\mathrm{Tr}\, P_8|\rangle$ obtained from adjoint gauge links over T from a $32^3 \times 4$ lattice.

where s is the colour symmetry state with $D \neq D'$ and some suitable A, B. The direct product of this representations does not contain a singlet representation and therefore we are dealing here with colourful objects, which have to be screened by the gluonic medium and are not $\mathbb{Z}(3)$-symmetric. This results in zero expectation values in the confined phase. In chapter 5 we will nevertheless calculate diquark correlators in SU(3) pure gauge theory along the lines of (2.43) and (2.44) from sources in the fundamental representation, where we utilise a global $\mathbb{Z}(3)$-transformation that leaves the Polyakov loop in the real sector. Moreover, it is of course possible to compute baryonic or even higher correlators from thermal Wilson lines in the adjoint or other representations [34], which is, however, beyond the scope of this work.

Since we are able to calculate $\langle|L_8|\rangle$ directly from the adjoint gauge links according to (2.89) and from the reduction procedure (2.79), we can check whether both methods agree. We have calculated the unrenormalised $\langle|L_8|\rangle$ with both methods on a $32^3 \times 4$ lattice for various temperatures. The result is shown in fig. 2.3. For all analysed temperatures $0.907T_c$ to $14T_c$ we see no deviations, which is reassuring.

2.4.3 Center Symmetry revisited

Let us recall the behaviour of the Polyakov loop in the fundamental representation under global $\mathbb{Z}(N)$ transformations $zg(x_0, \mathbf{x})$ described in (2.21)

$$^{g}L(\mathbf{x}) = e^{i\phi}L(\mathbf{x}),$$

where

$$z = e^{i\phi}\mathbb{1}, \qquad \phi = \frac{2\pi n}{N}, \qquad n = 0, \ldots, N-1.$$

We are now interested in the behaviour under global $\mathbb{Z}(3)$ transformations zg of the Polyakov loop in an arbitrary representation D of SU(3). We find

$$^{g}L_D(\mathbf{x}) = e^{it\phi}L_D(\mathbf{x}), \tag{2.97}$$

where

$$z = e^{i\phi}\mathbb{1}_{D\times D}, \qquad \phi = \frac{2\pi n}{3}, \qquad n = 0, 1, 2 \tag{2.98}$$

and $t = (p - q) \bmod 3$ is the *triality*, where (p, q) is the canonical label of the representation. As (2.97) shows, the triality t acts as a $\mathbb{Z}(3)$-*charge* for L_D. For representations with vanishing triality, i. e. $D = 8, 10, 27$ in our work, the corresponding Polyakov loops L_D are invariant under global $\mathbb{Z}(3)$ transformations and thus do not feel the breakdown of the center symmetry.

In order to illustrate the effect of different trialities we have computed l_D following the direct product route discussed in 2.4.1 on a $8^3 \times 4$ lattice in pure gauge theory at one temperature below and one above T_c. A histogram in the complex plane of l_D calculated on 10^5 different lattice configurations for $D = 3, 6, 8, 10$ is shown in fig. 2.4. These four lowest irreducible representations cover all three possible values for the triality, where for both $D = 8$ and $D = 10$ the triality vanishes and additionally L_8 is purely real. Let us briefly explain what we expect to see and why we expect to see it, before we discuss the results of the calculations. We start with those representations which have a non-vanishing triality. Below T_c we are in the confinement phase, where the center symmetry is realised and consequently the expectation value of l_D vanishes. Thus, far away from the critical temperature, we expect to see the values cluster around the origin of the complex plane in a spherical symmetric manner. As the system approaches T_c, the values start to wander outwards along the lines of the three unit roots, since in a finite volume a sharp transition at the critical temperature is not possible and thus a gradual transition into the $\mathbb{Z}(3)$-broken phase has to take place. There, the Polyakov loop acquires a non-vanishing expectation value *in the thermodynamic limit*, where its values cluster around one of the $\mathbb{Z}(3)$-sectors. In a finite volume, however, tunnelling between the three $\mathbb{Z}(3)$-vacua is possible, leading to a vanishing expectation value even above T_c. Therefore, we expect to see values clustered around the three possible vacua, which have wandered outwards and have lost their connection to the origin. These considerations apply to both $t = 1$ and $t = 2$ representations. The only difference concerning the behaviour of the $t = 2$ representations to the ones with $t = 1$ outlined above is, that the Polyakov loops residing in one of the two $\mathbb{Z}(3)$-vacua with non-vanishing imaginary part are interchanged. Representations with vanishing triality are blind to the center symmetry and therefore cluster around their expectation value in a spherical symmetric fashion in both phases. As will be shown further below, due to string breaking, the expectation value of these representations is non-zero even below T_c. This property also survives the thermodynamic limit. We finally remark, that $\langle |l_D| \rangle$ becomes smaller with larger D at the temperatures considered here.

Let us now turn to the concrete histograms in fig. 2.4. In the first line we show L_3, which has triality $t = 1$. Below T_c (left column) we see a pronounced star like shape oriented along the axis of the three roots of unity, thus leading to a vanishing expectation value $\langle l_3 \rangle = 0$. In fact, as described above, the star like shape suggests that the system is already close to the phase transition.

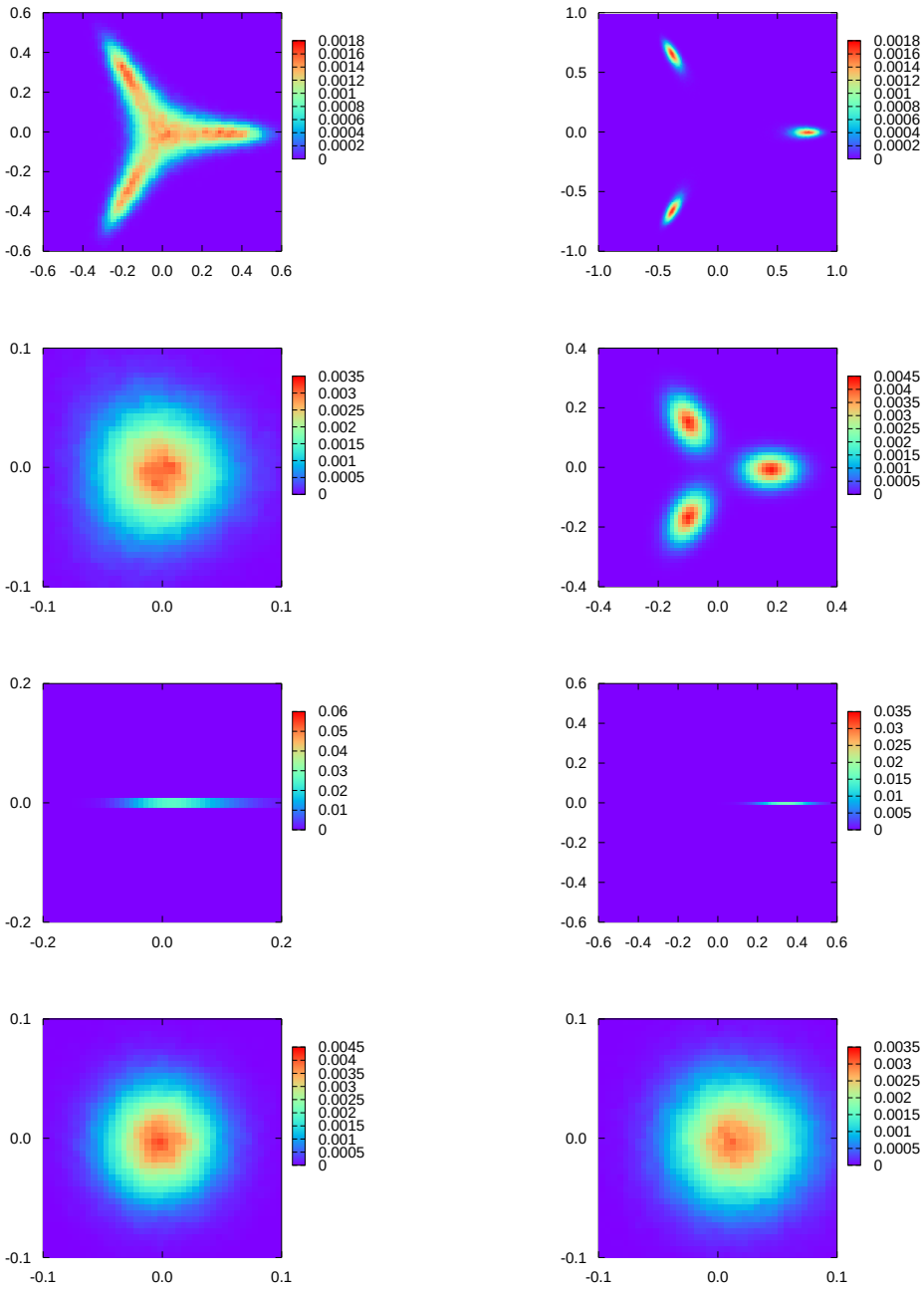

Figure 2.4: Histogram of l_D in the complex plane from a $8^3 \times 4$ lattice for $T/T_c = 0.959$ (left column) and $T/T_c = 1.682$ (right column) and for $D = 3, 6, 8, 10$ (from top to bottom), which have the trialities $t = 1, 2, 0, 0$.

Above T_c (right column), the system is in the $\mathbb{Z}(3)$-broken phase, and we see three distinct clusters around the three $\mathbb{Z}(3)$-vacua, in accordance with the considerations above. In the second line we show l_6, which has triality $t = 2$, cluster around the origin below T_c, thus showing $\mathbb{Z}(3)$-symmetry. In comparison to l_3, the distribution is not star shaped but spherical, which is explained by the fact that the absolute value of the Polyakov loop $\langle |l_D| \rangle$ becomes smaller in higher representations and thus the different $\mathbb{Z}(3)$-sectors have a larger overlap. Above T_c we observe basically the same as in the l_3 case, but with the two $\mathbb{Z}(3)$-sectors with negative real part interchanged with respect to those of l_3. Moreover, $\langle |l_6| \rangle$ is obviously smaller than in the fundamental representation, as we already noticed below T_c. The third line shows l_8, which has vanishing triality $t = 0$ and is purely real, $l_8 \in \mathbb{R}$. All values are distributed on the real axis with the maximum in the positive part in both phases. While this is easy to see above the critical temperature, it is harder to see for $T < T_c$, but will be shown to be correct in chapter 4 in more detail. These arguments also apply to l_{10} plotted in the last line, which has vanishing triality as well but assumes in general complex values. We observe a spherical symmetric distribution, which is below the critical temperature close to but not quite zero and clearly real and positive above T_c.

2.4.4 String Breaking in Pure Gauge Theory

We will now discuss the phenomenon of *string breaking* in SU(3) pure gauge theory. In the fundamental representation the $Q\bar{Q}$ free energies below the critical temperature rise forever, thus confining the participating two heavy quarks into a meson. In some higher representations, however, the heavy quarks can be screened by the surrounding gluonic medium (or vacuum for $T = 0$) and form a singlet state. Then, similar to the string breaking mechanism in full QCD (see sec. 2.3), the quark-anti-quark pair decays into two disjoint gluonlumps. This has been observed for the adjoint potential at $T = 0$ [35, 36] and at finite temperature [37]. The observations can be made systematic with the help of group theory [4]. Considering the direct product formed by a quark in some representation D and the gluon field, which is in the adjoint representation 8, we can reduce it out into the sum of irreducible representations. For instance, let the quark be in the sextet representation $D = 6$. We then obtain

$$6 \otimes 8 = 24 \oplus \overline{15} \oplus 6 \oplus \bar{3}, \tag{2.99}$$

where all representations higher than the anti-fundamental one will at least be partially screened by the gluons. Therefore, the remaining (anti-)fundamental component causes the corresponding free energy to show confinement. Contrary to that, for $D = 8$, i. e. a quark in the adjoint representation, we find

$$8 \otimes 8 = 27 \oplus \overline{10} \oplus 10 \oplus 8 \oplus 8 \oplus 1. \tag{2.100}$$

Now, we have obtained a singlet component, which leads to the observed string breaking at large distances in SU(3) pure gauge theory below T_c. In general, all representations with non-vanishing triality $t \neq 0$ will form a residual (anti-)fundamental component

with the gluon field and thus the corresponding free energy will rise forever. The representations with vanishing triality $t = 0$ can be screened completely by the surrounding gluons and form a singlet component at large separations, which leads to the breaking of the string. The distance, at which this takes place, is called the *string breaking distance* r_{string} and its value in the vacuum is related to the mass of the "gluonlump" m_{glump}, when the Polyakov loop is in the adjoint representation. In this case, the heavy quark in the adjoint representation may be thought of as being a static *gluino* $\tilde{G}$, which is the fermionic superpartner of the gluon. Thus a gluelump in our approach is the bound state $\tilde{G}g$ of a heavy gluino $\tilde{G}$ and a dynamical gluon g [36]. At finite temperature the string breaking distance observed in the adjoint singlet free energy is related to the binding energy of the gluelump.

The findings above again highlighten the rôle of the center symmetry for confinement, that can be explored by employing higher representations of the SU(3) gauge group. As a consequence of string breaking and the cluster property of free energies, we expect the Polyakov loop in a $t = 0$-representation to stay finite in the thermodynamic limit also below T_c. We will proof this to be correct for the adjoint representation $D = 8$ and determine the string breaking distance and the binding energy of the gluelump in chapter 4.

2.4.5 Casimir Scaling

The *Casimir scaling hypothesis* states, that potentials between sources in different representations are proportional to each other with their ratios given by the respective ratios of eigenvalues of the corresponding quadratic Casimir operators [4]. To be definite, let $V_D(r)$ be the potential between charges in the irreducible representation D and $C(D)$ is the respective eigenvalue of the Casimir operator of that representation. Let us define the ratio of the Casimirs for two arbitrary representations D_1, D_2 to be

$$d(D_2, D_1) = \frac{C(D_2)}{C(D_1)} \quad \text{and} \quad d_D = d(D, 3). \tag{2.101}$$

Then, Casimir scaling means that

$$V_{D_2}(r) = d(D_2, D_1) V_{D_1}(r) \tag{2.102}$$

is fulfilled. In the lowest order of the perturbation series the Coulomb potential in SU(3) pure gauge theory is given by

$$V_D(r) = -C(D)\frac{g^2}{4\pi r}, \tag{2.103}$$

which fulfils (2.102) obviously. Moreover, Casimir scaling is realised in perturbation theory in the vacuum for small distances, where one gluon exchange dominates, up to two loop order and furthermore at high temperatures and large distances up to the same order, since the contribution of non-planar loops vanishes to this order [5]. In lattice perturbation theory of full QCD in the vacuum Casimir scaling holds up to $\mathcal{O}(g^4)$ [38]. A

lattice calculation at finite temperature employing an effective action for the Polyakov loop in SU(3) has found that Casimir scaling is realised between Polyakov loops in different representations as well [39]. Numerical calculations on the lattice at $T = 0$ in pure gauge theory show that (2.102) is realised also for distances smaller than the string breaking distance to an accuracy of 5 % [4]. This very good agreement of the lattice data with the Casimir scaling hypothesis at non-perturbative distances in the vacuum has considerable ramifications on models for non-perturbative QCD, especially for the confinement mechanism [40]. This can be seen as follows. If (2.102) holds also for distances where a flux tube is present, we obtain a rule for the string tension σ_D in some representation D, which is

$$\sigma_D = d_D \, \sigma_3, \tag{2.104}$$

where σ_3 is the string tension in the fundamental representation. This would exclude other possibilities like center vortex models [41], which state that the scaling is proportional to the number of fundamental flux tubes embedded into the higher representation vortex and predict for SU(3)

$$\sigma_D = (p + q) \, \sigma_3, \tag{2.105}$$

where (p, q) is the canonical label for a representation with dimension D. This prediction coincides with Casimir scaling in the large N-limit [42, 43] and is supported by the finding, that the vacuum seems to act as a type I superconductor [44, 45], i. e. flux tubes repel each other. Another possibility is based on considerations in M-theory for SU(N) theories [46, 47],

$$\sigma_D = \frac{\sin\left(\frac{t\pi}{N}\right)}{\sin\left(\frac{\pi}{N}\right)} \, \sigma_3, \tag{2.106}$$

where t is the triality and which is called *Sine-law scaling*. It coincides with Casimir scaling in the large N-limit as well.

In order to study the properties of the confinement mechanism at finite T and their behaviour at the phase transition into the deconfined phase and for the renormalisation procedures presented in chapter 3, we wish to calculate free energies in higher representations in the non-perturbative finite temperature region. Work that has been done so far on the correlators of Polyakov loops in higher representations for SU(3) finite temperature pure gauge theory can be found in [48, 49, 50].

3 Renormalisation of the Polyakov Loop

We will now introduce two different renormalisation methods for the Polyakov loop in arbitrary representations of the SU(3) gauge group obtained from lattice calculations. To this end, the first method using the short distance behaviour of the $Q\bar{Q}$ free energies has to be extended from the fundamental to higher representations, while the second method can be applied easily to any representation. We will then compare the results of these two methods, thus allowing us to check their consistency. In the last part of this chapter we will discuss a third renormalisation method which starts from different assumptions.

3.1 General Remarks

Polyakov suggested a surprisingly simple separation of the divergence structure of $\langle L_3 \rangle$ [51]. According to this the linear divergent parts that appear in any order perturbation theory can be combined giving an exponential factor, while the rest consists only of finite contributions and logarithmic divergences summed up here in G_{ren}, so that we obtain

$$\langle L_3 \rangle \propto e^{-Kf(l/a)}\, G_{\mathrm{ren}}, \tag{3.1}$$

where K is a proportionality constant, $f(l/a)$ is linear in its argument, l is the length of the loop and a the lattice spacing. All logarithmic divergences can be removed order by order in perturbation theory [52]. Although a composite operator, the Polyakov loop does not mix with any other operator under renormalisation. Thus, the Polyakov loop expectation value is a standard renormalisable object and physically meaningful. We note, that we address in this work only Polyakov loops which have a differentiable contour. For contours with cusps or intersecting contours new divergencies arise, which have been dealt with in perturbative calculations [53].

Renormalising the Polyakov loop calculated on the lattice means now to eliminate the linear divergence in (3.1). To this end we use a *multiplicative* renormalisation scheme [51] for the thermal Wilson line

$$P_3^R(\mathbf{x}) = \left(Z_3^R(g^2)\right)^{N_\tau} P(\mathbf{x}). \tag{3.2}$$

where P_3^R is the renormalised thermal Wilson line and $Z_3^R(g^2)$ is an effective renormalisation constant depending only on the square of the bare gauge coupling g. The renormalisation scheme for the Polyakov loop is now readily obtained to be

$$L_3^R(\mathbf{x}) = \left(Z_3^R(g^2)\right)^{N_\tau} L_3(\mathbf{x}). \tag{3.3}$$

The lattice and configuration averages can now readily be taken. We note here, that the multiplication with Z_3^R respects the center symmetry and the projection operators (2.29) do not act on it. Therefore also $(n, \bar{n})$-point correlation functions can be renormalised by

$$C^{s,R}_{n\bar{n},3} = \left(Z_3^R(g^2)\right)^{(n+\bar{n})N_\tau} C^s_{n\bar{n},3}, \tag{3.4}$$

where s stands for the symmetry state of the n quarks and $\bar{n}$ anti-quarks including the average correlator. We like to stress the point that the effective renormalisation constants $Z_3^R(g^2)$ depend *only* on the bare gauge coupling and not on the temperature or the volume [53] and the renormalised Polyakov loop expectation value on the temperature and not on g or N_τ. We will discuss a different approach, where the renormalisation constants are assumed to be explicitly T-dependent, in chapter 3.4.

We also adopt the multiplicative renormalisation scheme laid out in (3.2) and (3.3) for thermal Wilson lines and Polyakov loops in higher representations of SU(3). This is possible, since the arguments in [51] for the divergence structure of the Polyakov loop (3.1) do not depend on the particular representation employed. We can now generalise (3.2) and (3.3) to arbitrary representations D to obtain

$$P_D^R(\mathbf{x}) = \left(Z_D^R(g^2)\right)^{d_D N_\tau} P_D(\mathbf{x}) \quad \text{and} \quad L_D^R(\mathbf{x}) = \left(Z_D^R(g^2)\right)^{d_D N_\tau} L_D(\mathbf{x}). \tag{3.5}$$

Though we have included d_D in the exponent of the effective renormalisation constant, this definition does not implicitly assume Casimir scaling to hold, since *a priori* the Z_D^R are not connected to the Z_3^R in some obvious way. If Casimir scaling is realised for the bare Polyakov loop in some representation D at some temperature, by (3.5) we also obtain Casimir scaling in the renormalised Polyakov loop together with the relation $Z_D^R = Z_3^R$ for the effective renormalisation constants.

As we have seen in chapter 2.4.5, Casimir scaling is realised in high temperature perturbation theory. We therefore expect for the $T \to \infty$-limit of $\langle L_D^R \rangle$

$$\lim_{T\to\infty} \langle L_D^R \rangle = \lim_{T\to\infty} \langle L_3^R \rangle^{d_D} = 1, \tag{3.6}$$

where $\langle L_D^R \rangle$ approaches unity from above, because $\langle L_3^R \rangle$ does [54].

The renormalisation scheme (3.5) can again immediately be applied to $(n, \bar{n})$-point correlators, where the sources are in some representation D, with the same arguments that lead to (3.4) to give

$$C^{s,R}_{n\bar{n},D} = \left(Z_D^R(g^2)\right)^{d_D(n+\bar{n})N_\tau} C^s_{n\bar{n},D} \tag{3.7}$$

for some colour symmetry state s.

3.2 Renormalising L through $Q\bar{Q}$ Free Energies

We will now give a description of the renormalisation procedure for the Polyakov loop in the fundamental representation on the lattice that uses the $Q\bar{Q}$ free energies. Afterwards,

we will extend this scheme to the adjoint representation, in which we have calculated the $Q\bar{Q}$-singlet free energies. For the sake of convenience we will suppress in this part mentioning the fundamental representation in all quantities where no ambiguity exists. The renormalisation procedure was first conjectured for SU(3) pure gauge theory [24] and can easily be extended to arbitrary $(n, \bar{n})$-point correlation functions of the thermal Wilson line and to the case of full QCD [29]. The basic idea is to renormalise the $Q\bar{Q}$ free energies calculated at small separations first. The renormalised Polyakov loop can then be obtained through the cluster property of the free energies.

The renormalised finite temperature $Q\bar{Q}$-singlet free energy $F^{1,R}_{Q\bar{Q}}(r,T)$ is given at short distances by the zero temperature heavy quark potential $V(r)$, because in this regime the dominating scale is the distance and not the temperature and thus the surrounding thermal medium does not change the properties of the $Q\bar{Q}$-system. Therefore the divergent self-energy contribution in the bare finite temperature $Q\bar{Q}$ free energy can be removed by *matching* it to the zero temperature heavy quark potential at small distances, which is known from lattice studies [26] and from perturbation theory [55, 26]. Thus, at small distances $r \ll 1/T$, we obtain the renormalisation group equation for the renormalised $Q\bar{Q}$-singlet free energy

$$T\frac{\mathrm{d}F^{1,R}_{Q\bar{Q}}(r,T)}{\mathrm{d}T} = 0. \tag{3.8}$$

On the lattice we use the smallest distance attainable for the matching procedure, which is given by $r_{\min} = (TN_\tau)^{-1}$. Therefore we have the matching prescription for the singlet free energy

$$F^{1,\mathrm{match}}_{Q\bar{Q}}(r_{\min},T)\Big|_{N_\tau} = V(r_{\min}), \tag{3.9}$$

where the temperature T is held fixed. It can be shown [24], that for temperatures $T \lesssim 20\,T_c$ the T-independence of the $Q\bar{Q}$-singlet free energies at small distances can be observed on lattices with a temporal extent of $N_\tau = 4$ and thus the matching prescription can be successfully applied. Since the $Q\bar{Q}$-singlet free energies show T-independence already at larger separations than the average or octet free energies, it is more convenient to use $F^1_{Q\bar{Q}}$ to extract the effective renormalisation constant, because lattices with smaller temporal extent can be employed, which limits the numerical effort. All $Q\bar{Q}$ free energies are, due to their symmetry under global $\mathbb{Z}(3)$ transformations, known to be independent from the volume they are calculated on [24] and therefore the thermodynamic limit is well behaved. This is crucial, since otherwise the effective renormalisation constants we are going to extract would be volume dependent. At fixed temperature T the continuum limit of the renormalised $Q\bar{Q}$-singlet free energy can now be obtained by

$$F^{1,R}_{Q\bar{Q}}(r,T) = \lim_{N_\tau\to\infty}\left(F^{1,\mathrm{match}}_{Q\bar{Q}}(r,T)\Big|_{N_\tau}\right), \tag{3.10}$$

which is equally well behaved. In fig. 3.1(left) we show the renormalised $Q\bar{Q}$-singlet free energies together with the $Q\bar{Q}$ potential at zero temperature. We observe, that

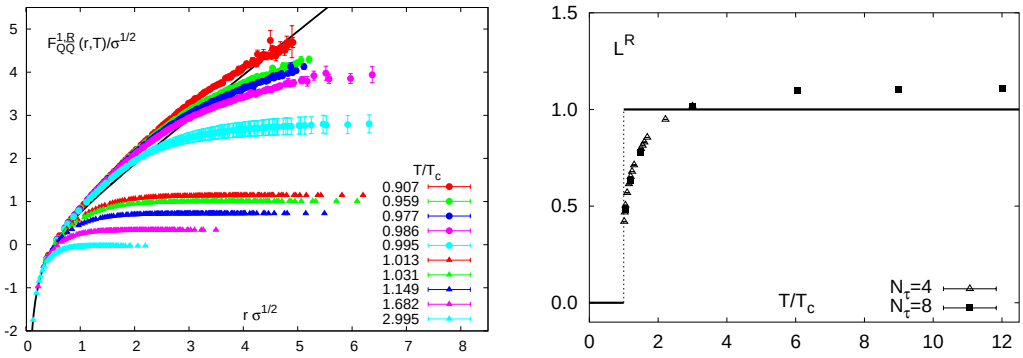

Figure 3.1: Left: $F^{1,R}_{Q\bar{Q}}(r,T)$ and the $Q\bar{Q}$ potential $V(r)$ at $T=0$ (black line). Right: L^R obtained from lattices with different temporal extend $N_\tau = 4, 8$.

for all temperatures the curves coincide with $V(r)$ at the smallest distances and depart smoothly with growing separations. Thus $F^{1,R}_{Q\bar{Q}}(r,T)$ is indeed T-independent at small r. For temperatures below T_c the singlet free energies overshoot the $T=0$ potential at intermediate distances, eventually becoming smaller than $V(r)$ again. This shows again the temperature dependence of the string tension for the confining singlet free energies. Above T_c screening is present and the $F^{1,R}_{Q\bar{Q}}(r,T)$ approach their asymptotic values, which are now well defined in the continuum limit.

Once the $Q\bar{Q}$-singlet free energy has been successfully renormalised at small distances, its large distance behaviour at finite temperature is fixed as well through the cluster property (2.59). We can now define the modulus of the expectation value of the Polyakov loop through

$$L^R(T) = \lim_{r\to\infty} \exp\left(-\frac{F^{1,R}_{Q\bar{Q}}(r,T)}{2T}\right). \tag{3.11}$$

In fig. 3.1(right) we show L^R obtained from the matching procedure from lattices with different temporal extent $N_\tau = 4, 8$ over the temperature. As the figure clearly shows, all systematic effects due to the presence of the lattice have been removed and L^R is a smooth function of T alone for temperatures $T > T_c$. Below T_c, L^R must clearly vanish, as the renormalised $Q\bar{Q}$ free energies rise forever. Therefore the renormalised expectation value of the Polyakov loop through the suggested renormalisation prescription is well behaved in the continuum limit. Furthermore, we see a finite jump in L^R at T_c, which is characteristic for a (weakly) first order phase transition. For higher temperatures $T \gtrsim 3T_c$ the renormalised Polyakov loop attains values larger than unity, where $L^R \to 1$ is its asymptotic high temperature perturbative value. Therefore we expect L^R to approach unity from above, when going to higher temperatures, which is also predicted by high-T perturbation theory [54].

We note here, that the renormalised free energies are, due to gauge freedom, only defined up to an additive normalisation of the zero temperature potential $V^c(r) = V(r) +$

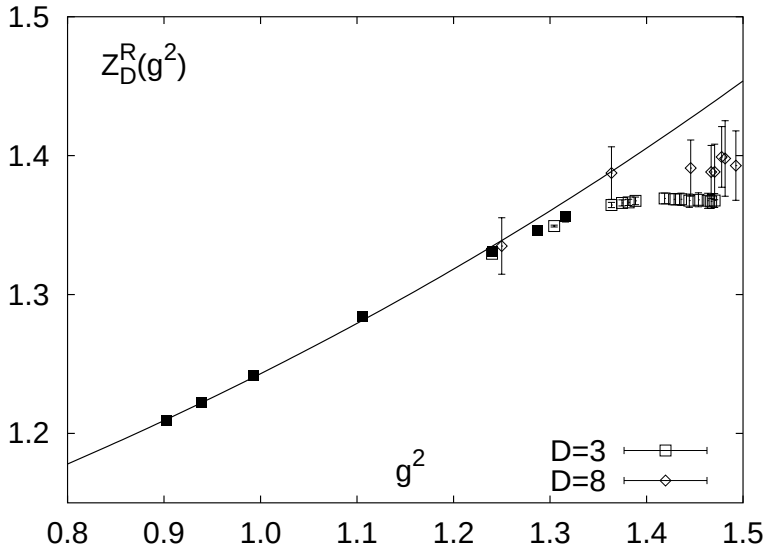

Figure 3.2: Effective renormalisation constant Z_D^R over g^2 from lattices with $N_\tau = 4$ (open symbols) and $N_\tau = 8$ (filled symbols) for $D = 3$ and $N_\tau = 4$ for $D = 8$. The solid black line is the result of the fit ansatz (3.14).

c. Consequently, L^R is only fixed up to a multiplicative term $e^{-c/2T}$, which nevertheless approaches unity exponentially when going to high temperatures.

In order to determine $Z^R(g^2)$ we could use the ratio $\left(L^R/\left\langle|L|\right\rangle\right)^{1/N_\tau}$, which is, however, only possible in the deconfined phase. It is more convenient to consider the shift in the $Q\bar{Q}$-singlet free energies due to the matching prescription

$$\delta F^1_{Q\bar{Q}}(T) = F^{1,R}_{Q\bar{Q}}(r,T) - F^1_{Q\bar{Q}}(r,T), \tag{3.12}$$

which is independent of r and can now be used to extract the effective renormalisation constants also below T_c through applying

$$Z^R(g^2) = \exp\left(-\frac{\delta F^1_{Q\bar{Q}}(T)}{2TN_\tau}\right), \tag{3.13}$$

which should not explicitly dependent on the temperature T, but only on the bare gauge coupling g. In fig. 3.2 we show the effective renormalisation constant Z^R from the fundamental representation over the square of the gauge coupling g from lattices with $N_\tau = 4, 8$. We see, that they are independent of the temporal lattice extent and collapse onto a common curve, indicating the dependence of Z^R on g^2 only. From the knowledge of the divergency structure of the Polyakov loop we can give a fit ansatz

$$Z^R(g^2) = \exp\left(g^2\frac{8}{3}Q^{(2)} + g^4 Q^{(4)}\right), \tag{3.14}$$

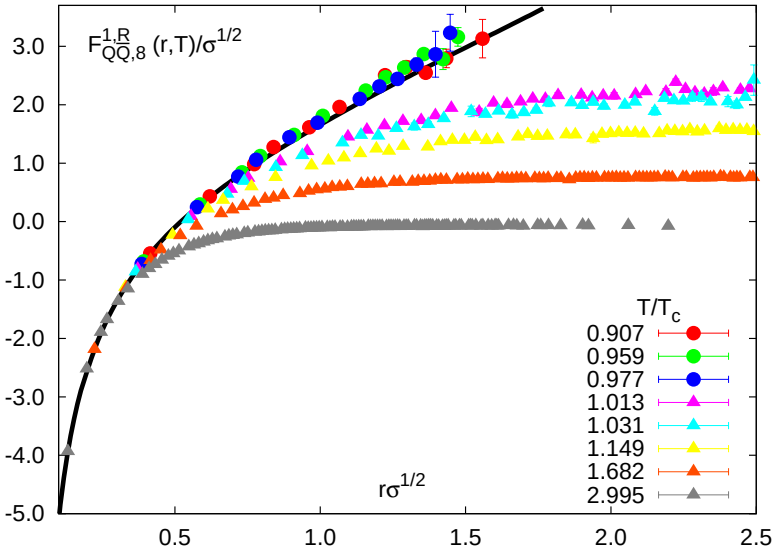

Figure 3.3: $F^{1,R}_{Q\bar{Q},8}$ renormalised to $V_8(r)$ (black line) from a $32^3 \times 4$ lattice.

which results in $Q^{(2)} = 0.0576(25)$ and $Q^{(4)} = 0.0639(68)$ from a best fit analysis in the range $0.9 - 1.33$ for g^2.

We are now in position to renormalise the adjoint singlet free energy $F^{1,R}_{Q\bar{Q},8}$ with the matching procedure outlined above. As the zero temperature potential to which the adjoint singlet free energies is going to be matched we choose according to Casimir scaling at zero temperature and small distances (2.102)

$$V_8(r) = d_8 V_3(r), \tag{3.15}$$

where $V_3(r)$ is the $T = 0$ potential in the fundamental representation [26]. The renormalised $F^{1,R}_{Q\bar{Q},8}$ are shown in fig. 3.3 together with $V_8(r)$. We observe $F^{1,R}_{Q\bar{Q},8}$ to coincide for small distances with V_8, departing smoothly to smaller values for $T > T_c$ and to higher ones for $T < T_c$. Thus, it is clear from fig. 3.3, that also $F^{1,R}_{Q\bar{Q},8}$ becomes temperature independent at small distances and the matching procedure can be successfully applied. We have determined the effective renormalisation constants $Z_8^R(g^2)$ using in analogy to (3.13) the expression

$$Z_8^R(g^2) = \exp\left(-\frac{\delta F^1_{Q\bar{Q},8}(T)}{2T d_8 N_\tau}\right) \tag{3.16}$$

for the adjoint singlet free energies. The results are shown in fig. 3.2. We observe Z_3^R and Z_8^R to agree within errors, though except for the highest temperature of $3T_c$ calculated ($g^2 = 1.25$), the Z_8^R are bigger than the Z_3^R. This may be due to insufficient statistics or may indicate a violation of the Casimir relation of the effective renormalisation constants at large couplings.

We conclude that the renormalisation of the adjoint $Q\bar{Q}$-singlet free energies through the matching procedure to the corresponding $T = 0$ potential is possible and gives reasonable results. We will discuss other properties of the adjoint singlet free energy like string breaking and the value of the renormalised adjoint Polyakov loop in chapter 4.

3.3 Renormalising L through N_τ Variation

We now discuss a new way on how to determine the value of the renormalised Polyakov loop in an arbitrary representation above T_c and the corresponding effective renormalisation constants Z_D^R from lattices with different temporal extent N_τ. For representations with vanishing triality, it can also be applied for temperatures below the critical temperature. The algorithm of the scheme is laid out in the box on page 44, see also fig. 3.4.

We choose the value of the renormalised Polyakov loop in some representation D, $L_D^R(T_{\text{start}})$, at T_{start}, which serves as a seed value for the procedure and has to be bigger than T_c for representations with non-vanishing triality. Computing the bare Polyakov loop $\langle|L_D|\rangle(g^2, N_{\tau,1})$ in that representation on the lattice, where we have to choose the gauge coupling g such, that $a(g)N_{\tau,1} = T_{\text{start}}^{-1}$ is fulfilled, we can extract the effective renormalisation constant $Z^R(g^2)$ by applying

$$Z_D^R(g^2) = \left(\frac{L_D^R(T_{\text{start}})}{\langle|L_D|\rangle(g^2, N_{\tau,1})}\right)^{1/d_D N_{\tau,1}} . \tag{3.17}$$

We now compute the bare Polyakov loop with the same gauge coupling g on a lattice with different temporal extent $N_{\tau,2} > N_{\tau,1}$, which is chosen such, that the corresponding temperature $T_1 = T_{\text{start}}\frac{N_{\tau,1}}{N_{\tau,2}}$ is still bigger than T_c for representations with non-vanishing triality. Since the effective renormalisation constant extracted through (3.17) depends only on g^2, we can apply it to $\langle|L_D|\rangle(g^2, N_{\tau,2})$ and obtain the renormalised Polyakov loop at T_1, $L_D^R(T_1)$. This procedure can be iterated with $L_D^R(T_1)$ acting as the new seed value. We thereby obtain a sequence of renormalised Polyakov loops in some representation D for several temperatures and a sequence of effective renormalisation constants for that representation for several gauge couplings g.

It is important to note at this point, that the $\langle|L_D|\rangle(g^2, N_{\tau,i})$ calculated on the lattices have to be in the thermodynamic limit. Otherwise the effective renormalisation constants would assume volume dependent values and consequently would be of no value at all. Therefore the iteration has to terminate at T_c at the latest for representations that show confinement below T_c, i. e. those with non-vanishing triality, because they vanish for $V \to \infty$ below T_c. For representations with $t = 0$, i. e. $D = 8, 10, 27$ as used in this work, the Polyakov loop stays finite for $V \to \infty$ also below T_c, as we have argued in 2.4.4, and are thus not subject to this constraint. We will discuss the thermodynamic limit for the Polyakov loop in the representations $D = 8, 10, 27$ at temperatures below T_c in chapter 4 and restrain our discussion here to the case $T > T_c$ for all representations.

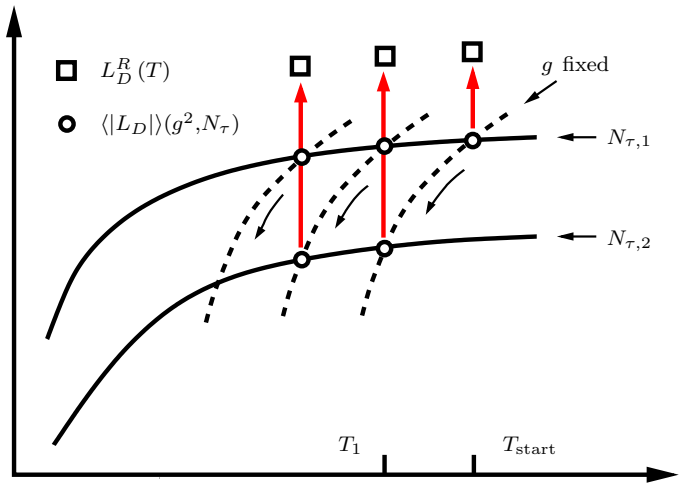

Figure 3.4: Renormalisation scheme using N_τ variation, resulting in a shark fin shaped saw tooth like path.

1. Choose some temperature T_{start}, where $T_{\text{start}} > T_c$ for representations with triality $t \neq 0$.
2. Choose $L_D^R(T_{\text{start}})$ as a seed value.
3. Choose a lattice with temporal extent $N_{\tau,1}$.
4. Determine gauge coupling g such that $T_{\text{start}} = 1/(a(g)N_{\tau,1})$.
5. Compute $\langle|L_D|\rangle(g^2, N_{\tau,1})$ from the lattice.
6. Determine $Z_D^R(g^2)$ by employing (3.17).
7. Choose a lattice with temporal extent $N_{\tau,2}$, where $N_{\tau,2} > N_{\tau,1}$, such that $T_1 = T_{\text{start}}\frac{N_{\tau,1}}{N_{\tau,2}}$ obeys $T_1 > T_c$ for representations with triality $t \neq 0$.
8. Compute $\langle|L_D|\rangle(g^2, N_{\tau,2})$ from the lattice.
9. Determine $L_D^R(T_1) = Z^R(g^2)^{N_{\tau,2}}\ \langle|L_D|\rangle(g^2, N_{\tau,2})$.
10. Jump to 3 with $T_{\text{start}} = T_1$ and $L_D^R(T_1)$ as seed value.

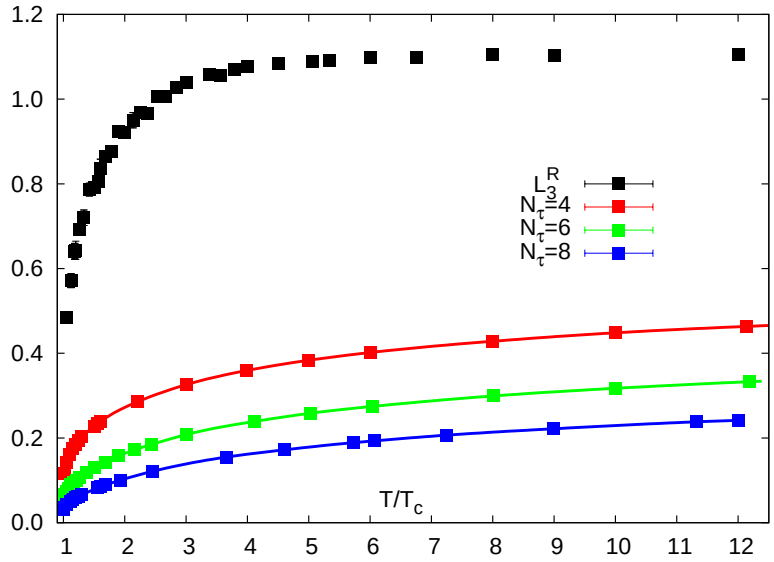

Figure 3.5: Bare Polyakov loops in the fundamental representation from lattices $32^3 \times N_\tau$ with $N_\tau = 4, 6, 8$, their cubic spline interpolation and the resulting L_3^R from the N_τ-variation method.

We now come to the application of this method to our data. We have calculated the Polyakov loop for all irreducible representations $D \leq 27$ on lattices $32^3 \times N_\tau$ with $N_\tau = 4, 6, 8$. The highest temperature at our disposal was $T_{\text{start}} = 12T_c$. As we will show in chapter 4.2, Casimir scaling is realised for the bare Polyakov loop $\langle |L_D| \rangle$ for all representations $D \leq 27$ at this temperature. Therefore we set

$$L_D^R(T_{\text{start}}) = \left(L_3^R(T_{\text{start}})\right)^{d_D} . \tag{3.18}$$

The renormalisation constants Z_D^R are therefore obtained independently of Z_3^R.

As seed value for the renormalised Polyakov loop in the fundamental representation we use $L_3^R(T_{\text{start}}) = 1.106(15)$, which has been obtained from the matching procedure of the fundamental $Q\bar{Q}$-singlet free energy at T_{start}. We will address the issue of different seed values below. In order to avoid simulations with a large number of different gauge couplings matching the constraints appearing through the choice of the $N_{\tau,i}$, we have used a cubic spline to interpolate between the data obtained from simulations roughly equally distributed in T. The values of the cubic spline have then be employed to compute $\langle |L_D| \rangle (g^2, N_{\tau,i})$ for some g. The result of the interpolation is shown in fig. 3.5. For the application of the renormalisation scheme to our data we have used the combinations $(4, 6)$ and $(6, 8)$ as pairs of temporal extent $(N_{\tau,1}, N_{\tau,2})$. Thereby we obtain more values for the renormalised Polyakov loop and the effective renormalisation constant in the given temperature interval $(T_c, 12T_c]$ than we would have with the combination $(4, 8)$.

The results for $Z_D^R(g^2)$ and the renormalised Polyakov loop L_D^R for $D = 3, 6, 8, 10, 15$ obtained with this method are shown in fig. 3.6(top). The errors are obtained from

a jackknife analysis. In this plot we have also included the results from the matching procedure of the fundamental and adjoint $Q\bar{Q}$-singlet free energy done in chapter 3.2. The plot clearly shows that all Z_D^R extracted by the N_τ-variation method collapse onto a single curve, which follows the result of the fit ansatz (3.14) for gauge couplings $g^2 \lesssim 1.35$ and then assumes a nearly constant value of $\sim 1.35 - 1.4$. Moreover, we find a very good agreement with the renormalisation constants obtained with the matching procedure of the fundamental and adjoint $Q\bar{Q}$-singlet free energies for all gauge couplings g calculated in this work.

For the representations $D = 10, 15$, we had to terminate the iteration process at $2T_c$, because below this temperature volume effects became visible in $\langle |L_D| \rangle$. For higher representations $D = 15', 24, 27$ this was already the case at the highest temperature of $12T_c$ used here, and thus we refrain from discussing them. The volume dependence of $\langle |L_D| \rangle$ will be investigated in detail in chapter 4 for the case $T < T_c$, but the findings are also applicable above T_c. We just note here, that this V-dependence can be explained by the fact that the distribution function of L_D computed on different lattice configurations stretches out into the negative part of the real axis, if its expectation value is small. This leads to a deviation of $\langle |L_D| \rangle$ to higher values, where the size of the deviation depends on the lattice volume used. This problem can be overcome partly by using $\langle L_D \rangle$ instead of $\langle |L_D| \rangle$ in the renormalisation method. For large temperatures, both observables agree, and for $D = 3, 6, 8$ we find agreement of $\langle L_D \rangle$ and $\langle |L_D| \rangle$ down to T_c on all volumes used in this work. For $D = 10, 15$ the errors become too large for a meaningful application of the N_τ-variation method at temperatures lower than $2T_c$. For $D = 15', 24, 27$ the values for $\langle L_D \rangle$ from the $N_\tau = 6, 8$ lattices was too noisy for all $T \leq 12T_c$. To sum up, we find for $D = 3, 6, 8, 10, 15$ that the simple relation

$$Z_D^R(g^2) = Z_3^R(g^2) \tag{3.19}$$

holds for temperatures above T_c for $D = 3, 6, 8$ and for $T > 2T_c$ for $D = 10, 15$. The good agreement of the two renormalisation methods shows that the renormalisation constants indeed only depend on the bare coupling and that both methods are equivalent. Furthermore the renormalisation constants in different representations agree within the present accuracy, indicating that the Casimir scaling relation (3.19) holds in the coupling range analysed here.

In fig. 3.6(bottom) we show the renormalised Polyakov loops obtained from the N_τ-variation method for $D = 3, 6, 8, 10, 15$ over the temperature. We have again included the results from the matching procedure of the fundamental and adjoint $Q\bar{Q}$-singlet free energy discussed in chapter 3.2 in the plot. For all D, L_D^R shows qualitatively similar behaviour, i. e. starting from small values just above T_c, where the value is smaller the larger $C(D)$, assuming $L_D^R = 1$ at $\sim 2.5T_c$ and approaching a constant value, which is larger the larger $C(D)$. These facts already hint at a connection of L_D^R to the Casimir. We will discuss Casimir scaling for the Polyakov loop in chapter 4.2. Since Casimir scaling is realised up to 2-loop order in high temperature perturbation theory [5], all L_D^R have to approach unity for $T \to \infty$, because L_3^R does [54]. Fig. 3.6(bottom) makes clear, that for all D this value is approached from above.

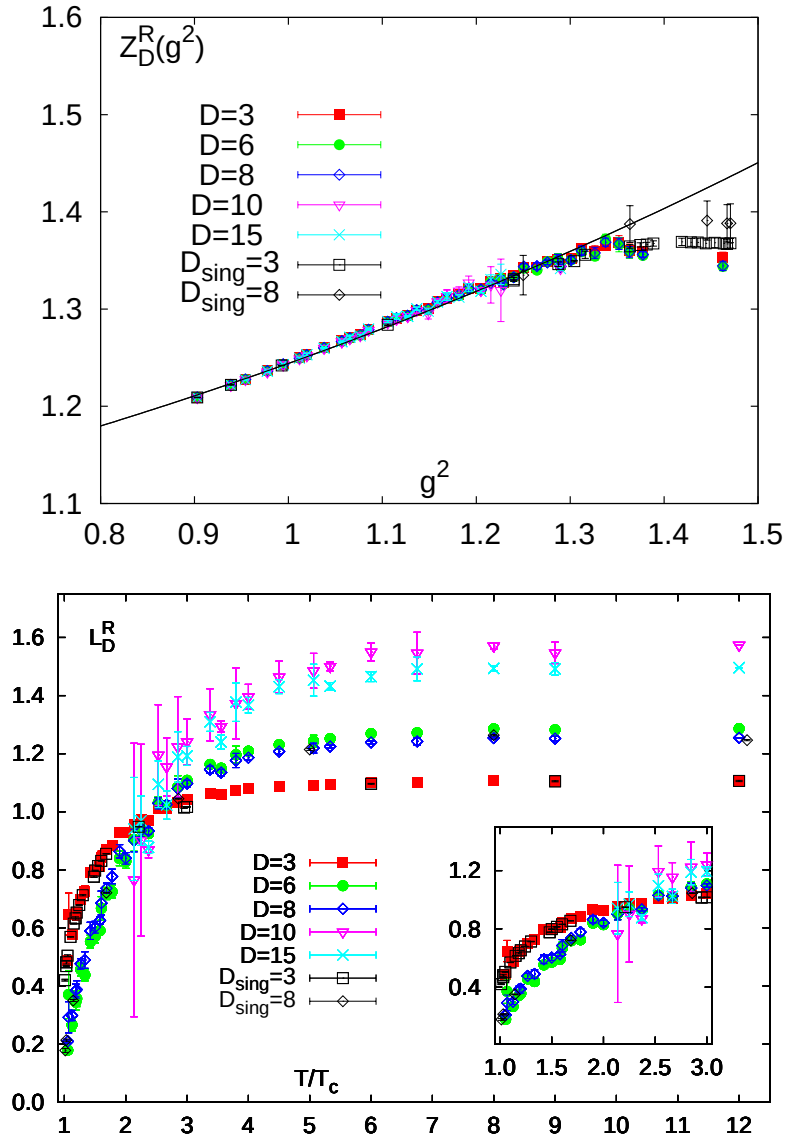

Figure 3.6: Top: Z_D^R for $D = 3, 6, 8, 10, 15$ obtained with the N_τ variation method and from lattices $32^3 \times N_\tau$ with $N_\tau = 4, 6, 8$ and Z_D^R from the matching procedure of the fundamental and adjoint $Q\bar{Q}$-singlet free energy (D_{sing}). The black line indicates the result of the fit ansatz (3.14). Bottom: resulting renormalised Polyakov loop L_D^R from both methods. The inset shows the region $T_c - 3T_c$.

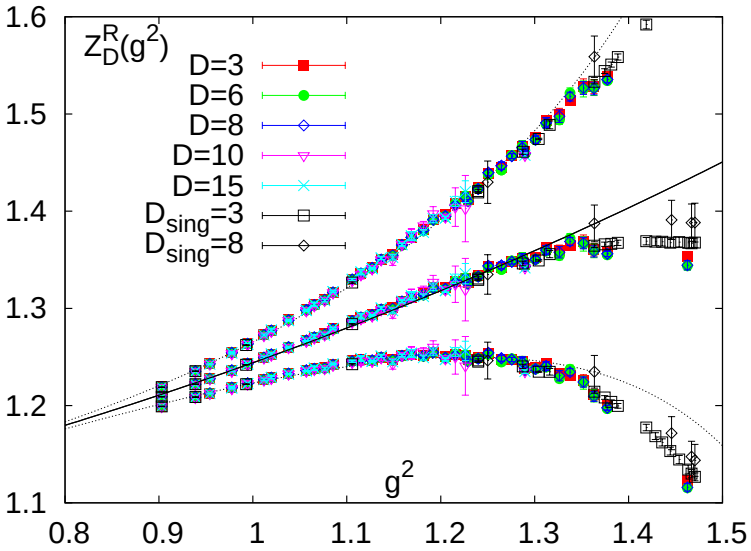

Figure 3.7: The same as fig. 3.6(top) for different seed values in the N_τ variation method and $T = 0$ potential $V_c(r)$ from the matching procedure of the fundamental and adjoint $Q\bar{Q}$-singlet free energy (D_{sing}). The fit results of the ansatz (3.14) have been changed accordingly. See text.

Any renormalisation procedure is only fixed up to a multiplicative constant, which translates into a multiplicative constant for both Z_D^R and L_D^R and thus to a change of the seed value in our method. In order to be consistent, we must still have, that

$$\lim_{g^2 \to 0} Z^R(g^2) = Z^R_{\text{pert}}(g^2) \tag{3.20}$$

is fulfilled if we change the seed value, where $Z^R_{\text{pert}}(g^2)$ is the perturbative renormalisation constant at weak coupling, given by the expansion of (3.14) at small g^2, i. e. $Z^R_{\text{pert}}(g^2) = 1 + g^2 \frac{8}{3} Q^{(2)} + \ldots$. We therefore investigate now the use of different seed values $L_3^R(T_{\text{start}})$ for the N_τ-variation method, which is also connected to the high temperature limit of the Polyakov loop. In fig. 3.7 we show the resulting effective renormalisation constants for different seed values. This have been obtained by applying the matching procedure to the fundamental $Q\bar{Q}$-singlet free energies to different $T = 0$ potentials

$$V^c(r) = V(r) + c, \qquad c\sqrt{\sigma} = \begin{cases} -1 & : \text{ upper branch} \\ 0 & : \text{ middle branch} \\ +1 & : \text{ lower branch} \end{cases}, \tag{3.21}$$

which is possible due to the gauge freedom of the potential. The renormalised Polyakov loop we used as the seed value then changes according to

$$L_3^{R,c} = L_3^R \, e^{-\frac{c}{2T}}. \tag{3.22}$$

The corresponding effective renormalisation constants then become

$$Z_3^{R,c} = Z_3^R \exp\left(-\frac{c\,a(g^2)}{2}\right), \tag{3.23}$$

which leaves the perturbative limit $g^2 \to 0$ unchanged. Fig. 3.7 shows that the renormalisation constants indeed approach a common value for g^2 for all three seed values used. It is clear from (3.22), that the high temperature limit of the Polyakov loop in all representation is not affected by the change of the seed value, as it should be.

3.4 Other Renormalisation Procedures for the Polyakov loop

We now want to discuss the renormalisation procedure for the Polyakov loop proposed in [56], that assumes the effective renormalisation constant to dependent explicitly and solely on the temperature, i. e. $z_D^R(T)$, and therefore extracts them in a different way. To be more precise, [56] proposes a multiplicative renormalisation scheme for the bare Polyakov loop in an irreducible representation D,

$$L_D^R(T) = \frac{1}{z_D^R(T)} \langle |L_D| \rangle (T). \tag{3.24}$$

The renormalisation constant is defined by

$$z_D^R(T) = \exp\left(\frac{-m_D^{\mathrm{div}}}{T}\right) \quad \text{and} \quad m_D^{\mathrm{div}} = \frac{f_D^{\mathrm{div}}}{a}, \tag{3.25}$$

where f_D^{div} is some proportionality constant and a is the lattice spacing. In order to extract $z_D^R(T)$, it is assumed that the logarithm of the bare Polyakov loop can be written as a power series in $1/N_\tau$,

$$-\ln(\langle |L_D| \rangle) = f_D^{\mathrm{div}} N_\tau + f_D^{\mathrm{ren}} + f_D^{\mathrm{lat}} \frac{1}{N_\tau}, \tag{3.26}$$

where f_D^{lat} is a finite lattice spacing correction and the renormalised Polyakov loop is obtained by

$$L_D^R = \exp(-f_D^{\mathrm{ren}}). \tag{3.27}$$

The main point is, that the f_D^i with $i \in \{\mathrm{div}, \mathrm{ren}, \mathrm{lat}\}$ are functions of the physical temperature only. The f_D^i are obtained by calculating bare Polyakov loops at fixed temperature but varying temporal lattice extent N_τ. It was found in [56], that $f_D^{\mathrm{lat}} \approx 0$, such that a linear fit to $-\ln(\langle L_D \rangle)$ suffices to extract f_D^{div} and f_D^{ren}. This procedure bears some resemblance to our N_τ variation method investigated in chapter 3.3, with the important difference that our effective renormalisation constants do *not* depend on the physical temperature but only on the bare gauge coupling g.

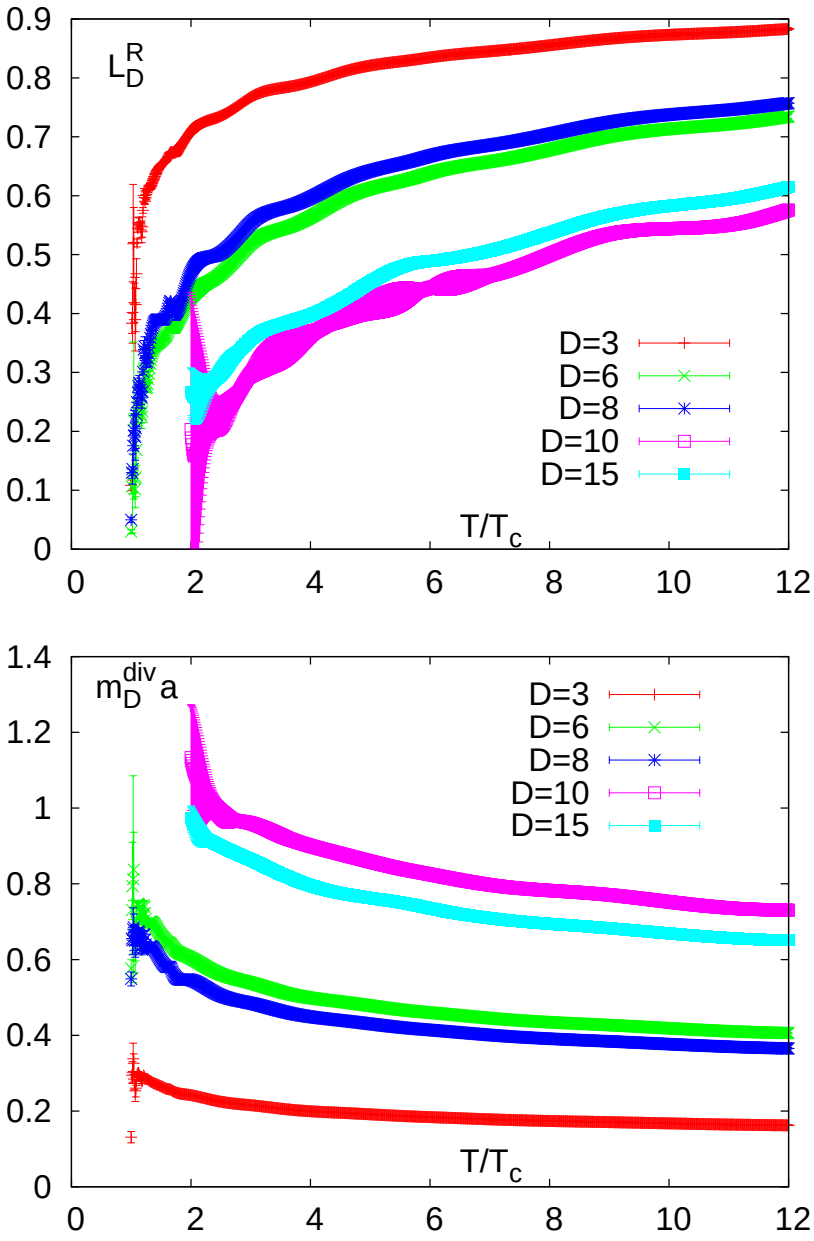

Figure 3.8: Top: Renormalised Polyakov loops for $D = 3, 6, 8, 10, 15$ above T_c obtained with the method proposed in [56] from our $32^3 \times N_\tau$ lattices with $N_\tau = 4, 6, 8$ pure gauge data. Bottom: Divergent mass m_D^{div} extracted by a linear fit with (3.26).

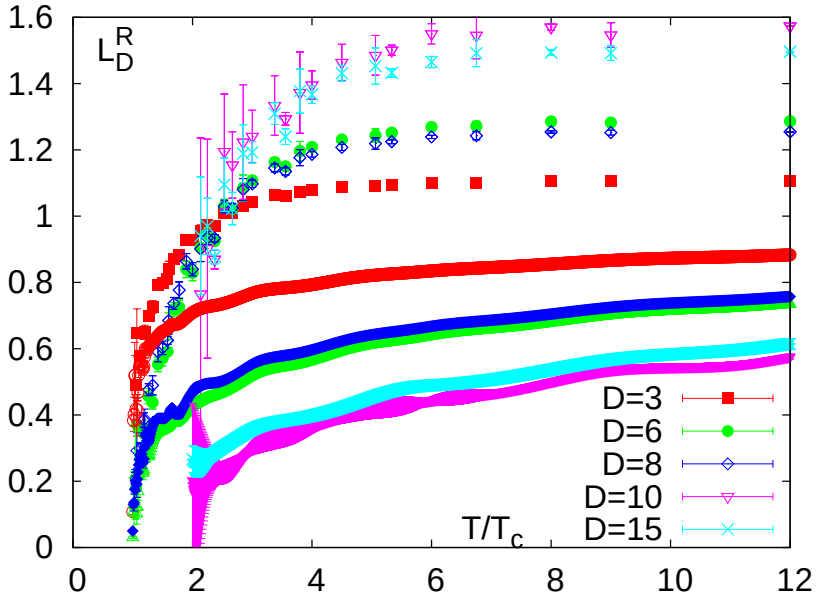

Figure 3.9: Comparison with the results for the renormalised Polyakov loops obtained with the N_τ-variation method in chapter 3.3.

We have performed the renormalisation procedure for the Polyakov loop in some irreducible representation proposed in [56] with our pure gauge data obtained from $32^3 \times N_\tau$ lattices with $N_\tau = 4, 6, 8$. We will show in chapter 4.3.2, that for small lattice volumes a severe volume dependence persists for small values of $\langle |L_D| \rangle$, which hampers the investigation of this quantity in the deconfined phase near T_c. Therefore we used $\langle L_D \rangle$ instead of $\langle |L_D| \rangle$ for the procedure. We have performed a best fit analysis to $-\ln(\langle L_D \rangle)$ with (3.26) at fixed temperature, where we neglect the f_D^{lat} term. The resulting renormalised Polyakov loops L_D^R can then be obtained by employing (3.27). In fig. 3.8(top) we show the resulting renormalised Polyakov loops for representations $D = 3, 6, 8, 10, 15$ in the temperature range $T_c - 12\,T_c$ and the divergent mass am_D^{div} in fig. 3.8(bottom). We observe L_D^R to rise strictly monotonic and staying smaller than unity for all $T < 12\,T_c$. Casimir scaling in L_D^R is preserved. High temperature perturbation theory requires $am_D^{\text{div}} \to 0$ when $T \to \infty$, which is also visible in fig. 3.8(bottom). The undulating behaviour of L_D^R and am_D^{div} especially near T_c is most probably an artifact of the cubic spline interpolation we applied to the bare Polyakov loops (see chapter 3.3).

In fig. 3.9 we compare the results for the renormalised Polyakov loops obtained with the method of [56] and the N_τ-variation method of chapter 3.3. It is clear, that the results from both methods are not connected by a multiplicative constant $e^{-c/2T}$ in the spirit of (3.22), since the L_D^R from the N_τ-variation become unity at $T \gtrsim 2.8\,T_c$, whereas the L_D^R from the method of [56] do not coincide at this temperature. A dependence of c on the representation D is prevented by Casimir scaling. Therefore both methods produce renormalised Polyakov loops that are *not equivalent* starting from the same bare

Polyakov loops. As was made clear in [53], the effective renormalisation constants for the Polyakov loop should depend on the bare gauge coupling g only and *not* on the physical temperature T.

4 Results for higher Representations of the Polyakov Loop

Having at hand a proper renormalisation procedures for Polyakov loops and the free energy in all representations, we are now able to embark on the investigation of the properties of the Polyakov loop and the free energy in higher representations in a physically meaningful way. Below the critical temperature we first have to study the thermodynamic limit of the Polyakov loops, before we can extract the binding energy of the gluelump and the string breaking distance from L_8^R.

4.1 $Q\bar{Q}$ Free Energies

Parallel to (2.102) we want to check Casimir scaling for the $Q\bar{Q}$ free energies at finite temperature,

$$F^{s,R}_{n\bar{n},D_2}(r,T) = d(D_2,D_1)F^{s,R}_{n\bar{n},D_1}(r,T), \tag{4.1}$$

where s is the colour symmetry state. We know already from lattice calculations at $T=0$ and from perturbative calculations in the vacuum and at high temperature, that Casimir scaling is realised to a reasonable degree in these regimes [4, 5]. Therefore (4.1) must be valid for $r\Lambda_{\mathrm{QCD}} \ll 1$ and $T \gg T_c$. For intermediate distances and temperatures not too far from the deconfinement phase transition, the situation is not clear.

Let us start with the case of the $Q\bar{Q}$-singlet free energy, which we have calculated in the fundamental and the adjoint representation on gauge configurations fixed to Coulomb gauge. The renormalisation for both of them was carried out in chapter 3.2. In fig. 4.1(top) we compare $F^{1,R}_{Q\bar{Q},8}$ with $F^{1,R}_{Q\bar{Q},3}$, where both free energies have been divided by their Casimir. If the Casimir scaling hypothesis for the singlet free energies (4.1) holds, both curves should coincide. We see that this is indeed the case for the highest two temperatures over the entire distance interval, whereas at lower temperatures deviations of $F^{1,R}_{Q\bar{Q},8}/C(8)$ to lower values become visible at large separations.

In order to get a more quantitative measure of how well Casimir scaling is realised, we have calculated the ratio

$$R_{3,8}(r,T) = d_8 \frac{F^{1,R}_{Q\bar{Q},3}}{F^{1,R}_{Q\bar{Q},8}}, \tag{4.2}$$

which should be unity, if (4.1) holds. The result is shown in fig. 4.1(bottom). We observe

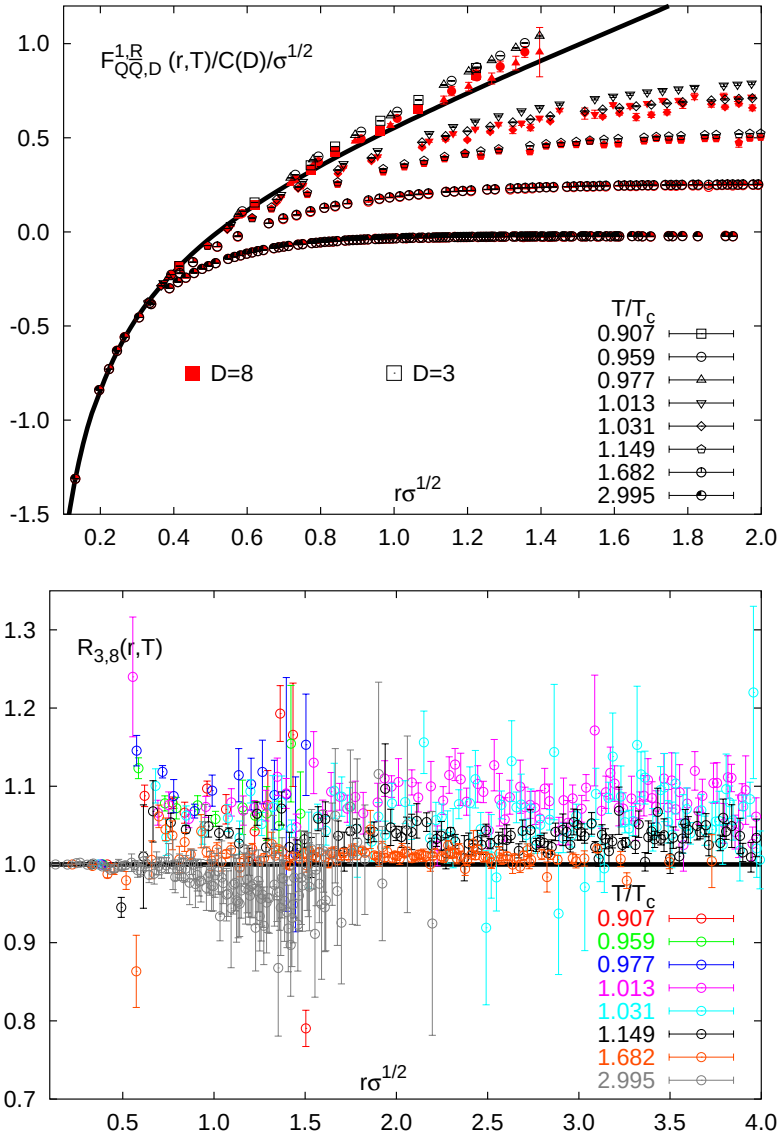

Figure 4.1: Top: $F^{1,R}_{Q\bar{Q},3}$ and $F^{1,R}_{Q\bar{Q},8}$ and $V_3(r)$ (black line) normalised by their Casimir $C(D)$ from a $32^3 \times 4$ lattice. Bottom: $R_{3,8}(r,T)$ of this free energies. See text.

$R_{3,8}$ to be one within errors for the highest two temperatures calculated. For $T/T_c = 1.149$ we see a deviation of 5 % and for the even smaller temperatures a value of slightly below 10 % is observed.

Thus we conclude that Casimir scaling is realised for $F^{1,R}_{Q\bar{Q},D}$ with $D = 3, 8$ for all separations r at temperatures $T/T_c \geq 1.682$ within errors. For lower temperatures above T_c and for all temperatures below T_c considered here, deviations occur already at small distances at the level of 5-10 %.

We now turn to the colour averaged $Q\bar{Q}$-free energies. Since the corresponding correlators can be obtained without a costly gauge fixing, we were able to calculate $F_{Q\bar{Q},D}(r,T)$ for representations $D = 3, 6, 8$ in the temperature range 0.9-3 T_c on $32^3 \times 4$ lattices. If Casimir scaling (4.1) holds for the average free energies, the curves should coincide with those of the fundamental representation.

Below T_c we show the renormalised average free energies for the three lowest temperatures divided by their Casimir in fig. 4.2. The renormalisation constants employed are the $(Z_3^R(g^2))^{d_D N_\tau}$, according to the renormalisation procedure described in chapter 3.2. Thus for the smallest distances all curves coincide as a consequence of the renormalisation procedure. However, for all $T < T_c$ and representations $D = 6, 8$ deviations to smaller values start to show up quite early, i. e. for separations $rT \gtrsim 0.8$ for $D = 6$ and $rT \gtrsim 0.6$ for $D = 8$, respectively. This effect is more pronounced for the adjoint average free energy than for the sextet. The effect of string breaking sets in at larger distances shown here and will be discussed in chapter 4.4.

Above T_c we show $\Delta F_{Q\bar{Q},D}$ divided by their Casimir for the same representations in fig. 4.3. We observe *screening* to take place in both higher representations. The curves for both $D = 6$ and $D = 8$ deviate to smaller values compared to the fundamental case. We find that the ordering

$$\frac{\Delta F_{Q\bar{Q},6}(r,T)}{C(6)} < \frac{\Delta F_{Q\bar{Q},8}(r,T)}{C(8)} < \frac{\Delta F_{Q\bar{Q},3}(r,T)}{C(3)} < 0, \qquad T > T_c \tag{4.3}$$

holds throughout the entire distance interval.

Thus, we conclude, that Casimir scaling is clearly *violated* for the average $Q\bar{Q}$ free energies in the temperature range $0.9 - 3\,\mathrm{T_c}$ for the fundamental, sextet and adjoint representations.

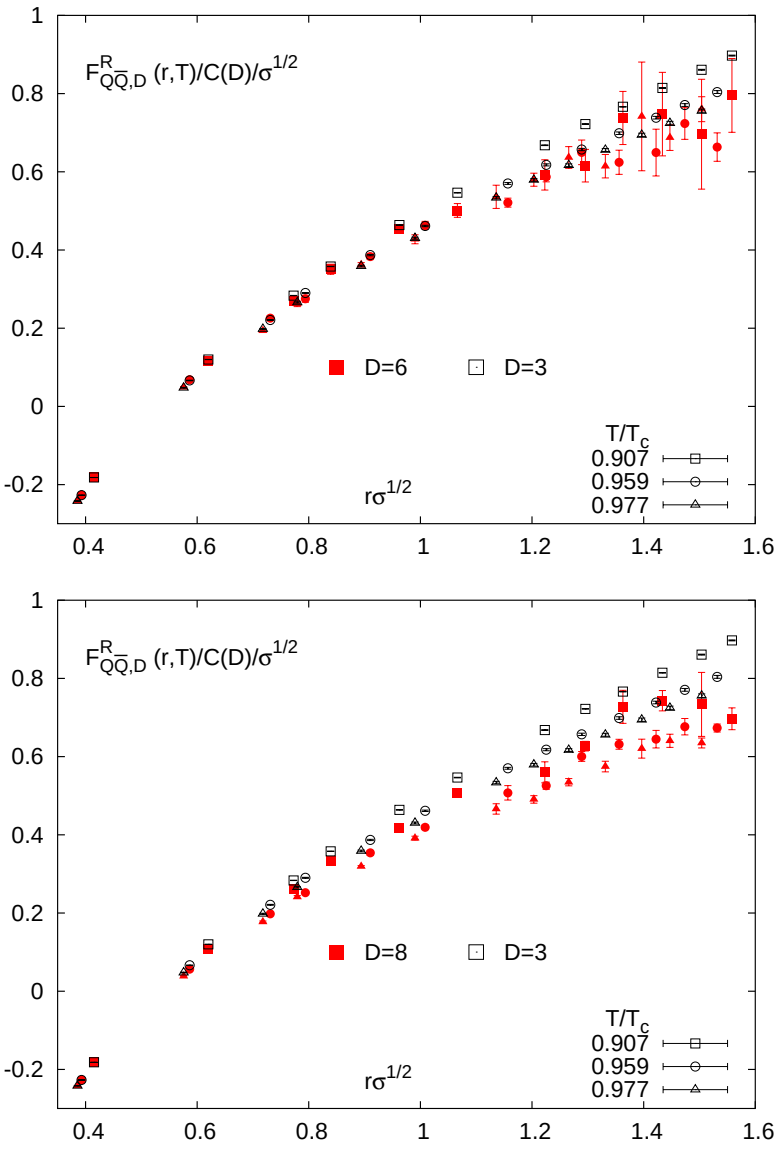

Figure 4.2: Average free energies for $D = 6$ (top) and $D = 8$ (bottom) compared to the fundamental free energy below T_c from a $32^3 \times 4$ lattice.

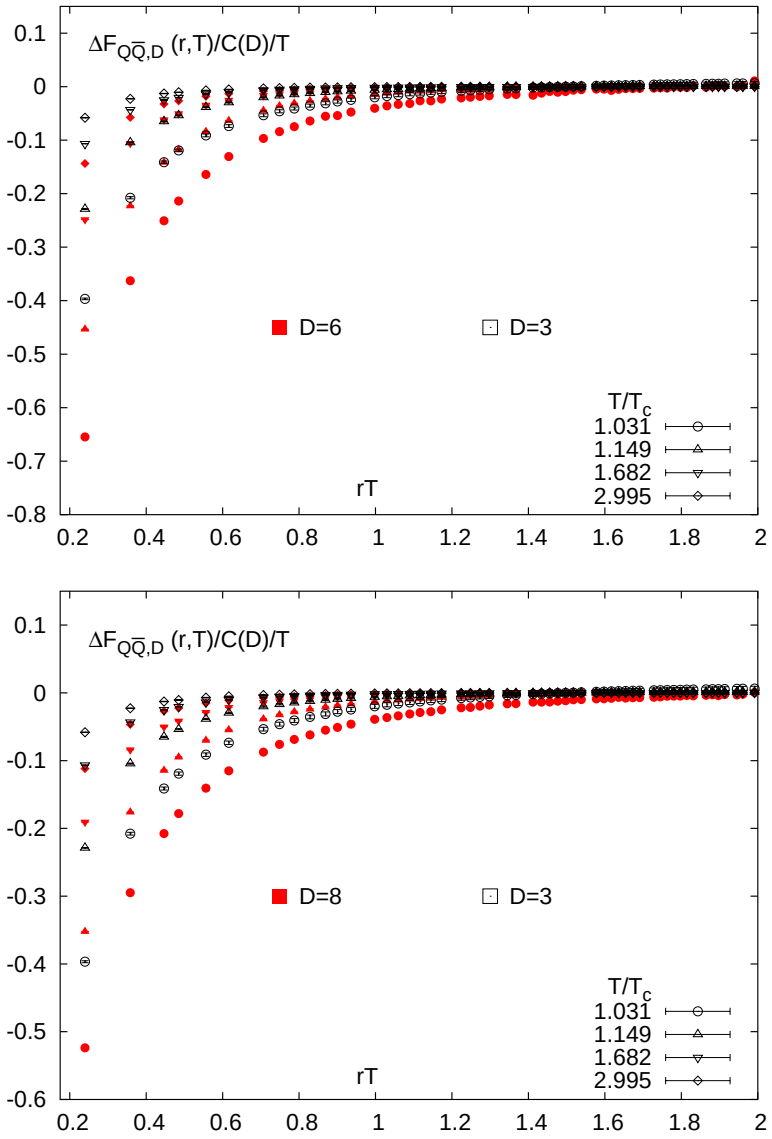

Figure 4.3: Average free energies for $D = 6$ (top) and $D = 8$ (bottom) compared to the fundamental free energy above T_c from a $32^3 \times 4$ lattice.

4.2 Casimir scaling for the Polyakov loop above T_c

Let us now discuss the question of Casimir scaling for the Polyakov loop above T_c. If Casimir scaling holds, we have the relation for the renormalised Polyakov loop in different representations D,

$$L_D^R(T) = \left(L_3^R(T)\right)^{d_D}, \tag{4.4}$$

for some temperature $T > T_c$. As we have already pointed out, this is true up to 2-loop order in high-temperature perturbation theory [5]. The effective renormalisation constants Z_D^R agree with each other for $D = 3, 6, 8, 10, 15$ for temperatures down to close to T_c, as we have shown in chapter 3.3. The missing ingredient for (4.4) to hold, is to show that this relation is also valid for the bare Polyakov loops $\langle |L_D| \rangle$. Therefore we display $\langle L_D \rangle^{1/d_D}$, which should be independent of D if Casimir scaling is realised, for temperatures above T_c from a $32^3 \times 4$ lattice in fig. 4.4. To minimise finite volume effects we follow the discussion given in chapter 3.3 and use $\langle L \rangle$ rather than $\langle |L| \rangle$. Furthermore we will not use the data for temperatures smaller than $1.5T_c$ for the representation $D = 15'$. We observed that all data collapse onto a common curve for all temperatures considered here. Thus Casimir scaling is realised for the bare Polyakov loop above T_c for representations $D = 3, 6, 8, 10, 15, 24, 27$ and above $1.5T_c$ also for $D = 15'$. Together with the results for the effective renormalisation constants in 3.3, we conclude, that Casimir scaling is realised for the renormalised Polyakov loop, (4.4), for temperatures $(T_c, 12T_c]$ for $D = 3, 6, 8$ and temperatures $(2T_c, 12T_c]$ for $D = 10, 15$. We note, that Casimir scaling for the renormalised Polyakov loop for $D = 10, 15$ could not be shown because the results for the effective renormalisation constants for this values of D are restricted to the temperature range $T > 2T_c$. Moreover, we were not able to obtain Z_D^R for $D = 15', 24, 27$, so that we can not make a statement on whether Casimir scaling is realised for the renormalised Polyakov loop in these representations.

4.3 Polyakov loops below T_c

We now investigate the behaviour of the Polyakov loop in different representations below T_c. To this end, we first study L_D at strong coupling ($\beta = 0$). Afterwards, we look at the volume dependence of $\langle L_D \rangle$ and $\langle |L_D| \rangle$ below T_c and compute the infinite volume, renormalised adjoint Polyakov loop for $T < T_c$. In connection with this, we can identify the binding energy of the gluelump and determine the string breaking distance for the adjoint $Q\bar{Q}$-singlet free energy.

4.3.1 Strong coupling

Random SU(3) gauge links U_4 for computing L_D at strong coupling ($\beta = 0$) can be diagonalised to assume the form

$$U_4 = \mathrm{diag}\left(e^{i\phi_1}, e^{i\phi_2}, e^{-i(\phi_1+\phi_2)}\right), \tag{4.5}$$

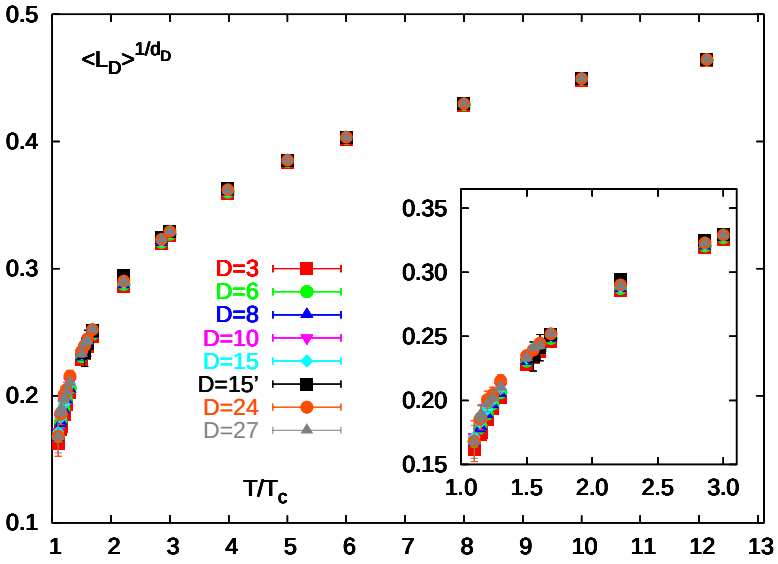

Figure 4.4: Testing Casimir scaling for the bare Polyakov loop. $\langle L_D \rangle^{1/d_D}$ from a $32^3 \times 4$ lattice for all D. The inset shows the region $T_c - 3T_c$.

where

$$0 \leq \phi_1, \phi_2, \quad \phi_1 < \phi_2, \quad \phi_2 < (-\phi_1 - \phi_2) \bmod 2\pi. \tag{4.6}$$

A simpler numerical implementation can be achieved by drawing $\phi_1, \phi_2 \in [0, 2\pi)$ uniformly, which introduces a six-fold overcounting of the fundamental domain (4.6). Nevertheless, due to the gauge symmetry of the system, the expectation values of L_D will be unaffected by this [57]. For reasons that will become apparent in a moment, we discuss the results of our lattice calculations in terms of the unnormalised Polyakov loop l. We have calculated $\langle |l_D| \rangle$ at $\beta = 0$ for volumes with spatial extent $N_\sigma = 16, 24, 32, 48, 64, 96$. The results of the calculations are shown in fig. 4.5 and 4.6. While $\langle |l_D| \rangle$ is finite on finite volumes, it vanishes in the thermodynamic limit when the triality of the representation D does not vanish, $t \neq 0$, i. e. for representations $D = 3, 6, 15, 15', 24$. The volume dependence of $\langle |l_D| \rangle$ for this representations can be understood in terms of a random walk model [58], which predicts

$$\langle |l_D| \rangle \sim \frac{1}{\sqrt{V}} \tag{4.7}$$

and is confirmed by the data displayed in fig. 4.5. The expectation value $\langle l_D \rangle$ for the representations with vanishing triality, i. e. $D = 8, 10, 27$ in this work, are constant with respect to V and therefore obviously finite in the thermodynamic limit. They assume the integer values (see fig. 4.6)

$$\langle l_D \rangle = \begin{cases} 2 & : \quad D = 8 \\ 1 & : \quad D = 10 \\ 3 & : \quad D = 27 \end{cases}, \tag{4.8}$$

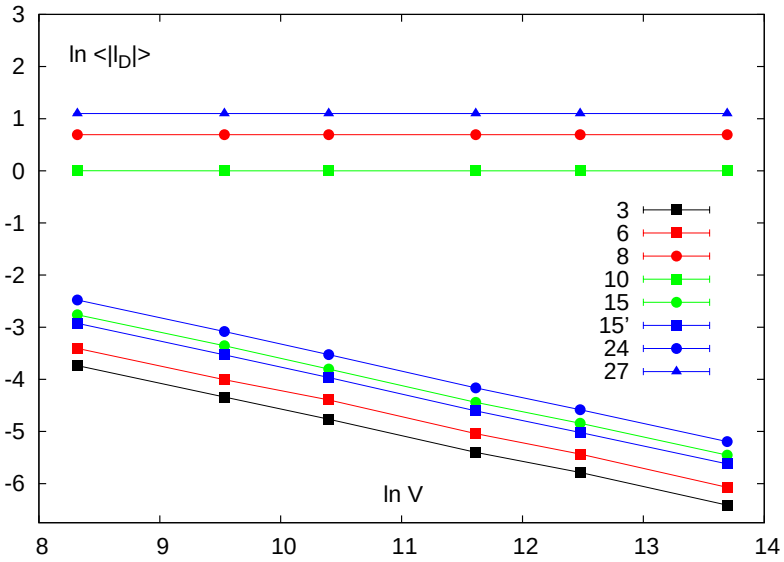

Figure 4.5: Double log plot of $\langle |l_D| \rangle$ over the volume V.

which would not have been so easily visible if we had used the normalisation version of the Polyakov loop. We note, that even stronger than (4.8), the integer values are assumed for the average over one configuration, $[l_D]$.

These findings can be understood as follows. The Polyakov loop in the fundamental representation l_3 is just the unnormalised trace of the random matrix (4.5). Therefore we have

$$l_3 = \operatorname{tr} U = e^{i\phi_1} + e^{i\phi_2} + e^{-i(\phi_1+\phi_2)}, \tag{4.9}$$

where $\phi_i \in [0, 2\pi)$ with $i = 1, 2$ uniformly distributed. We remind that $\operatorname{tr} \mathbb{1}_{D\times D} = D$ has been used here. We now want to consider the expectation value of terms

$$[l_3(\mathbf{x})^r l_{\overline{3}}(\mathbf{x})^s] \tag{4.10}$$

where $r, s \in \mathbb{N}$ and $[\cdot]$ denotes the lattice average from one configuration. It is clear from the remarks above, that the only combinations of r, s that survive the thermodynamic limit are those where $(r - s) \bmod 3 = 0$, i. e. those with vanishing triality. Plugging now (4.9) into (4.10) leads to sums of terms $be^{i\alpha}$, where $\alpha = \sum_i a_i\phi_i$ with $a_i, b \in \mathbb{Z}$ and the b are binominal coefficients. The α assumes in general non-uniform distributions in $[2\pi \min(0, a_i), 2\pi \max(a_i))$. If $a_i = 0$ for all i, then we readily obtain $[e^{i\alpha}] = 1$. Since (4.9) is symmetric under the permutation of ϕ_i with $i : (12)$, for any term $[e^{i\alpha}]$ we also obtain a term $[e^{-i\alpha}]$ in the expansion of (4.10) into a sum, such that their combined contribution to the average vanishes. Applying this recipe, we find for the combinations relevant for this work

$$[l_3(\mathbf{x}) l_{\overline{3}}(\mathbf{x})] = 3, \quad \left[l_3(\mathbf{x})^3\right] = \left[l_{\overline{3}}(\mathbf{x})^3\right] = 6, \quad \left[l_3(\mathbf{x})^2 l_{\overline{3}}(\mathbf{x})^2\right] = 15, \tag{4.11}$$

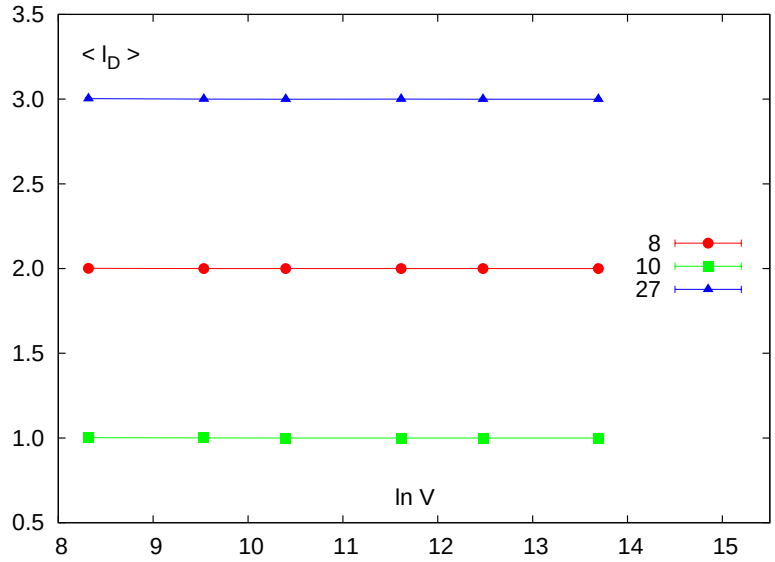

Figure 4.6: $\langle l_D \rangle$ over the log of the volume V for $D = 8, 10, 27$.

where the numbers are sums of binominal coefficients of the non-vanishing contributions. We can now derive the values of (4.8) by expressing l_D in terms of l_3 and $l_{\overline{3}}$ and apply the results in (4.11). In view of (2.79),(2.80) and (2.84) we obtain (suppressing the position dependence of the l_D)

$$\begin{aligned} [l_8] &= [l_3 l_{\overline{3}}] - 1 \\ &= 3 - 1 \\ &= 2 \end{aligned} \tag{4.12}$$

$$\begin{aligned} [l_{10}] &= [l_3 l_6] - [l_8] \\ &= \left[l_3^3\right] - 2\,[l_3 l_{\overline{3}}] + 1 \\ &= 6 - 2 \cdot 3 + 1 \\ &= 1 \end{aligned} \tag{4.13}$$

$$\begin{aligned} [l_{27}] &= \left[|l_6|^2\right] - [l_8] - 1 \\ &= \left[l_3^2 l_{\overline{3}}^2\right] - \left[l_3^3\right] - \left[l_{\overline{3}}^3\right] \\ &= 15 - 6 - 6 \\ &= 3, \end{aligned} \tag{4.14}$$

which reproduces (4.8) exactly.

We note, that these results can also be obtained from group theory. In the path integral representation of (4.10) at $\beta = 0$ the contribution of the action vanishes and we obtain

$$\left[l_3^r \, l_{\overline{3}}^s\right] = \frac{\int \mathcal{D}U \, l_3^r \, l_{\overline{3}}^s}{\int \mathcal{D}U}. \tag{4.15}$$

Employing group theoretical relations for the character l_3, see e. g. [17], one arrives at (4.8) as well.

4.3.2 Below T_c

We now turn to the Polyakov loop below T_c. As the considerations concerning string breaking in pure gauge theory 2.4.4 made clear, we expect the Polyakov loop to vanish in the thermodynamic limit below T_c for representations with non-vanishing triality. Moreover, the same considerations lead us to the expectation, that Polyakov loops in representations with vanishing triality do *not* vanish in the thermodynamic limit below T_c. In fig. 4.7(top) we have calculated $\langle |L_D| \rangle$ for all representations at $T/T_c = 0.959$ from lattices $N_\sigma^3 \times 4$ with $N_\sigma = 16, 24, 32, 48$. In fig. 4.7(top) the Polyakov loop of all representations except the adjoint seem to vanish according to a power law, as was proposed for $\beta = 0$ for the $t \neq 0$-representations. Only the adjoint Polyakov loop shows a different behaviour, deviating from the $1/\sqrt{V}$ behaviour to larger values with growing volume. We obtain similar plots for all other temperatures below T_c. This can be understood as follows. Let us consider the Polyakov in some representation $L = [L(\mathbf{x})]$, where $[\cdot]$ denotes the average on one configuration. For $D = 10$, where the Polyakov loop can assume complex values, we consider only the real part in the following, since the expectation value of the imaginary part is zero. At strong coupling ($\beta = 0$), the $L(\mathbf{x})$ are uncorrelated random variables. Therefore L has a Gaussian distribution due to the central limit theorem,

$$\rho(L) = \frac{1}{\sqrt{2\pi}\sigma} \exp\left(-\frac{(L - \overline{L})^2}{2\sigma^2}\right), \tag{4.16}$$

where $\overline{L}$ is the expectation value of L and σ its variance, which is dependent on the lattice volume

$$\sigma = \frac{a}{\sqrt{V}}, \tag{4.17}$$

where a is a proportionality constant. We assume this behaviour to be valid also for $\beta > 0$ as long as the correlation length of $L(\mathbf{x})$ is small compared to the spatial extent of the lattice.This assumption is fulfilled to a very good degree up to temperatures close to T_c on the largest lattices we employ in this work. Thus we can extend the findings at strong coupling concerning the thermodynamic limit of representations with non-vanishing triality (4.3.1) into the domain below T_c. We are now interested in the distribution function of $|L|$. It is given by

$$\tilde{\rho}\,(|L|) = \rho(L) + \rho(-L). \tag{4.18}$$

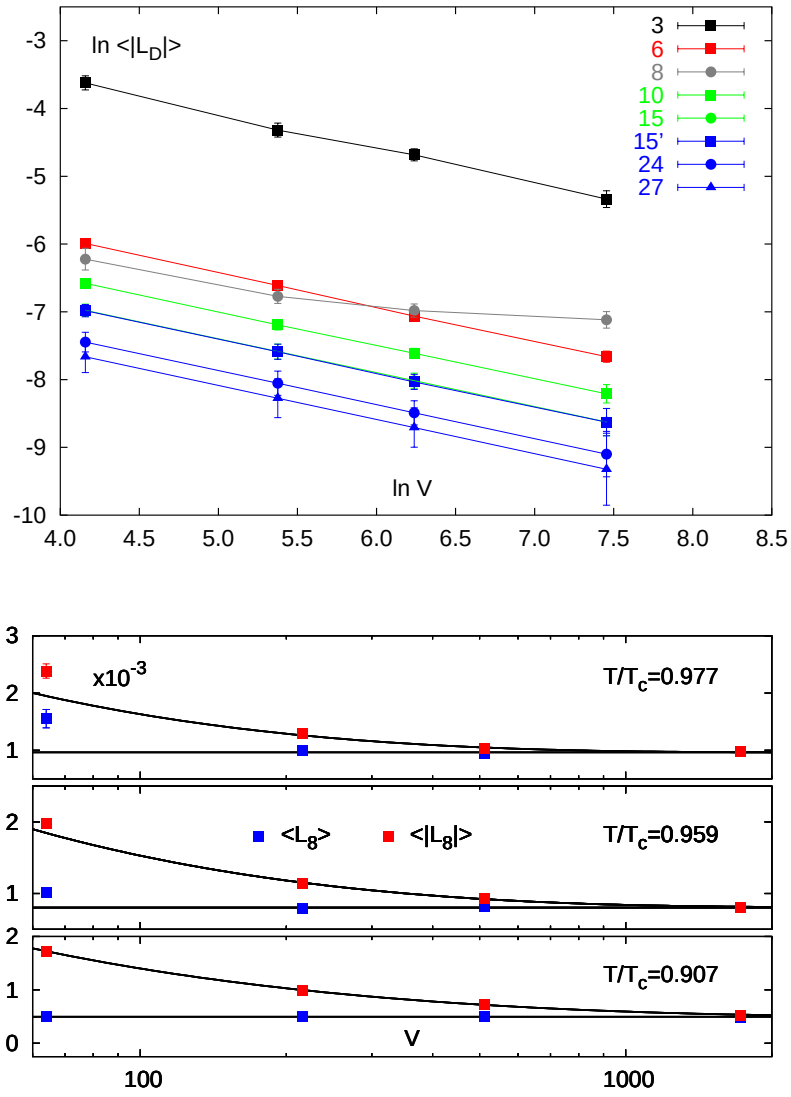

Figure 4.7: Top: $\langle |L_D| \rangle$ at $T/T_c = 0.959$ from lattices $N_\sigma^3 \times 4$ with $N_\sigma = 16, 24, 32, 48$. Bottom: $\langle L_8 \rangle$ for $T < T_c$ from the same lattices. The y-axises have been blown up by 10^3.

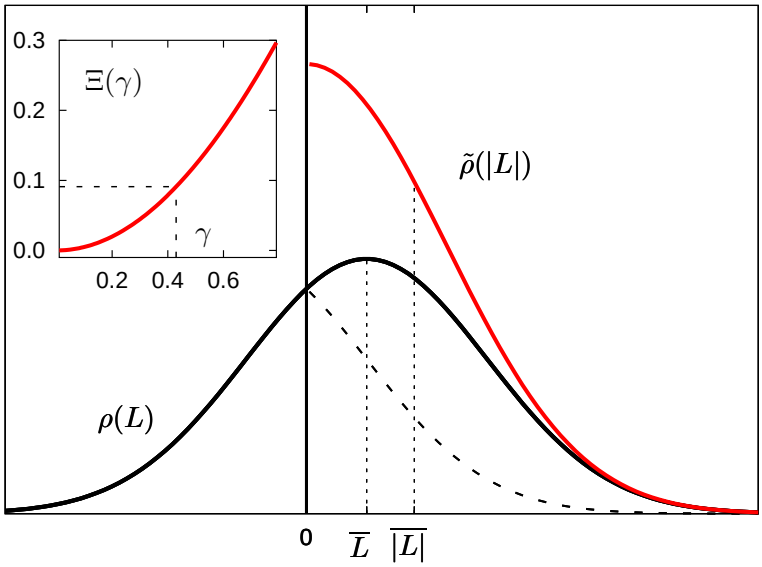

Figure 4.8: Distribution functions for L and $|L|$. The dotted black lines in the inset show $\gamma_{\text{th}} = 0.43$ and $\Xi(\gamma_{\text{th}}) = 0.091$.

Its mean $\overline{|L|} \equiv \langle |L| \rangle$ can be computed to give

$$\overline{|L|} = \int_0^\infty \mathrm{d}x \; x \, \tilde{\rho}(x) \tag{4.19}$$

$$= \sqrt{\frac{2}{\pi}} \, \sigma \exp\left(-\frac{\overline{L}^2}{2\sigma^2} \right) + \overline{L} \, \mathrm{erf}\left(\frac{\overline{L}}{\sqrt{2}\sigma} \right), \tag{4.20}$$

where $\mathrm{erf}\,(x) = \sqrt{\frac{2}{\pi}} \int_0^x e^{-t^2} \, \mathrm{d}t$ is the error function. We will later use $\overline{|L|}$ as a fit ansatz for $\langle |L| \rangle$. In fig. 4.8 we show the distribution functions. In the limit $\sigma \to 0$ ($V \to \infty$), we find $\overline{|L|} \to \overline{L}$. i. e. (4.20) is an unbiased estimator for the expectation value of the Polyakov loop. We note, that the estimate of $\langle L \rangle$ and $\langle |L| \rangle$ obtained from the average of N lattice configurations have, as usual when correlations are absent, an *error* proportional to $1/\sqrt{N}$. This does, however, not effect the considerations that lead to (4.20), since the σ appearing in there is connected to the volume average on *one* configuration.

For the representation with non-vanishing triality, that have $\overline{L} = 0$, the second term in (4.20) vanishes and we readily obtain together with (4.17) the behaviour

$$\overline{|L|}_0 = \sqrt{\frac{2}{\pi}} \, \sigma = \sqrt{\frac{2}{\pi}} \frac{a}{\sqrt{V}}. \tag{4.21}$$

For representations with $t = 0$, the mean $\langle L \rangle$ does not vanish and the term containing the error function in (4.20) will not disappear. We are faced with two different regimes

of $\overline{|L|}$ now. For the regime $\sigma \gg \overline{L}$, the second term in (4.20) becomes very small and the exponential in the first term reduces to one, such that we recover (4.21) again. This reflects the fact that when the variance of the distribution of L is large compared to its expectation value, we are not able to resolve the finite expectation value of L. For the regime $\sigma \ll \overline{L}$, however, the second term dominates and $\overline{|L|}$ approaches $\overline{L}$. We can make this observation systematic by considering the relative deviation of $\overline{|L|}$ for a finite $\overline{L}$ with respect to the case where $\overline{L} = 0$ defined by

$$\Xi = \frac{\overline{|L|} - \overline{|L|}_0}{\overline{|L|}_0}. \tag{4.22}$$

We can trade σ and $\overline{L}$ in Ξ for the single variable $\gamma = \frac{\overline{L}}{\sigma}$ and obtain

$$\Xi(\gamma) = \exp\left(-\frac{\gamma^2}{2}\right) + \sqrt{\frac{\pi}{2}}\gamma \operatorname{erf}\left(\frac{\gamma}{\sqrt{2}}\right) - 1. \tag{4.23}$$

In the inset of fig. 4.8 we show the behaviour of Ξ for some values of γ. We now have to give a threshold value γ_{th}, above which we can distinguish $\overline{L}$ being different from zero. We can say, that whenever $\gamma > \gamma_{\text{th}}$, i. e.

$$\overline{L} > L_{\text{min}} = \gamma_{\text{th}}\sigma, \tag{4.24}$$

we are able to resolve the finite expectation value of L on the lattice with volume V. The quantity L_{min} thus denotes the smallest expectation value that can be found on a lattice with volume V. We will give a reasonable value for γ_{th} below.

Let us now turn to the expectation value of the adjoint Polyakov loop below T_c. In fig. 4.7(bottom) we show a plot of $\langle L_8 \rangle$ and $\langle |L_8| \rangle$ over the volume for three temperatures below T_c from lattices $N_\sigma^3 \times 4$ with $N_\sigma = 16, 24, 32, 48$. We see both quantities coincide for all three temperatures at the largest volume ($N_\sigma = 48$) used in this work. For the lowest temperature, $\langle L_8 \rangle$ is clearly constant for all volumes calculated, whereas for the two higher temperatures deviations to higher values for the smallest volume with $N_\sigma = 16$ become visible. This is probably due to finite correlation lengths on the small lattice. We have performed a best fit analysis of the $\langle |L_8| \rangle$ data with a fit ansatz (4.20) and fit parameters $\overline{L}$ and a, where we have used the volume dependence (4.17) for σ. Additionally, we have fitted a constant to $\langle L_8 \rangle$. Since the two higher temperatures show deviations to higher values in $\langle L_8 \rangle$ for the smallest volume ($N_\sigma = 16$) due to finite correlation lengths, we have left these data points out for both fits at these temperatures. The results are listed in tab. 4.1. We observe, that the fit results for $\langle L_8 \rangle$ and $\overline{L}$ agree very well within errors. This vindicates the ansatz (4.20) for the Polyakov loop with $D = 8$. Moreover, we see, that the proportionality constant a changes only very little with temperature, as we expect it to be far enough from the critical temperature.

An important observation we can make from fig. 4.7(bottom) is, that at all $T < T_c$ calculated here, we find that $\langle L_8 \rangle$ is almost volume independent already on lattices with spatial extent $N_\sigma = 32$ (second point from the right). Therefore it is safe to consider $\langle L_8 \rangle$ from lattices $32^3 \times 4$ to be effectively in the thermodynamic limit. Together with the

T/T_c	$\langle L_8 \rangle$	$\overline{L}_8$	a	$L_{\min}$
0.907	$4.962(41) \times 10^{-4}$	$4.91(10) \times 10^{-4}$	0.01684(10)	1.74×10^{-4}
0.959	$8.040(62) \times 10^{-4}$	$8.07(11) \times 10^{-4}$	0.01731(35)	1.79×10^{-4}
0.977	$9.644(92) \times 10^{-4}$	$9.63(17) \times 10^{-4}$	0.01790(90)	1.85×10^{-4}

Table 4.1: Results of a best fit analysis: constant fit to $\langle L_8 \rangle$, fits with the ansatz given in (4.20) to $\langle |L_8| \rangle$ with fit variables $\overline{L}_8$ and proportionality constant a from (4.17). $L_{\min}$ is the resulting resolution limit from (4.24).

observation, that deviations from the $1/\sqrt{V}$ behaviour in $\langle |L_8| \rangle$ become already visible at $N_\sigma = 24$, we find a reasonable value for $\gamma_{\rm th}$ to be

$$\gamma_{\rm th} = \frac{\overline{L}_8(0.907\, T_c)}{\sigma} \approx 0.43, \tag{4.25}$$

where we have used $a = 0.01684$. We then have $\Xi(\gamma_{\rm th}) = 0.091$. We can now compute $L_{\min}$ for all three temperatures by employing (4.24), which results in the resolution limits given in the last column of tab. 4.1 for the biggest volume ($N_\sigma = 48$) used in this work.

We are now in position to renormalise $\langle L_8 \rangle$ in the thermodynamic limit below T_c with the renormalisation constant $(Z_8^R(g^2))^{N_\tau}$. The $Z_8^R(g^2)$ have been obtained by from the renormalisation of the $Q\bar{Q}$-singlet free energies in the adjoint representation (see chapter 3.2), which is applicable below T_c. We show L_8^R from the $32^3 \times 4$ lattice together with other quantities discussed in the next section in tab. 4.3.

In view of fig. 4.7(top) we are still in the regime where $\gamma < \gamma_{th}$ for the lattice volumes employed in this work for the representations $D = 10, 27$ and thus a fit with (4.20) is hopeless. A constant fit to $\langle L_D \rangle$ for these representations shows, that the resulting $\overline{L}$ are all compatible with zero and thus now definite answer to the value of $\langle L_D \rangle$ can be obtained from this approach either. We conclude, that the expectation values for $D = 10, 27$ are smaller than the resolution limit and therefore bigger lattice volumes must be employed than used in this work. We can nevertheless use the data for $\langle |L_D| \rangle$ for $D = 10, 27$ to test the assumption of Casimir scaling for the $t = 0$ representations. We set

$$\overline{L}_D = \langle L_8 \rangle^{d(D,8)} \tag{4.26}$$

for $D = 10, 27$ and use the ansatz for the volume scaling (4.20) to perform a best fit analysis for the proportionality constant a appearing in (4.17) to the $\langle |L_D| \rangle$ over the volume. For $D = 10$, we have only used the real part of the Polyakov loop for reasons discussed earlier. Table 4.2 shows the $\overline{L}_D$ obtained, where $\langle L_8 \rangle$ is taken from the above

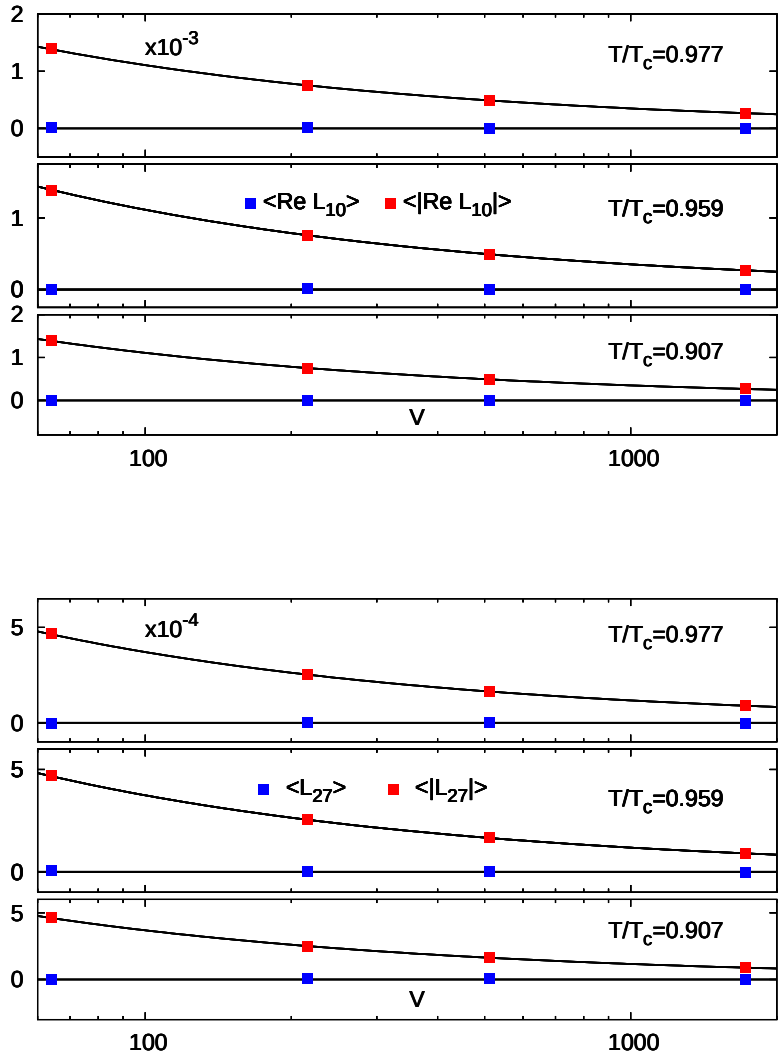

Figure 4.9: The same as fig. 4.7(bottom) for $D = 10, 27$ obtained with the ansatz (4.26). For $D = 10$, only the real part of L_{10} was used. The y-axises have been blown up by 10^3 for $D = 10$ and by 10^4 for $D = 27$.

T/T_c	$\langle L_8 \rangle$	$\overline{L}_{10}$	$\overline{L}_{27}$
0.907	$4.962(41) \times 10^{-4}$	$2.462(41) \times 10^{-7}$	$1.543(34) \times 10^{-9}$
0.959	$8.040(62) \times 10^{-4}$	$6.46(10) \times 10^{-7}$	$5.59(12) \times 10^{-9}$
0.977	$9.644(92) \times 10^{-4}$	$9.30(18) \times 10^{-7}$	$9.08(23) \times 10^{-9}$

Table 4.2: Results for $\overline{L}_D$ according to the Casimir scaling ansatz (4.26) using $\langle L_8 \rangle$ from table 4.1.

analysis of L_8. We find, that the resulting fit value of a is very stable for both representations and almost independent of temperature, as we already observed for $D = 8$. We obtain $a = 0.0139(9)$ for $D = 10$ and $a = 0.0046(2)$ for $D = 27$. The results are shown in fig. 4.9, where we also plot $\overline{L}_D$ from (4.26) in comparison to $\langle L_D \rangle$ for $D = 10, 27$. We see, that the Casimir scaling assumption (4.26) leads to fit functions that agree with the data. We therefore conclude, that the Casimir scaling ansatz (4.26) is not contradicted by our data obtained for $D = 10, 27$. We can give upper limits for the Polyakov loops in the thermodynamic limit in representation $D = 10, 27$ with the help of the proportionality constant a obtained above and (4.24). We find $\langle \mathrm{Re}\, L_{10} \rangle < 1.4 \times 10^{-4}$ and $\langle L_{27} \rangle < 4.75 \times 10^{-5}$.

4.4 The adjoint Polyakov loop

We are now in position to discuss the *renormalised adjoint Polyakov loop in the thermodynamic limit below* T_c. We have summarised the data to be discussed in this part in tab. 4.3. See also tab. C.10 in appendix C.

Let us start with the expectation value of the adjoint Polyakov loop and its temperature dependence. In fig. 4.10(top) we show L_8^R for temperatures close to T_c. For reference, we have also plotted L_3^R, which is exactly zero below T_c. We observe that L_8^R rises from 0.0087(16) at $T/T_c = 0.907$ to 0.0219(48) just below T_c at $T/T_c = 0.995$. Crossing the critical temperature into the deconfined phase, L_8^R jumps almost an order of magnitude to 0.154(37) at $T/T_c = 1.005$. This behaviour is clearly a remnant of the weakly first order phase transition that takes place at T_c.

Knowing L_8^R, we can now address the issue of string breaking and in connection with that, determine the binding energy of the gluelump. In fig. 4.10(bottom) we show the situation at $T/T_c = 0.959$ as an example. As $F^{1,R}_{Q\bar{Q},8}$ becomes too noisy at large distances,

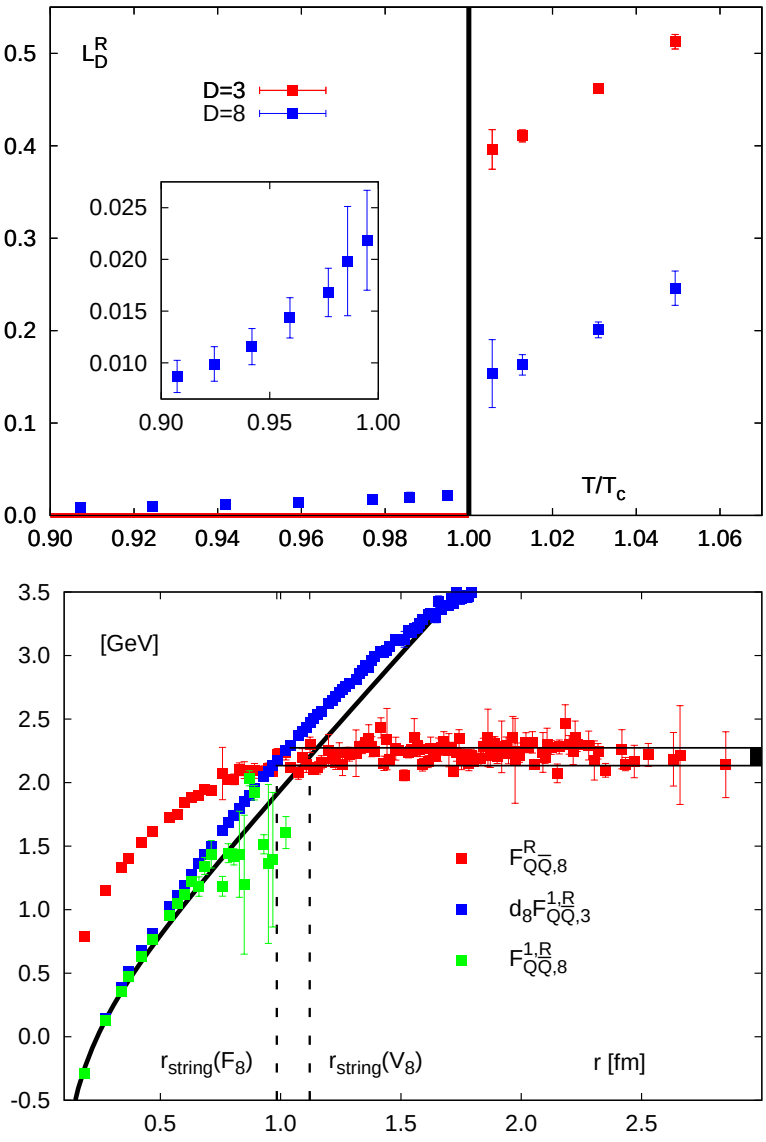

Figure 4.10: Top: L_8^R and L_3^R over the temperature. The inset shows L_8^R below T_c on a smaller scale. Bottom: string breaking distances and F_∞ at $T/T_c = 0.959$. The black line indicates d_8V_3.

T/T_c	F_∞ [GeV]	$r_{\text{string}}(V_8)$ [fm]	$r_{\text{string}}(F_8)$ [fm]	L_8^R
0.907	2.331(88)	1.180(61)	1.040(39)	0.0087(16)
0.924	2.310(84)	1.170(58)	1.01(10)	0.0099(17)
0.942	2.274(76)	1.153(53)	1.012(92)	0.0116(17)
0.959	2.204(70)	1.121(48)	0.984(26)	0.0143(19)
0.977	2.161(73)	1.101(50)	0.960(26)	0.0168(23)
0.986	2.09(14)	1.069(97)	0.93(12)	0.0198(53)
0.995	2.06(12)	1.053(81)	0.90(15)	0.0219(48)
$T=0$	$2.4-3.0$	~ 1.2		–

Table 4.3: Temperature dependence of F_∞, string breaking distance r_{string} for the adjoint singlet free energy with respect to V_8 and F_8 (see text) and the renormalised adjoint Polyakov loop L_8^R. The last line gives the values at $T=0$ for twice the mass of the gluelump [59] and for the string breaking distance [43].

we also show the colour average free energy $F^R_{Q\bar{Q},8}$, which has the same cluster value. We can easily calculate the free energy F_∞ at which string breaking in the adjoint $Q\bar{Q}$ free energy occurs below T_c by employing

$$F_\infty = -2T \ln\left(L_8^R\right), \tag{4.27}$$

which follows from the cluster property (2.93). This is the energy stored in the adjoint string which suffices to create a gluon pair from the surrounding gluonic medium to form two disjoint gluelumps. Gluelumps are bound states of an infinitely heavy test quark in the adjoint representation, which serves here as an infinitely heavy test gluino $\tilde{G}$, i. e. the fermionic superpartner of the gluon, and a dynamical gluon g. The mass of such an $\tilde{G}g$-lump in the vacuum is connected to $V_{8,\infty}$, the value of the adjoint potential at large separations, by

$$m_{\text{glump}} = \frac{V_{8,\infty}}{2}, \tag{4.28}$$

since two $\tilde{G}g$-lumps are created. At finite temperature we may identify the binding energy of the gluelump from F_∞, which we show in fig. 4.11(upper panel). We observe F_∞ to change only little with T, starting from 2.331(88) GeV at $T/T_c = 0.907$ and subsequently falling to 2.06(12) GeV just below T_c. This corresponds to a variation

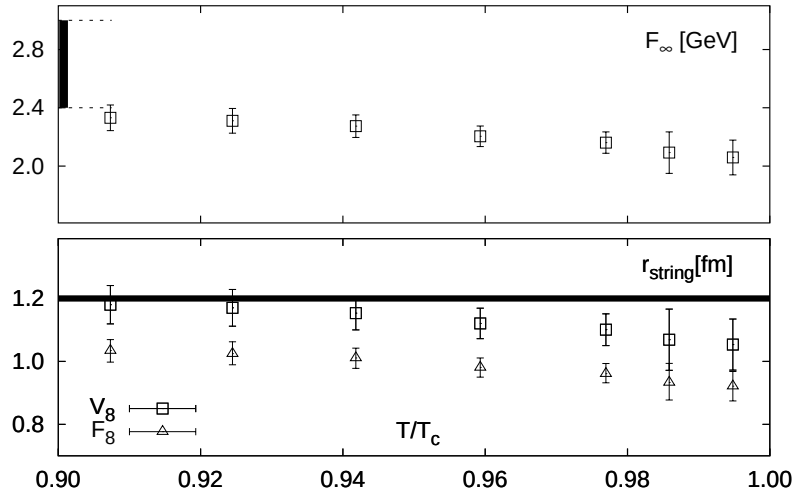

Figure 4.11: Upper panel: F_∞ over T/T_c. The black band indicates twice the mass of the gluelump at $T = 0$, where for m_{gluelump} $1.2 - 1.5\,\text{GeV}$ has been used [59]. Lower panel: String breaking distance r_{string} over T/T_c for the adjoint singlet free energy with respect to V_8 and F_8 (see text). The black line stands for the $T = 0$ value of $\sim 1.2\,\text{fm}$ [43].

smaller than 8 % in the temperature range $0.9 - 1.0\,\text{T}_\text{c}$. At the lowest temperatures discussed here, F_∞ indeed approaches the $T = 0$ value of $V_{8,\infty}$, $2.4 - 3.0\,\text{GeV}$, which is twice the mass of the gluelump [59]. This is reassuring and gives confidence in the $\tilde{G}g$-approximation we consider here.

We finally determine the string breaking distance r_{string} of the adjoint $Q\bar{Q}$ free energy, which can be done in two different ways. Firstly, we consider the string breaking distance with respect to the adjoint potential V_8 at $T = 0$, which is connected to the fundamental potential by Casimir scaling and can be determined from the condition

$$V_8(r_{\text{string}}(T)) = F_\infty(T). \tag{4.29}$$

The second possibility is to replace V_8 in (4.29) by $F_8(r,T) = d_8 F_3^{1,R}(r,T)$ and define analogously

$$F_8(r_{\text{string}}(T),T) = F_\infty(T), \tag{4.30}$$

which coincides with (4.29) at $T = 0$. However, due to the overshooting of $F_3^{1,R}(r,T)$ with respect to the $T = 0$ potential at intermediate distances [24], we expect to find systematically lower values for the string breaking distance implicitly defined through F_8 compared to those defined through V_8. In fig. 4.11(lower panel) we show the resulting r_{string} from the two definitions over the temperature. We first discuss the string breaking distances obtained with respect to V_8. In view of the findings for the binding energy

of the gluelump, it is not surprising that r_{string} changes only little with increasing T, starting from 1.180(61) fm at $T/T_c = 0.907$ and falling to 1.053(81) fm just below T_c. At the smallest temperature r_{string} almost coincides with the $T = 0$ value of 1.2 fm [43], which strongly suggests that temperature effects for the string breaking distance become only mildly important close to T_c. The string breaking distance obtained with respect to F_8 shows similar behaviour to that obtained from V_8, but has, as already noted above, a value that is systematically smaller by about ~ 0.15 fm, due to the overshooting of the fundamental free energy.

4.5 The Polyakov loop in 2-flavour QCD

Let us now discuss the Polyakov loop in different representations in $N_f = 2$ QCD. We have reexamined configurations generated with staggered quarks on a $16^3 \times 4$ lattice at several temperatures above and below the transition temperature into the deconfined phase with a quark mass of $m/T = 0.4$. For further details on the simulations and data tables see appendices A.1, A.2 and C.

Since the presence of the dynamical quark field breaks the center symmetry explicitly, as we have argued in chapter 2, the thermodynamic limit of the quantities studied here is finite. Nevertheless a volume dependence on the lattice used here might persist. Moreover, since $N_f = 2$ QCD shows a crossover behaviour [7], L_3^R changes rapidly but smoothly in the transition region and, because of the explicitly broken center symmetry, is non-zero for all temperatures. As a consequence, the discussion of $\langle L_D \rangle$ is sufficient.

In fig. 4.12(top) we show $\langle L_D \rangle^{1/d_D}$ for $D = 3, 6, 8, 10, 15$ versus the temperature, where we refrain from showing data below T_c for the representations $D = 10, 15$ due to noise. The quantity $\langle L_D \rangle^{1/d_D}$ is independent of the representation D when Casimir scaling is realised for the bare Polyakov loop. We observe this to be the case for the highest temperatures calculated down to $\sim 1.5T_c$ for all D analysed here. Below this temperature we observe deviations to smaller values for the fundamental representation, whereas the values for higher D still coincide within errors. Therefore we see a *violation* of Casimir scaling when entering the transition region which continues to the smallest temperatures analysed. We note however, that these violations are relatively mild and a difference between $\langle L_D \rangle^{1/d_D}$ for $D = 6$ and $D = 8$ can not be confirmed even at the smallest temperatures, as the inset of fig. 4.12(top) shows.

Since only configurations for $N_\tau = 4$ where available, we can not apply the N_τ variation method in order to obtain the effective renormalisation constants Z_D^R in $N_f = 2$ QCD. Moreover, we did not compute the adjoint singlet free energies. Since Casimir scaling for the bare Polyakov loop is realised for temperature $T \gtrsim 1.5T_c$, we *assume* Casimir scaling to hold also for the effective renormalisation constants, i. e. $Z_D^R = Z_3^R$, in this temperature regime. The effective renormalisation constants for the fundamental representation Z_3^R using the $Q\bar{Q}$-singlet free energy for $N_f = 2$ QCD have been obtained in [29, 60]. The resulting renormalised Polyakov loops are shown in fig. 4.12(bottom), where we display the whole temperature range. For temperatures $T > 1.5T_c$ the behaviour is qualitatively similar to the pure gauge case displayed in fig. 3.6(bottom). We observe $L_D^R = 1$ for all

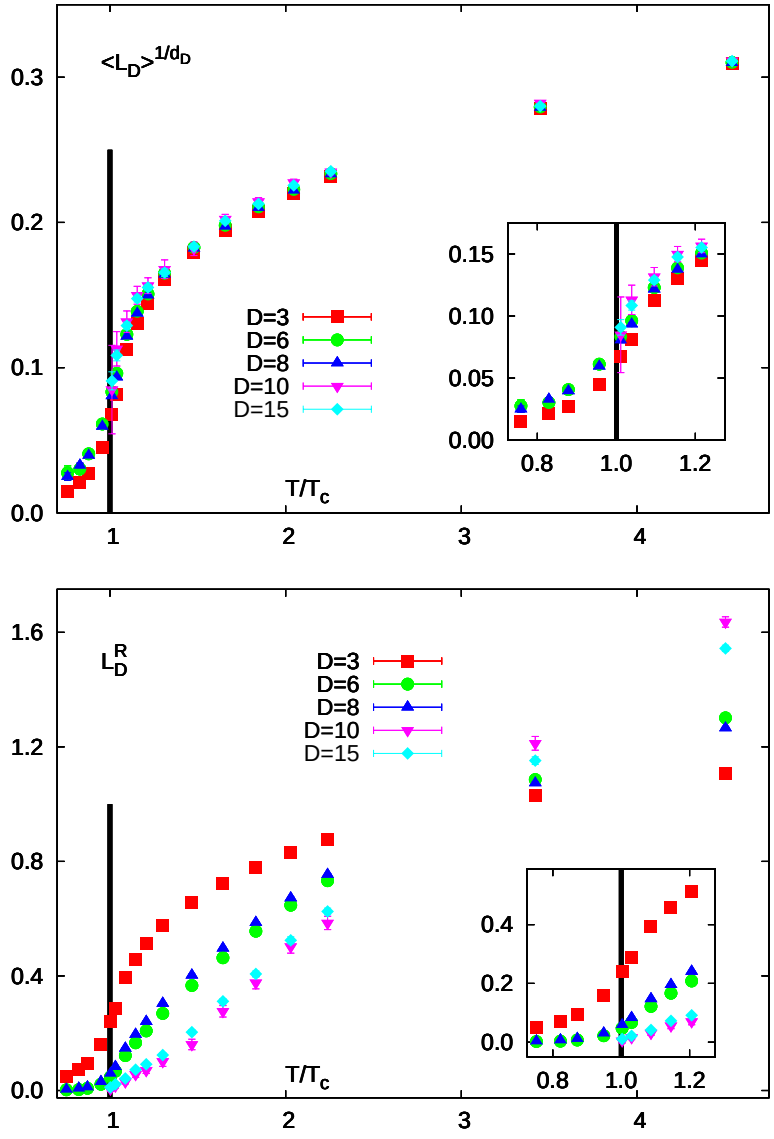

Figure 4.12: Top: testing Casimir scaling for the bare Polyakov loop in 2-flavour QCD. $\langle L_D \rangle^{1/d_D}$ from a $16^3 \times 4$ lattice for all $D = 3, 6, 8, 10, 15$. Bottom: renormalised Polyakov loop L_D^R in full QCD assuming Casimir scaling in Z_D^R for representations $D = 3, 6, 8, 10, 15$. The insets show the regions $0.725T_c - 1.275T_c$.

representations at $T \approx 3T_c$ and L_D^R becomes larger than unity for even higher temperatures. Though our assumption of Casimir scaling in Z_D^R in the transition region can not be trusted in view of the findings for the bare Polyakov loop from fig. 4.12(top), the violations found were not too big. We therefore expect to have caught at least the qualitative behaviour of L_D^R correctly in the transition region.

5 Diquark Free Energy

We now turn to the discussion of the behaviour of heavy diquark systems at finite temperature. We have calculated static diquark free energies from the correlation functions of the anti-triplet and the sextet colour state shown in (2.43) and (2.44). The results are compared to free energies of quark anti-quark systems. As an immediate application, we discuss whether heavy quark bound states may be supported above T_c for the case of coloured diquark systems. For previous discussions on static diquark free energies in finite temperature lattice QCD see [61, 62].

5.1 $\mathbb{Z}(3)$ symmetry and thermodynamic limit

The QQ-correlation functions are not $\mathbb{Z}(3)$ symmetric and therefore their expectation values are exactly zero in pure gauge theory when averaging over all $\mathbb{Z}(3)$ sectors. We perform a global $\mathbb{Z}(3)$ transformation on each configuration such that the Polyakov loop in the fundamental representation L_3 (averaged over one configuration) lies in the real $\mathbb{Z}(3)$ sector. This represents the correct infinite quark mass limit $m_q \to \infty$ of full QCD, where the center symmetry is explicitly broken and $\langle L_3 \rangle$ is real and positive. In the infinite volume limit this procedure, as well as calculating $\langle |L_3| \rangle$, is equivalent to the introduction of an explicit symmetry breaking term in the action. While this expectation value is finite on finite volumes (even in the confined phase), it vanishes in the thermodynamic limit when the system shows confinement, as was made clear in the preceding chapters. The volume dependence can be understood in terms of a random walk model [58]. We expect this behaviour to be valid for the QQ-correlators below T_c as well.

To check the validity of the finite volume scaling behaviour for the QQ correlation functions we use calculations on lattices of size $N_\sigma^3 \times 4$ with various spatial extents $N_\sigma = 16, 24, 32$ and 48. The results for $C^{\overline{3}}_{QQ}(r,T)$ at a temperature of $T/T_c = 0.959$ for some values of the quark separation r are shown in fig. 5.1. We also show $\langle |L_3| \rangle$ for reference. We observe that the expected scaling behaviour holds for all temperatures below T_c for the correlation functions at all distances. Deviations from a linear behaviour in fig. 5.1 are visible for large distances r on the smallest lattice ($N_\sigma = 16$) which may show the influence of the periodic boundary conditions.

We have used the data for a fit of the scaling ansatz

$$C^{\overline{3}}_{QQ}(r,T) \propto N_\sigma^{-3\nu(r,T)} \propto V^{-\nu(r,T)}. \tag{5.1}$$

The results for the exponent ν at temperatures below T_c, shown in fig. 5.2, are within errors in agreement with the expected value of 0.5 from the random walk model. The

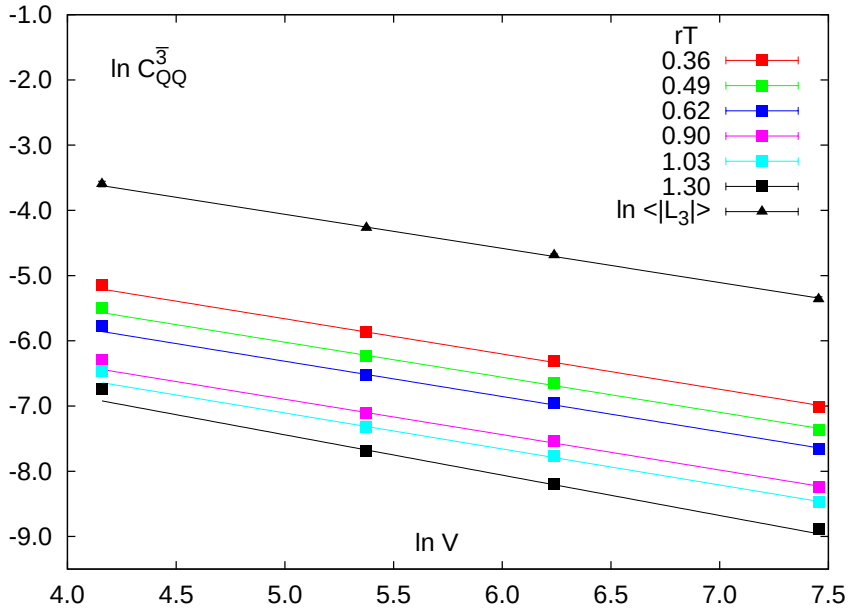

Figure 5.1: Scaling analysis of $C^{\bar{3}}_{QQ}(r,T)$ at $T/T_c = 0.959$ from lattices $N_\sigma^3 \times 4$ and $N_\sigma = 16, 24, 32, 48$. $\langle|L_3|\rangle$ is given as a reference. The lines show the results of the linear fits.

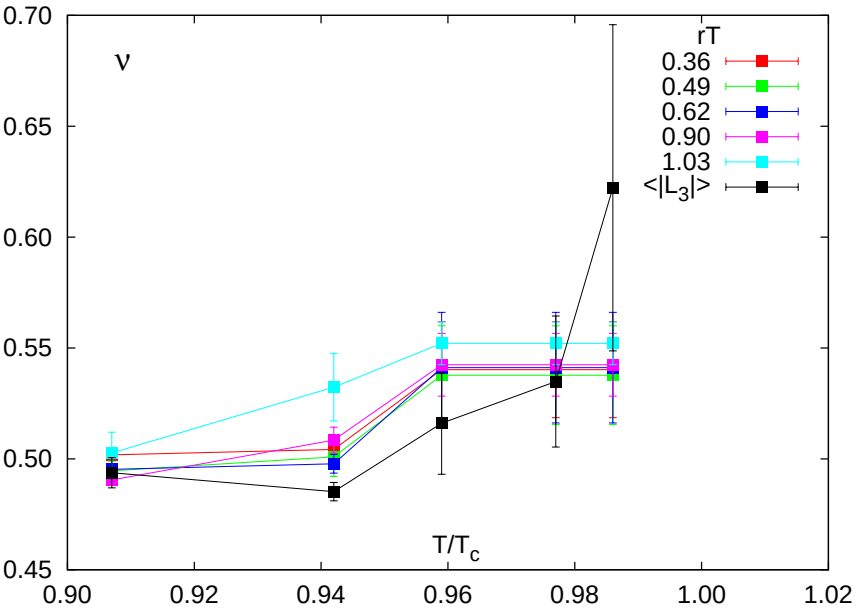

Figure 5.2: T-dependence of ν for $C^{\bar{3}}_{QQ}(r,T)$ and $\langle|L_3|\rangle$ for reference.

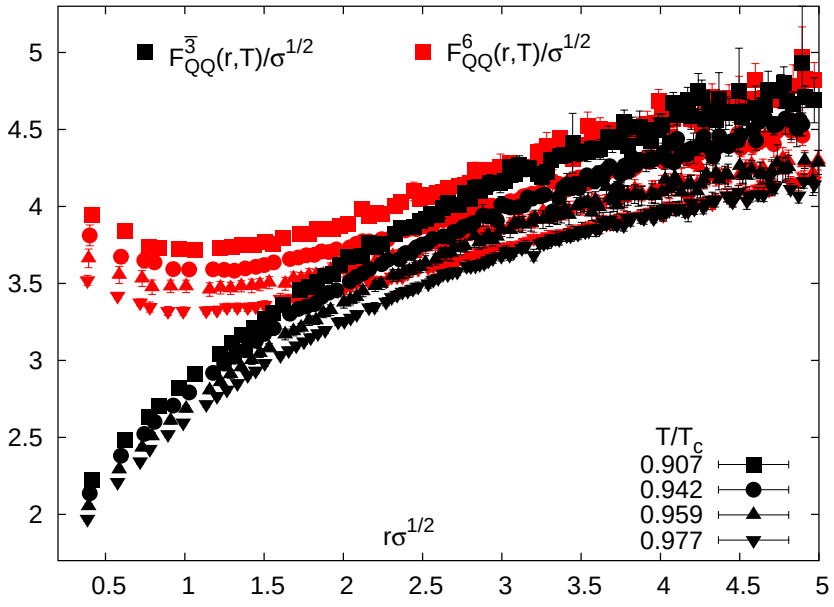

Figure 5.3: $F^{\overline{3}}_{QQ}(r,T)$ (black) and $F^{6}_{QQ}(r,T)$ (red) below T_c.

increase near T_c may be explained by an increase of the correlation length near the phase transition and indicates that the lattice volumes used may be too small near the critical temperature to obtain the correct scaling. This is also supported by the observation that the increase of the slope is largest for large r and decreases towards $1/2$ for smaller separations.

We note here again that the vanishing of all non $\mathbb{Z}(3)$ symmetric operators can only be seen in the confined phase of quenched QCD while in the deconfined phase due to the spontaneous breaking of the $\mathbb{Z}(3)$ symmetry and in QCD with dynamical quarks, where the center symmetry is explicitly broken, the expectation values of all Polyakov loops and the QQ-correlation functions are finite in the infinite volume limit.

Despite the trivial thermodynamic limit in the confined phase, the r-dependence of the diquark free energies might show a non-trivial behaviour and will be discussed in the following.

5.2 General Properties of $F^{\overline{3}}_{QQ}$ and F^{6}_{QQ}

At zero temperature the short distance behaviour of the diquark potential is related to the quark-antiquark potential by the ratio of the different Casimir operators, i.e.

$$V_{QQ}(r) \simeq \frac{1}{2} V_{Q\bar{Q}}(r), \quad \text{for } r\Lambda_{QCD} \ll 1. \tag{5.2}$$

As for the quark-antiquark free energies [24], we assume that the r-dependence of the diquark free energies at short separations becomes independent of the temperature. We

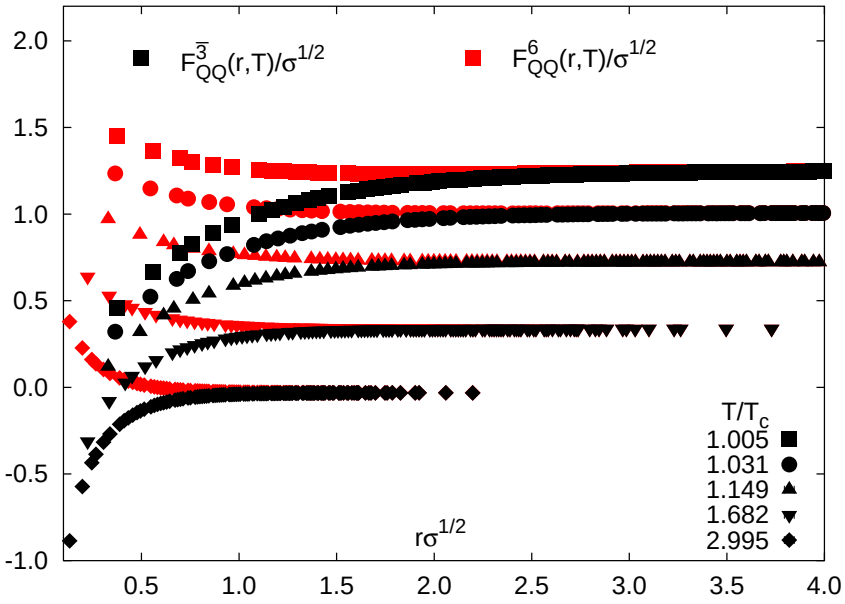

Figure 5.4: $F^{\bar{3}}_{QQ}(r,T)$ (black) and $F^{6}_{QQ}(r,T)$ (red) above T_c.

only discuss the r-dependence of the diquark free energies without specifying any T or V dependent terms.

Fig. 5.3 shows $F^{\bar{3}}_{QQ}(r,T)$ and $F^{6}_{QQ}(r,T)$ for four different temperatures below T_c. We observe clearly that $F^{\bar{3}}_{QQ}(r,T)$ is attractive over the entire distance interval calculated here, assuming an almost linear behaviour for large distances.

$F^{6}_{QQ}(r,T)$ is attractive for distances $r\sqrt{\sigma}\gtrsim 1.0$, at $r\sqrt{\sigma}\approx 1.0$ it assumes a minimum and becomes repulsive for even smaller distances, remaining T-dependent as well. This qualitative behaviour is already known from $Q\bar{Q}$-octet free energies. For large distances $F^{\bar{3}}_{QQ}(r,T)$ and $F^{6}_{QQ}(r,T)$ coincide.

In contrast to the results below T_c, the static diquark free energies in the deconfined phase are finite in the thermodynamic limit and, moreover, can be renormalized in the same way as in the case of quark-antiquark free energies. In the following the static diquark free energies obtained through (2.43) and (2.44) are renormalized using the method described in chapter 3.2.

From now on we drop the superscript R for renormalized quantities, when we are using the $\sqrt{\sigma}$ scale. The effective renormalisation constants used are obtained from the $Q\bar{Q}$-singlet free energies. In fig. 5.4 we show the anti-triplet, $F^{\bar{3}}_{QQ}(r,T)$, and the sextet free energies, $F^{6}_{QQ}(r,T)$, for five temperatures above T_c. While $F^{\bar{3}}_{QQ}(r,T)$ is attractive over the entire distance range, the QQ-sextet free energies are repulsive for all distances. At large separations the free energies in both colour channels tend towards the same asymptotic value. In this limit the colour sources get screened independently of their colour orientation.

The diquark free energies show a temperature dependence over the entire distance range analyzed in this work. In contrast to the $Q\bar{Q}$ free energies we observe a temperature dependence of the diquark free energies even at the smallest distances accessible here. This behaviour suggests that entropy contributions play an important role for the diquark free energies even at very small separations. This may be explained by the fact that the diquarks are not colour singlets and the surrounding gluon cloud has to arrange the whole system to be in a colour singlet state. As we have mentioned in chapter 2.4.2, this results in general in small values for cross correlators in the vacuum, since these represent coloured states of heavy quarks. At finite temperature, however, the thermal medium possesses additional screening power and therefore coloured states might persist in the deconfined phase.

5.3 Comparison between diquark and quark-anti-quark free energies

We will now compare the diquark free energies to the quark-antiquark free energies in pure gauge theory. Using the perturbative short and large distance relation from one gluon exchange [16, 20, 21] one can deduce the perturbative relation between $F^{\overline{3}}_{QQ}$ and $F^{1}_{Q\bar{Q}}$. In the limit $r\Lambda_{QCD} \ll 1$ zero temperature perturbation theory yields

$$F^{\overline{3}}_{QQ}(r,T) \sim -\frac{2}{3}\frac{\alpha(r)}{r}, \tag{5.3}$$

while high temperature perturbation theory gives

$$F^{\overline{3}}_{QQ}(r,T) \sim -\frac{2}{3}\frac{\alpha(T)}{r}e^{-m_D r}. \tag{5.4}$$

Therefore leading order perturbation theory suggests the connection between static diquark and quark-antiquark free energies to be given by

$$F^{\overline{3}}_{QQ}(r,T) \sim \frac{1}{2}F^{1}_{Q\bar{Q}}(r,T), \tag{5.5}$$

i. e. the ratio of their Casimirs. Note that these relations can only be valid up to an additive (in general temperature dependent) constant. In the following we will analyse if this simple relation holds beyond the perturbative regime and where deviations from (5.5) occur.

To remove any constant contributions with respect to the quark separation we will compare the static diquark and quark-antiquark forces defined by

$$K_i(r,T) = -\frac{\mathrm{d}F_i(r,T)}{\mathrm{d}r} \tag{5.6}$$

for $i = QQ$ and $Q\bar{Q}$. The results for $2K^{\overline{3}}_{QQ}$ compared to $K^{1}_{Q\bar{Q}}$ for some temperatures below and above T_c are shown in fig. 5.5. With the present data it is not possible to perform a quantitative comparison below T_c. While the quark-antiquark force is

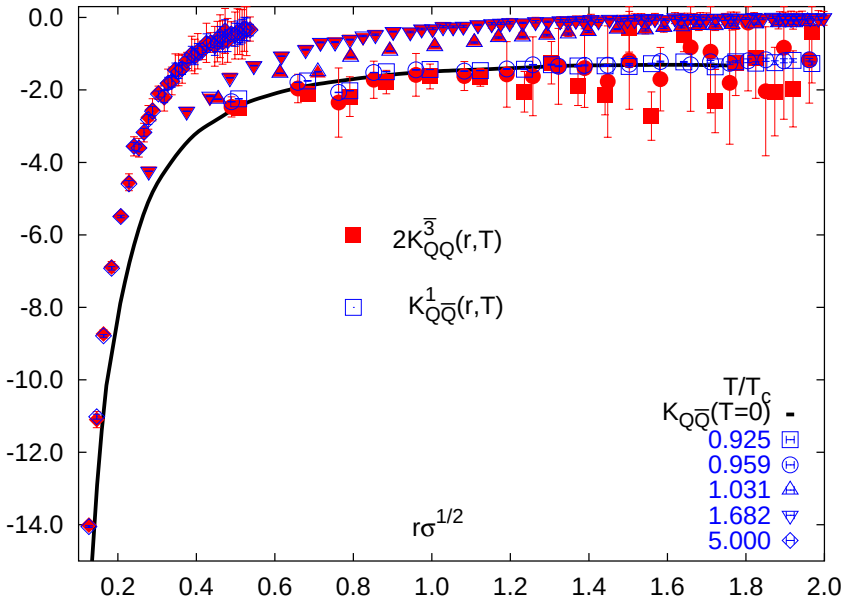

Figure 5.5: Force $K(r,T)$ for the QQ-anti-triplet (red) and the $Q\bar{Q}$-singlet (blue).

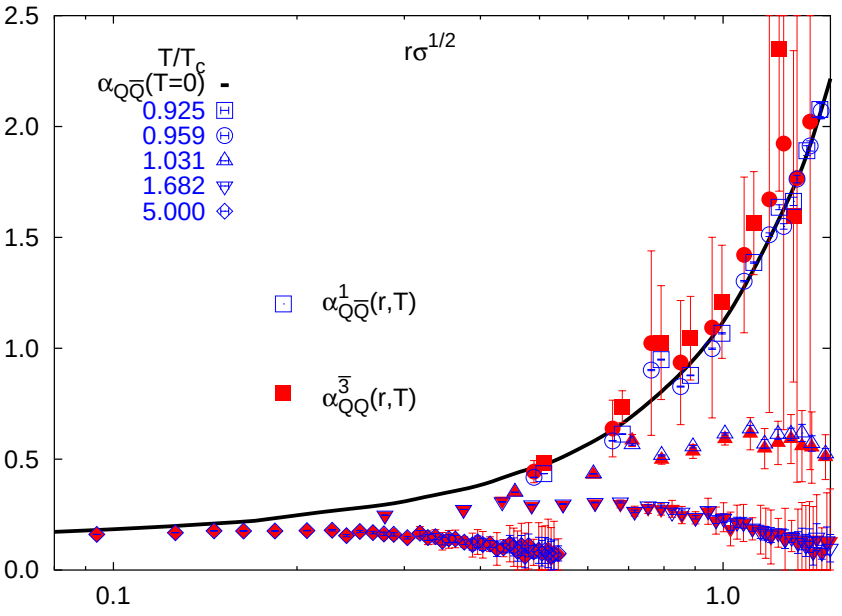

Figure 5.6: Effective running coupling $\alpha(r,T)$ for the QQ-anti-triplet (red) and the $Q\bar{Q}$-singlet (blue).

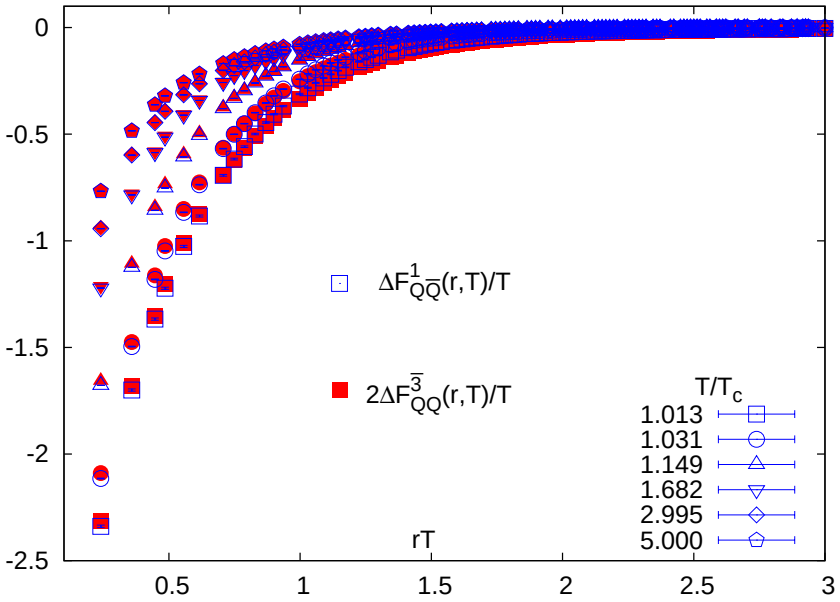

Figure 5.7: $Q\bar{Q}$-singlet and twice the QQ-anti-triplet free energy renormalized by their cluster value above T_c.

consistent with the zero temperature force up to $r\sqrt{\sigma} \sim 2.0$, the diquark force gets very noisy already at small distances. Above T_c both coincide remarkably well for all analysed distances and all temperatures within errors. This indicates that the simple relation (5.5) is a good approximation already just above T_c.

A closely related way to analyse the relation (5.5) is to calculate from the force the effective running coupling

$$\alpha^{\bar{3}}_{QQ}(r,T) = \frac{3}{2}r^2\frac{\mathrm{d}F^{\bar{3}}_{QQ}(r,T)}{\mathrm{d}r} \tag{5.7}$$

$$\alpha^{1}_{Q\bar{Q}}(r,T) = \frac{3}{4}r^2\frac{\mathrm{d}F^{1}_{Q\bar{Q}}(r,T)}{\mathrm{d}r}, \tag{5.8}$$

where again all constant contributions are removed and a direct comparison to $\alpha^1_{Q\bar{Q}}$ is possible. The results in fig. 5.6 show that the effective running coupling constants for both systems agree within errors above the critical temperature, while below T_c the diquark running coupling agrees with $\alpha^1_{Q\bar{Q}}$ within errors, but again the data is too noisy to draw a definite conclusion.

In the deconfined phase we can compare the relation of the free energies for the diquark pair and the quark-antiquark free energies more directly by using free energies normalised by their cluster value $\Delta F_i(r,T)$. The comparison in fig. 5.7 shows that (5.5) is a good approximation for all temperatures and all distances in the deconfined phase.

The comparison of the forces and running coupling constants indicates that the results

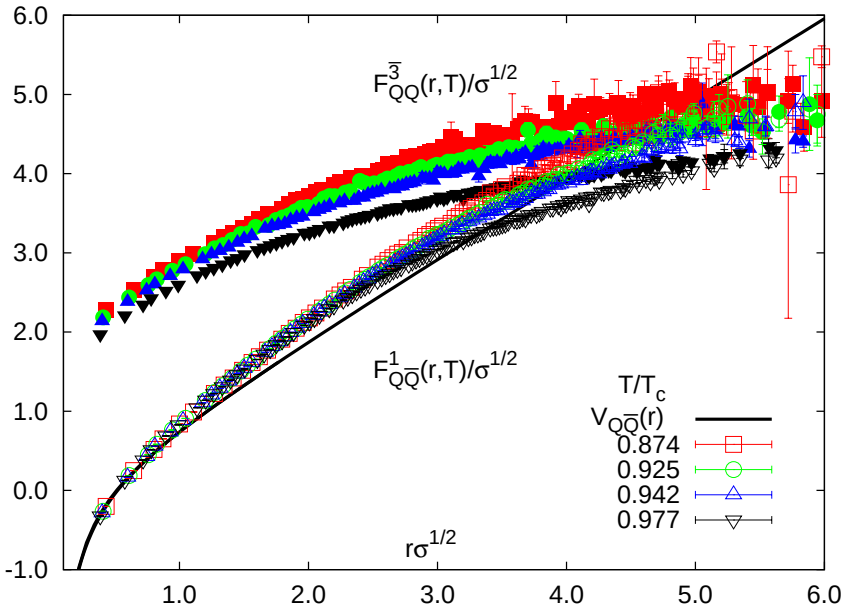

Figure 5.8: $F^{\bar{3}}_{QQ}(r,T)$ and $F^{1}_{Q\bar{Q}}(r,T)$ below T_c, renormalized to the $V_{Q\bar{Q}}(r)$-potential (solid black line).

on the running coupling and the screening properties obtained for the quark-antiquark free energy [63] can in good approximation be transfered to the static diquark free energies.

After this discussion of the r-dependence of the diquark free energies we now compare the renormalized free energies of the diquark to the quark-anti-quark system. Below T_c (fig. 5.8) we have to note that the diquark free energies diverge in the thermodynamic limit and therefore a discussion of the temperature dependence is not possible. Note that the comparison to the quark-antiquark free energies indicate that at first sight also at large distances the relation (5.5) holds which would imply that the string tension of the diquark system is half of the string tension of the quark-antiquark system. A detailed analysis of the distance behaviour, i. e. different string fluctuation components or the equivalence of the string tension of QQ- and $Q\bar{Q}$-systems as predicted by AdS/CFT [64] is not possible with the present data and and should be analysed in future.

The results above T_c in fig. 5.9 show that in contrast to the quark-antiquark case, we see a temperature dependence in the diquark free energies over the whole distance regime. This indicates that entropy contributions play an important role even at small distances. This may be explained by the fact that the diquark system is no colour singlet and the surrounding gluon cloud has to arrange the whole system to be in a colour singlet state in contrast to the case of a colour singlet quark-antiquark pair. This can in fact be more explicit together with the observation that in the limit of large distances the diquark free energies tend towards the same asymptotic value as the quark-antiquark free energies. This indicates that the quarks in both systems are screened independently

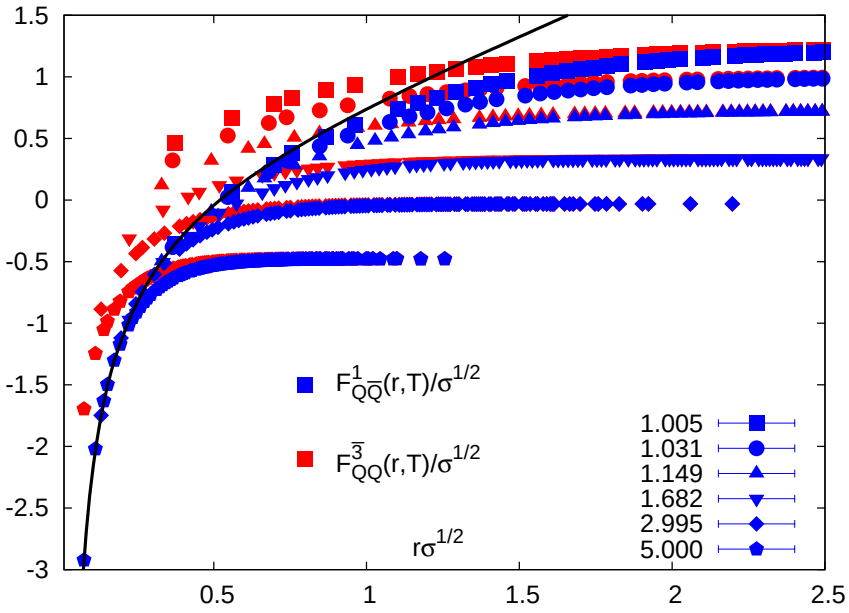

Figure 5.9: $F^{\bar{3}}_{QQ}(r,T)$ (red) and $F^1_{Q\bar{Q}}(r,T)$ (blue) above T_c from a $32^3 \times 4$ lattice, renormalized to the $V_{Q\bar{Q}}(r)$-potential (solid black line).

by the gluonic medium. If we define the difference of the free energy of the system due to the presence of a single test quark in the deconfined phase

$$F_Q(T) := \frac{1}{2} \lim_{r\to\infty} F^1_{Q\bar{Q}}(r,T), \tag{5.9}$$

we obtain together with the findings from fig. 5.7 and fig. 5.9

$$\Delta F^1_{Q\bar{Q}}(r,T) \quad = \quad 2\Delta F^{\bar{3}}_{QQ}(r,T) \tag{5.10}$$

$$\lim_{r\to\infty} F^1_{Q\bar{Q}}(r,T) \quad = \quad \lim_{r\to\infty} F^{\bar{3}}_{QQ}(r,T) = 2F_Q(T). \tag{5.11}$$

Combining (5.10) and (5.11) yields

$$F^1_{Q\bar{Q}}(r,T) = 2\left(F^{\bar{3}}_{QQ}(r,T) - F_Q(T)\right) \tag{5.12}$$

as a good description for the relation of the $Q\bar{Q}$-singlet and the diquark anti-triplet free energy in the deconfined phase. As $F^1_{Q\bar{Q}}$ is known to become T-independent for small distances, so must the rhs of (5.12), thereby identifying the T-dependent contribution to $F^{\bar{3}}_{QQ}$ at small distances. This means, that besides the contribution of the Coulomb interaction at small distances, we find that the free energy necessary to screen the QQ-system in the colour anti-triplet state for $r \to 0$ is that of a single heavy quark, in agreement with elementary SU(3) relations [56].

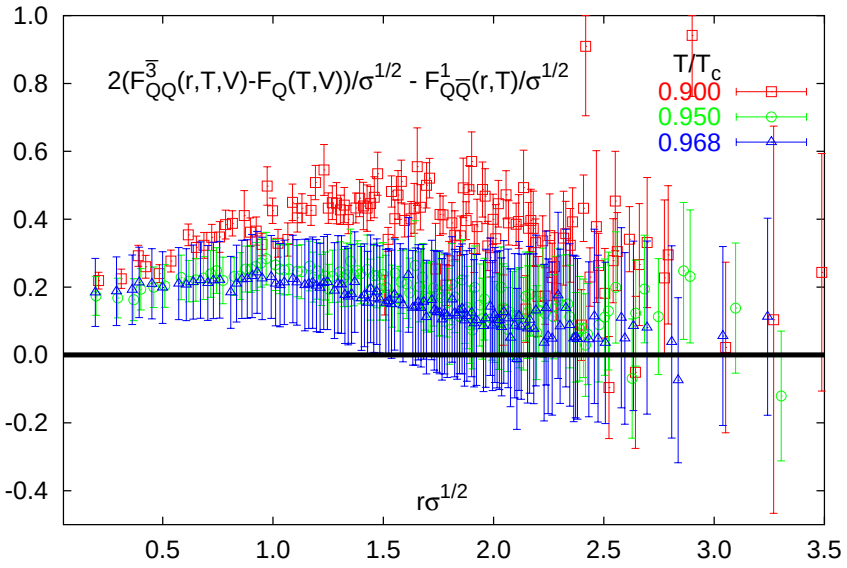

Figure 5.10: $2\left[F^{\bar{3}}_{QQ}(r,T,V) - F_Q(T,V)\right] - F^1_{Q\bar{Q}}(r,T)$ below T_c from a $32^3 \times 8$ lattice.

Furthermore since the entropy contribution in the singlet free energy vanishes for small distances [60], i. e. $S^1_{Q\bar{Q}}(r \to 0, T) = 0$, we must have for the entropy of QQ-antitriplet at small distances $S^{\bar{3}}_{QQ}(r \to 0, T) - S_Q(T) = 0$ and hence

$$S^{\bar{3}}_{QQ}(r \to 0, T) = S_Q(T). \tag{5.13}$$

This shows that the entropy contribution to the QQ-anti-triplet free energy at small distances above T_c stems entirely from the single quark entropy defined by $S_Q = -\frac{\partial F_Q}{\partial T}$. The relation (5.12) can also be used to identify the relation between the internal energies of both colour channels, where the internal energy is defined by $U = -T^2 \frac{\partial F/T}{\partial T}$. This gives

$$U^1_{Q\bar{Q}}(r,T) = 2\left(U^{\bar{3}}_{QQ}(r,T) - U_Q(T)\right), \tag{5.14}$$

and since in the limit $r \to 0$ the internal energy of the $Q\bar{Q}$ singlet system $U^1_{Q\bar{Q}}$ reduces to the potential at $T = 0$ [24], we obtain

$$\lim_{r\to 0} V_{Q\bar{Q}}(r) = 2\left(\lim_{r\to 0} U^{\bar{3}}_{QQ}(r,T) - U_Q(T)\right). \tag{5.15}$$

Since the lhs of (5.15) is T-independent, we find

$$\frac{\partial U^{\bar{3}}_{QQ}(r \to 0, T)}{\partial T} = \frac{\partial U_Q(T)}{\partial T} = T\frac{\partial S_Q(T)}{\partial T}, \tag{5.16}$$

where the last equality follows from standard thermodynamic relations.

We now want to test whether the relation (5.12) can be extended to the confined phase. We show the difference

$$2\left[F^{\overline{3}}_{QQ}(r,T,V) - F_Q(T,V)\right] - F^1_{Q\bar{Q}}(r,T) \tag{5.17}$$

in fig. 5.10, where $F_Q(T,V) = -\ln(\langle|L_3(T,V)|\rangle)$. We observe, that the curves approach zero at large distances, but remaining different from zero at small distances. At intermediate separations, we see the difference (5.17) having a hump, which is more pronounced for smaller temperatures. The interesting finding is that the difference (5.17) does not go to zero for $r \to 0$, but seems to approach a finite value.

5.4 Results in 2-flavour QCD

In QCD with dynamical quarks the $\mathbb{Z}(3)$-symmetry is explicitly broken by the finite quark mass. The Polyakov loops are distributed only in the real sector. Therefore we expect that the diquark free energies are finite in the thermodynamic limit and show no volume dependence even at temperatures below the critical one. Here we will show results obtained for 2-flavour QCD using p4-improved staggered fermions with a quark mass of $m/T = 0.4$. For details on the simulation see [65, 66] and appendix A.1, A.2 and A.3. We use only renormalised quantities in this section and suppress the superscript R. The renormalisation procedure applied is that of chapter 3.2.

In fig. 5.11 the results for $F^{\overline{3}}_{QQ}(r,T)$ are shown in comparison to the singlet $Q\bar{Q}$ free energies below T_c. We observe a behaviour that is quite similar to the results obtained for the diquark and quark-anti-quark free energies. String breaking is seen in both systems and the free energies tend towards the same values at large separations.

The results above T_c in fig. 5.12 show a comparable behaviour to the results in the quenched case. The screening properties of the diquark system are the same as for the quark-antiquark system and in the limit of large distances both free energies tend towards the same asymptotic value.

In the deconfined phase the relation between both free energies and the temperature dependence of the diquark free energies can again be understood in terms of (5.12). This is evident from fig. 5.13(bottom). Below T_c, where a finite $F_Q(T)$ in the thermodynamic limit exists in full QCD, we observe in fig. 5.13(top) both quantities coincide only for large distances, whereas for smaller separations again a hump becomes visible. Fig. 5.14 shows the difference (5.17), which is not V-dependent in full QCD. As in fig. 5.10 in pure gauge theory, we observe that the difference stays finite at small separations. Calculations at even smaller distances may elucidate the situation here further.

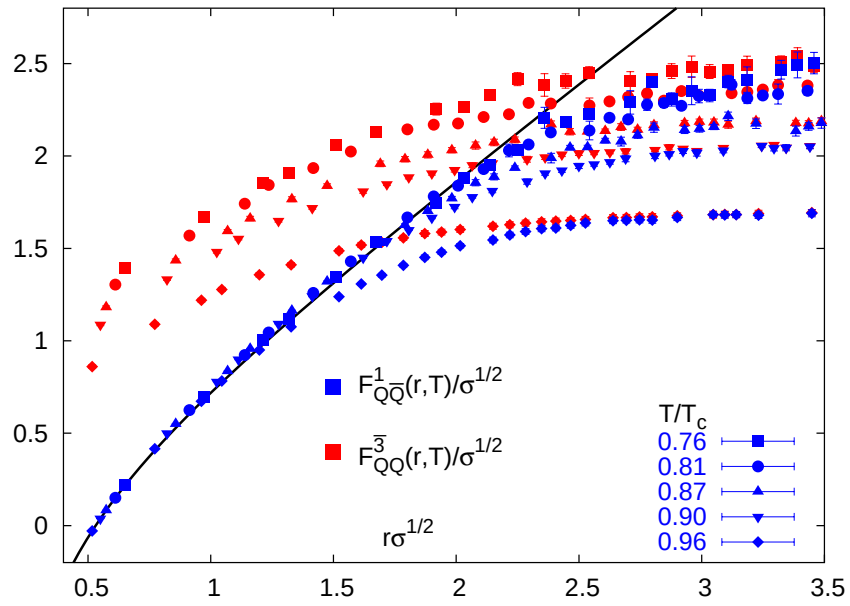

Figure 5.11: $F^{\bar{3}}_{QQ}(r,T)$ (red) and $F^1_{Q\bar{Q}}(r,T)$ (blue) below T_c from a $16^3 \times 4$ lattice in full QCD, renormalized to the $V_{Q\bar{Q}}(T=0)$-potential (solid black line).

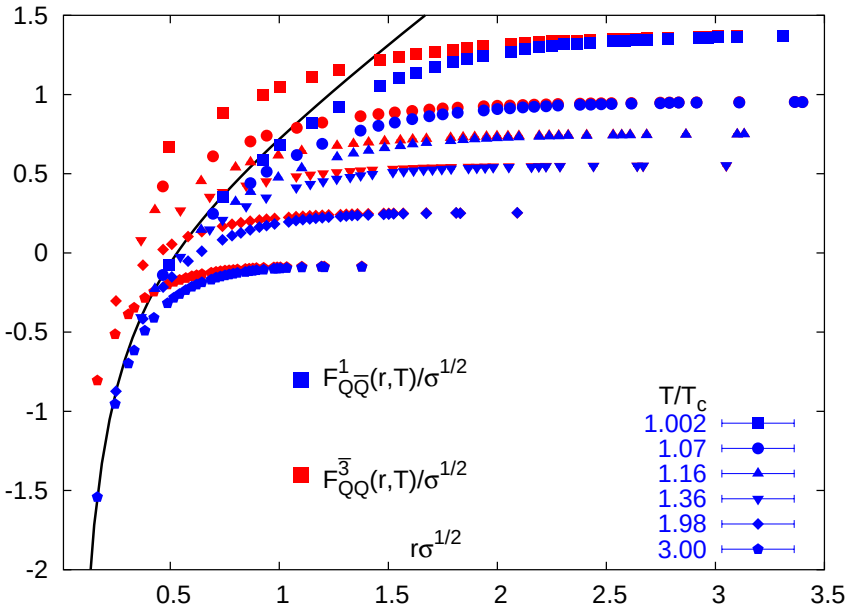

Figure 5.12: $F^{\bar{3}}_{QQ}(r,T)$ (red) and $F^1_{Q\bar{Q}}(r,T)$ (blue) above T_c from a $16^3 \times 4$ lattice in full QCD, renormalized to the $V_{Q\bar{Q}}(T=0)$-potential (solid black line).

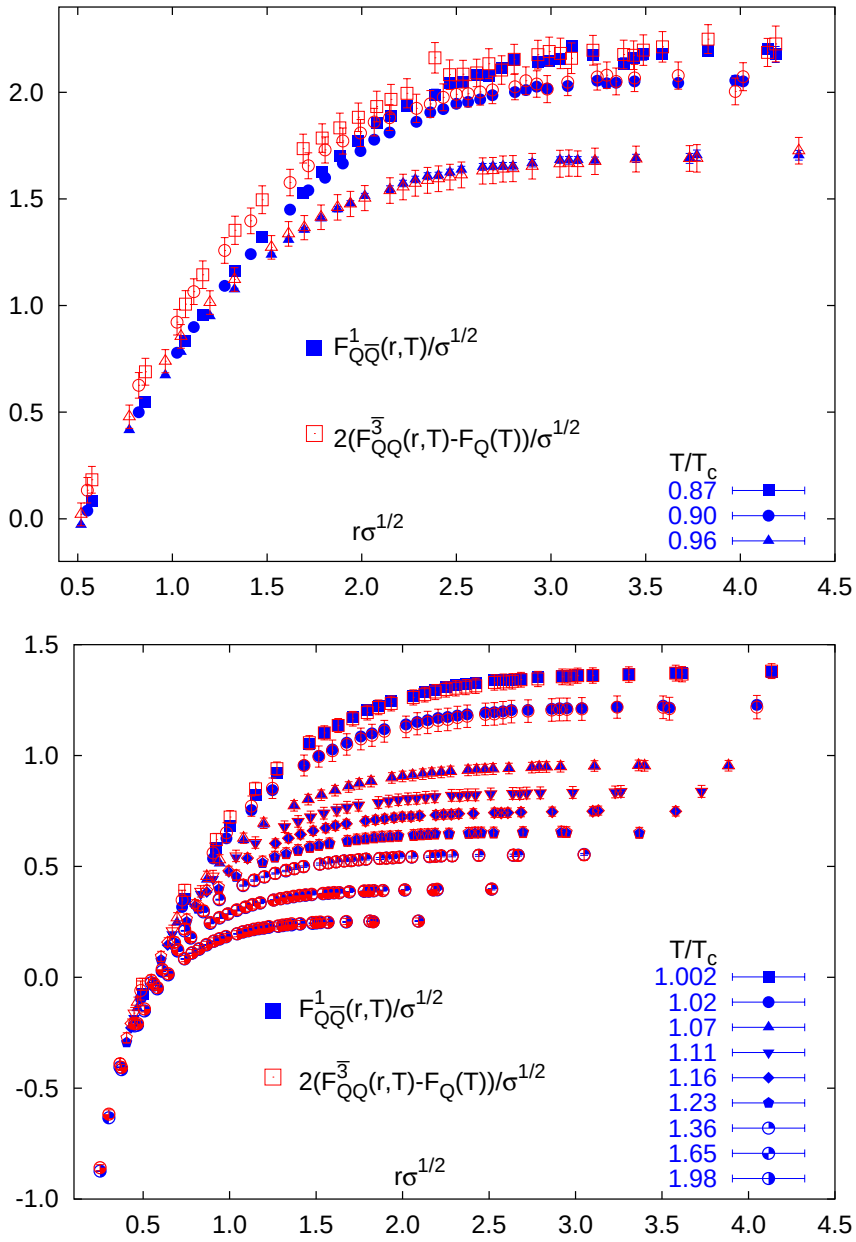

Figure 5.13: $F^{1,R}_{Q\bar{Q}}(r,T)$(blue) compared to $2(F^{\bar{3},R}_{QQ}(r,T) - F^R_Q(T))$ (red) from a $16^3 \times 4$ lattice in full QCD.

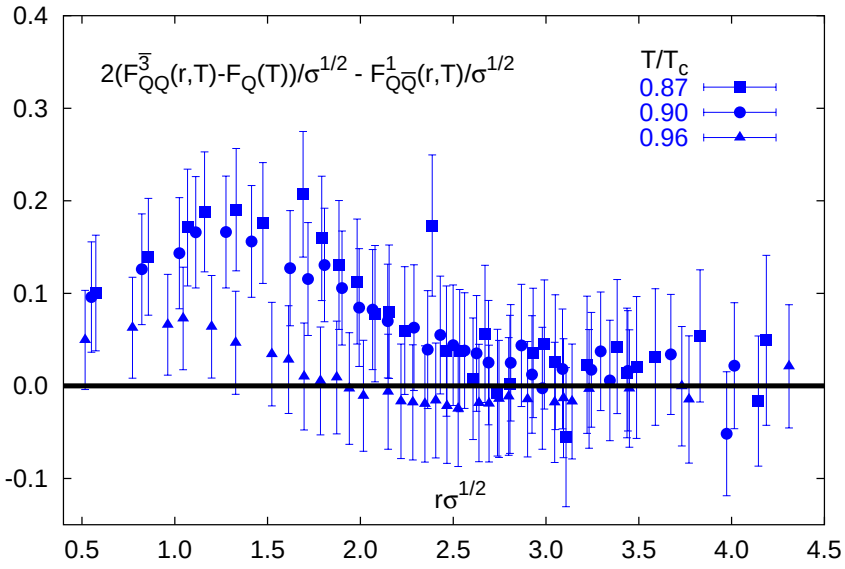

Figure 5.14: $2\left[F^{\overline{3}}_{QQ}(r,T) - F_Q(T)\right] - F^1_{Q\bar{Q}}(r,T)$ below T_c.

6 Baryonic Free Energy

The study of static three quark systems can shed light on the internal structure of the baryon. Of particular interest is the question whether a genuine three body force exists between the quarks below the critical temperature and how the system behaves at finite temperature. At zero temperature the Y-string shape of a baryonic system is supported by recent calculations in lattice QCD [67, 68]. At finite temperature work so far has concentrated on simulations in the maximal Abelian gauge [68, 69], showing a Y-shaped string as well. In this chapter, we address the question of the flux tube shape of the QQQ-singlet colour state below the critical temperature in the quenched approximation of QCD and discuss the appearance of string breaking in 2-flavour QCD. Moreover, we find a simple relation for the free energies in the different colour channels of the baryonic system and the free energies of the QQ-system above T_c.

6.1 Notation and Distance Measure

We first fix the notation for the geometries of the three quark system. In fig. 6.1 we show three quarks Q_i forming a triangle and their distances r_{ij}, where $i, j = 1, 2, 3$. The perimeter of the triangle is then simply

$$P = \sum_{i<j} r_{ij}. \tag{6.1}$$

This is also the total length of a Δ-shaped string, i. e. a string connecting the three quarks along the edges of the triangle. Another possible string shape is a Y-shaped string, where the flux tube emanates from each of the three quarks and has a junction at the Fermat point F of the triangle. The total length of such a Y-shaped string is

$$L = \left[\frac{1}{2} \sum_{i<j} r_{ij}^2 + 2\sqrt{3} A_\Delta \right]^{\frac{1}{2}}, \tag{6.2}$$

where A_Δ is the area of the triangle. The inner angles at the vertices of the triangle are assumed to be smaller than $\frac{2\pi}{3}$, which is the case for all triangles considered in this work. The angle between any two arms of the Y-shaped flux tube is always $\frac{2\pi}{3}$. For equilateral triangles we have the simple relation $P = \sqrt{3}L$. In this work we examine only isosceles triangles, where we set $r_{12} = r_{13} = r_s$ to be the equally long edges and $r_{23} = r_b$ to be the length of the base edge. For equilateral triangles we use $r_{ij} = r$ for all $i, j = 1, 2, 3$.

The three point correlation functions of the Polyakov loop are now obtained as follows (see fig. 6.2). At the positions of the Q_i, we calculate the correlation functions (2.52) -

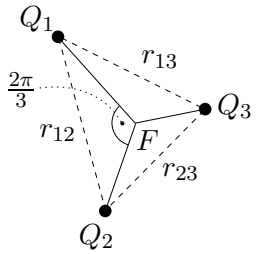

Figure 6.1: Inter quark distances. F is the Fermat point of the triangle. Taken from [22].

(2.55) and compute the average for those Q_i with the same $\{r_{ij}\}$. We obtain a new set of $\{r_{ij}\}$ by holding Q_1 fixed, whereas the two other vertices of the triangle Q_2 and Q_3 are moved simultaneously one point of the lattice in one direction (here:to the left). The base edge r_b connecting this two points preserves thereby its length, which is $r_b = na\sqrt{2}$, where a denotes the lattice spacing and $1 \leq n < \frac{N_\sigma}{2}$ is an integer and describes the number of elementary cells the procedure starts with. The two other edges have equal lengths $r_s = a\sqrt{m^2+n^2}$, where m is another integer which runs between $n \leq m < \frac{N_\sigma}{2}$ for every n by this procedure. Therefore for every n we obtain one equilateral ($n = m$) and several isosceles ($n < m < \frac{N_\sigma}{2}$) triangles. We start with $n = 1$ and repeat the procedure until $n = \frac{N_\sigma}{2} - 1$. We apply this method in both directions of all three spatial dimensions before sweeping Q_1 over the entire spatial lattice. As a consequence of this averaging procedure, the correlators (2.53) and (2.54) for the two colour octet states of the QQQ-system can not be calculated separately. Instead, we only extract the mean of both, which we call $C^8_{QQQ}(r,T)$ from now on. The colour average free energy of the QQQ-system at finite temperature has also been studied in [22].

6.2 $\mathbf{F}^s_{QQQ}$ in Perturbation Theory

In the perturbation series of the free energy of the QQQ-system the contribution of the three gluon vertex vanishes for symmetry reasons [70]. Therefore, neglecting self energy contributions, to order in g^4 the free energy F^s_{QQQ}, where s is the colour symmetry state of the QQQ-system, decomposes into the sum of diquark free energies F^t_{QQ}, which can be in an anti-symmetric anti-triplet ($t = \overline{3}$) or in a symmetric sextet ($t = 6$) state. In order to obey the permutation relations found for the QQQ-system in (2.52) and (2.55) we must then have

$$F^1_{QQQ}(\mathbf{r},T) = \sum_{i<j} F^{\overline{3}}_{QQ}(r_{ij},T) + k_1(T) \tag{6.3}$$

$$F^{10}_{QQQ}(\mathbf{r},T) = \sum_{i<j} F^{6}_{QQ}(r_{ij},T) + k_{10}(T), \tag{6.4}$$

where r_{ij} denotes the distance between the ith and jth quark, $\mathbf{r} = (r_{12}, r_{13}, r_{23})^t$ and $k_n(T)$ with $n = 1, 8, 10$, accounts for the self energy contributions. As can be seen easily

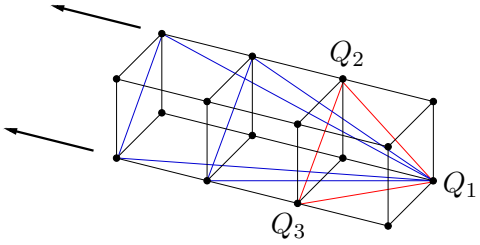

Figure 6.2: Calculation of the three point correlation function of the Polyakov loop. Taken from [22].

from (6.3) and (6.4), the singlet state of the QQQ-system is attractive, because the QQ-anti-triplet is, and the decuplet state repulsive, as the QQ-sextet is (see chapter 5). The QQQ-system in the adjoint colour state is expected to be attractive as well, but weaker than the singlet state [22]. We refrain from discussing the QQQ-octet colour channel here in more detail, since due to the mixture of both octet free energies in our lattice correlator C^8_{QQQ}, we can only gain limited insight in the behaviour of this observable. We note here, that the distance dependence of the free energies in (6.3) and (6.4) can be expressed by the perimeter $P = \sum_{i<j} r_{ij}$ of the triangle.

As for the $Q\bar{Q}$-singlet free energy [24], we expect the QQQ-singlet free energy to become temperature independent at small distances. It was shown in chapter 5, that the residual T-dependence of the QQ-anti-triplet free energy at small distances in the deconfined phase can be removed by subtracting the free energy of a single heavy test quark $F_Q(T) := \frac{1}{2}\lim_{r\to\infty} F^1_{Q\bar{Q}}(r,T)$. Therefore we expect to find in the deconfined phase at small distances the relations

$$F^1_{QQQ}(P,T) = \sum_{i<j} F^{\overline{3}}_{QQ}(r_{ij},T) - 3F_Q(T) \tag{6.5}$$

$$F^{10}_{QQQ}(P,T) = \sum_{i<j} F^{6}_{QQ}(r_{ij},T) - 3F_Q(T), \tag{6.6}$$

where P is the perimeter of the triangle. We will test below, for which quark separations and temperatures the relations (6.5) and (6.6) hold.

6.3 Results in Pure Gauge

We now discuss the results of our calculations in pure gauge theory from $32^3 \times 4$ and $32^3 \times 8$ lattices. We use the renormalisation procedure discussed in chapter 3.2 for the QQ- and the QQQ-free energies. For more details on the simulation see appendices A.1 - A.3 and C. We drop the superscript R for the renormalised quantities, which are plotted using $\sqrt{\sigma}$ to set the scale. The renormalisation procedure applied is that of chapter 3.2.

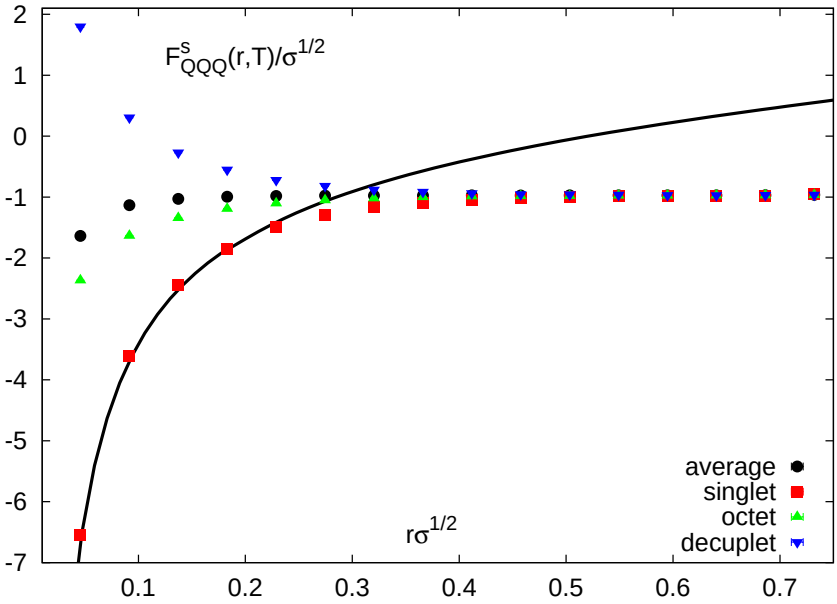

Figure 6.3: Free energies of the colour channels from $32^3 \times 8$ lattice at $T/T_c = 6$. The black line indicates $V_{QQQ}(r)$.

6.3.1 Colour Channels

In fig. 6.3 we show the free energies of the different colour channels and the average free energy for the QQQ-system for equilateral triangles on a $32^3 \times 8$ lattice at $T/T_c = 6$. One can see clearly, that the singlet is strongly, the octet weaker attractive and the decuplet repulsive in agreement with the findings in section 6.2. For large r at a given temperature, all colour channels become flat and approach a common value. The singlet free energy becomes temperature independent at small distances and coincides with the baryonic $T = 0$ potential, which is related to the quark-antiquark potential at vanishing temperature by the ratio of the different Casimir operators, i. e. $V_{QQQ}(r) = \frac{3}{2} V_{Q\bar{Q}}(r)$ for $r\Lambda_{QCD} \ll 1$. We obtain similar plots for all other temperatures above T_c.

6.3.2 Equilateral geometries above T_c

We now compare the free energies of the QQQ-system with the free energy of the QQ-system above T_c. In fig. 6.4 we show $F^1_{QQQ}(r,T)$ and $3F^{\bar{3}}_{QQ}(R,T) - 3F_Q(T)$ over the edge length r of the equilateral triangles and the QQ distance respectively. The second term should be equal to the QQQ-singlet free energy if genuine three body forces are absent, see (6.5). For every temperature we indeed observe $F^1_{QQQ}(r,T)$ and $3F^{\bar{3}}_{QQ}(r,T) - 3F_Q(T)$ coincide throughout the entire distance interval. We find also, that the same is true for $F^8_{QQQ}(r,T)$ and $3\left[\frac{1}{2}F^{\bar{3}}_{QQ}(r,T) + \frac{1}{2}F^6_{QQ}(r,T) - F_Q(T)\right]$, as can be seen in fig. 6.5. Close to T_c, however, F^8_{QQQ} is slightly larger for small separations. In fig. 6.6 we plot

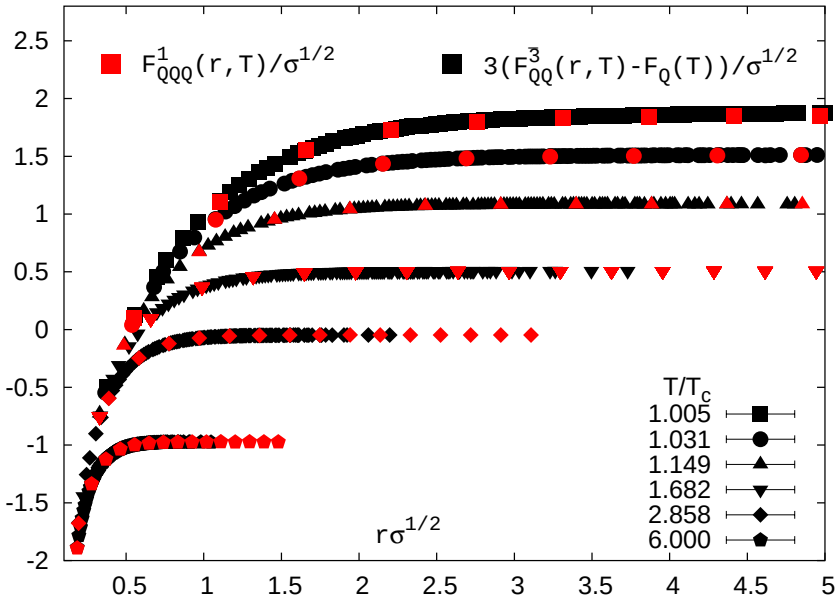

Figure 6.4: $F^1_{QQQ}(r,T)$ and $3\left(F^{\bar{3}}_{QQ}(r,T) - F_Q(T)\right)$ above T_c over r, the edge length r of the equilateral triangles and QQ-distance respectively.

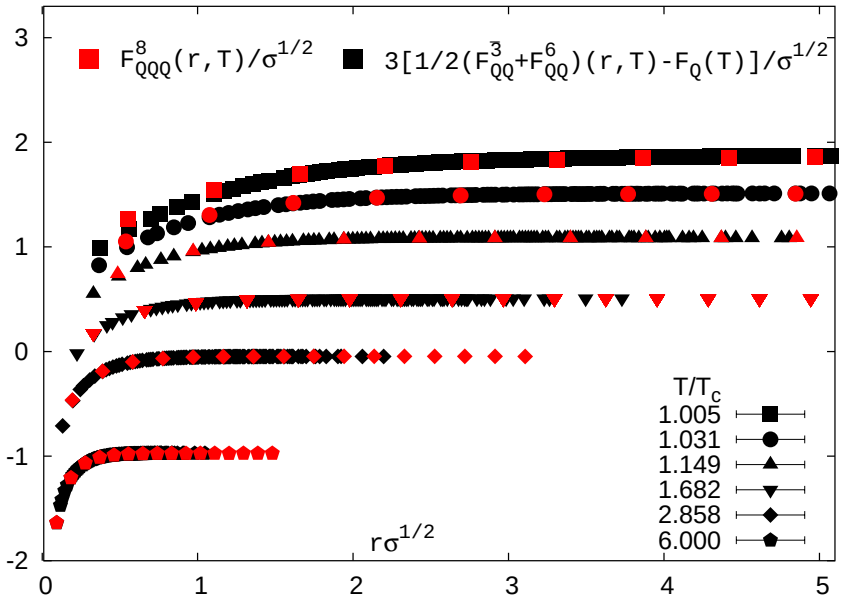

Figure 6.5: $F^8_{QQQ}(r,T)$ and $3\left[\frac{1}{2}F^{\bar{3}}_{QQ}(r,T) + \frac{1}{2}F^6_{QQ}(r,T) - F_Q(T)\right]$ above T_c over r, the edge length r of the equilateral triangles and QQ-distance respectively.

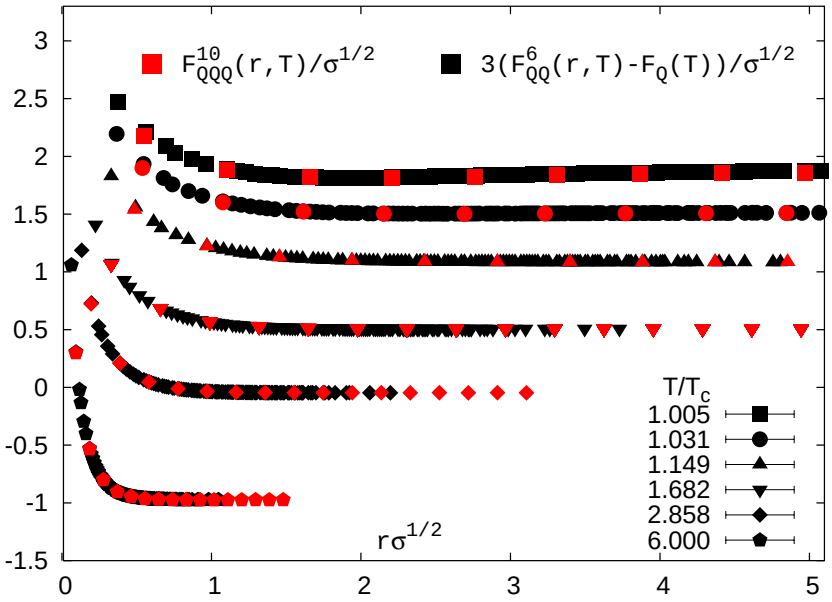

Figure 6.6: $F^{10}_{QQQ}(r,T)$ and $3\left(F^{6}_{QQ}(r,T) - F_Q(T)\right)$ above T_c over r, the edge length r of the equilateral triangles and QQ-distance respectively.

$F^{10}_{QQQ}(r,T)$ and $3F^{6}_{QQ}(r,T) - 3F_Q(T)$. Again we observe that both observables coincide and therefore we find (6.6) to be valid above T_c for all separations considered here.

6.3.3 Isosceles geometries above T_c

In order to subject the data for all geometries and temperatures above T_c calculated to this test, we plot $\Delta F(P,T) = F^{1}_{QQQ}(P,T) - \sum_{i<j} F^{3}_{QQ}(r_{ij},T) + 3F_Q$ in fig. 6.7. If the QQQ-singlet free energy can be expressed in terms of QQ-anti-triplet free energies and $F_Q(T)$ according to (6.5), $\Delta F(P,T)$ should vanish. This is fulfilled to a very good degree for all perimeters except the smallest ones close to the critical temperature, which is probably due to the vicinity of the phase transition. Again, the same findings can be drawn for the QQQ-decuplet free energy in fig. 6.8. We omit the investigation of the non-equilateral baryonic octet free energies here, since their analysis is more complicated due to the contribution of both anti-triplet and sextet QQ-free energies.

In total, we find F^{1}_{QQQ} and F^{10}_{QQQ} are related to the QQ-free energies according to (6.5) and (6.6) for all separations and temperatures in the deconfined phase. For the QQQ-octet free energy we have found the average of QQ-anti-triplet and -sextet free energies to describe F^{8}_{QQQ} well for equilateral geometries except close to T_c at the smallest separations.

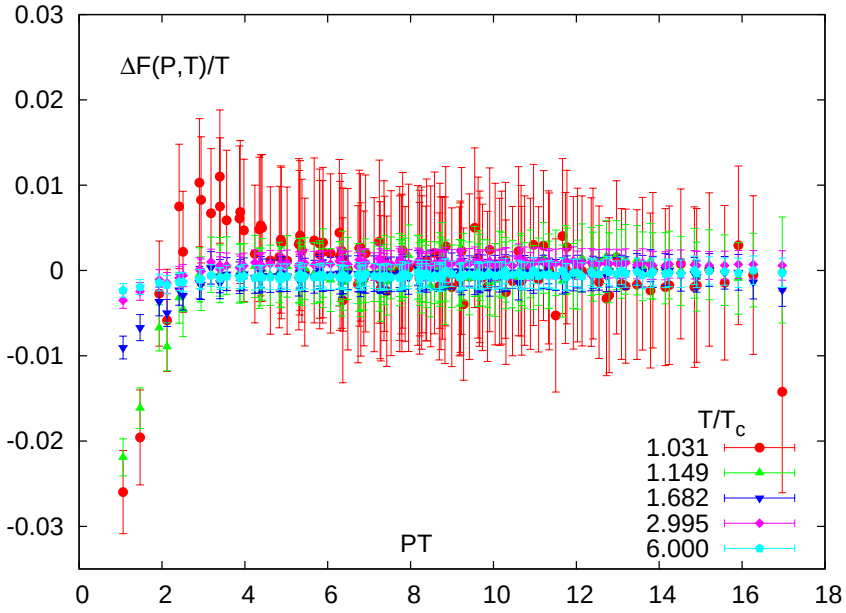

Figure 6.7: $\Delta F(P,T) = F^1_{QQQ}(P,T) - \sum_{i<j} F^{\bar{3}}_{QQ}(r_{ij},T) + 3F_Q$ above T_c over the perimeter P for all geometries calculated.

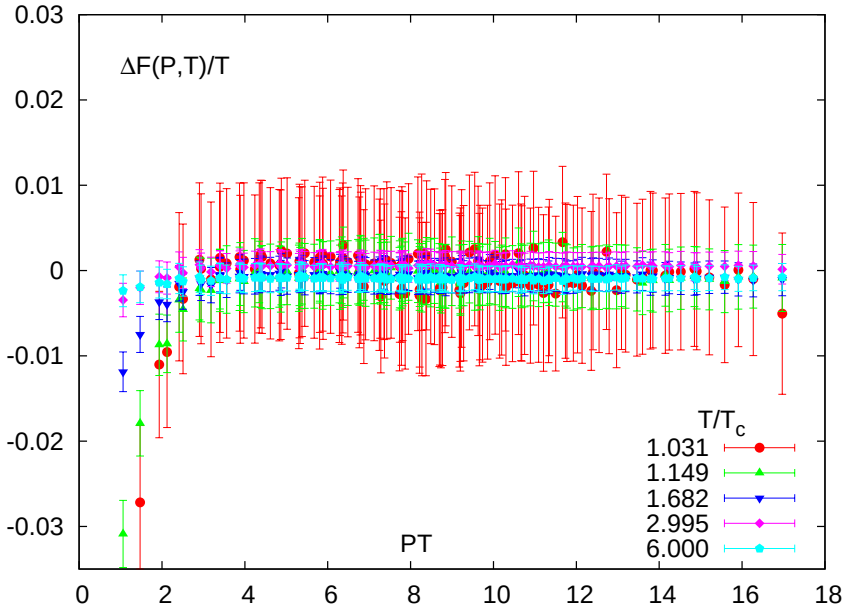

Figure 6.8: $\Delta F(P,T) = F^{10}_{QQQ}(P,T) - \sum_{i<j} F^{6}_{QQ}(r_{ij},T) + 3F_Q$ above T_c over the perimeter P for all geometries calculated.

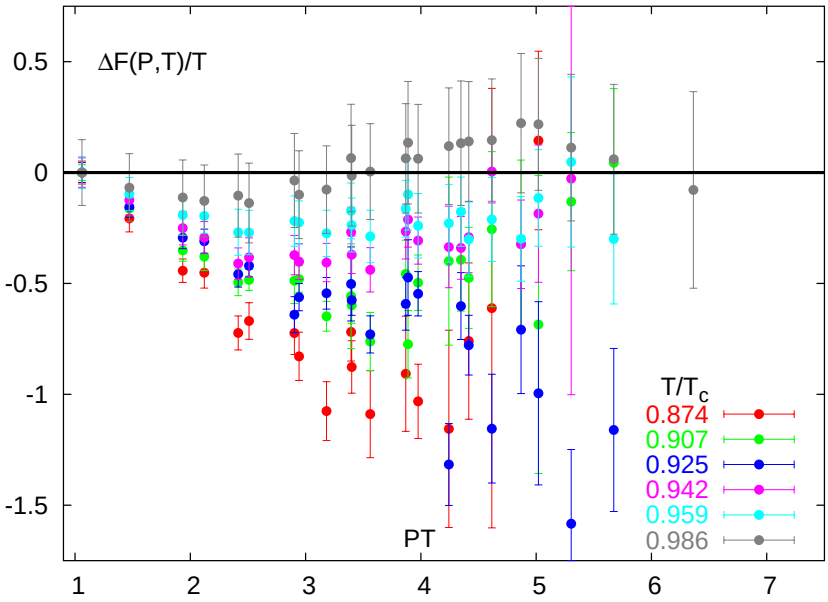

Figure 6.9: $\Delta F(P,T) = F^1_{QQQ}(P,T) - \sum_{i<j} F^{\bar{3}}_{QQ}(r_{ij},T)$ below T_c over the perimeter P for all geometries calculated. $\Delta F(P_{\min},T)$ has been set to zero, where $P_{\min}$ is the smallest perimeter calculated.

Together with the findings for the entropy and internal energy of $F^{\bar{3}}_{QQ}$ in the deconfined phase in chapter 5.3, we can follow from (6.5), that

$$U^1_{QQQ}(P,T) = \frac{1}{2}\sum_{i<j} U^1_{Q\bar{Q}}(r_{ij},T) \quad \text{and} \quad S^1_{QQQ}(P,T) = \frac{1}{2}\sum_{i<j} S^1_{Q\bar{Q}}(r_{ij},T) \tag{6.7}$$

are valid for all isosceles geometries studied in this work above T_c in pure gauge theory.

6.3.4 Free energies below T_c

We now examine the QQQ-free energies below T_c. We start by looking at the relation of the QQQ-singlet and the QQ-anti-triplet free energies. If $F^1_{QQQ}(P,T)$ can be expressed in terms of the sum of $F^{\bar{3}}_{QQ}(r_{ij},T)$ also below T_c, i. e. a Δ-ansatz for the flux tube shape together with the same string tension holds, then $\Delta F(P,T) = F^1_{QQQ}(P,T) - \sum_{i<j} F^{\bar{3}}_{QQ}(r_{ij},T)$ should be equal to a T-dependent constant $k(T)$ for all P, in the spirit of (6.3). In fig. 6.9 we show $\Delta F(P,T)/T$ for $T < T_c$ over the perimeter of the geometries P. Since below T_c no proper $F_Q(T)$ can be defined, we have set $\Delta F(P_{\min},T) = 0$, where $P_{\min}$ is the smallest perimeter calculated. Therefore $k(T)$ should vanish. We can see clear deviations of $\Delta F(P,T)$ to smaller values, most strongly for the lowest temperatures, deviations from zero becoming smaller with growing temperature. For $T/T_c = 0.986$ we have $\Delta F(P) \approx 0$.

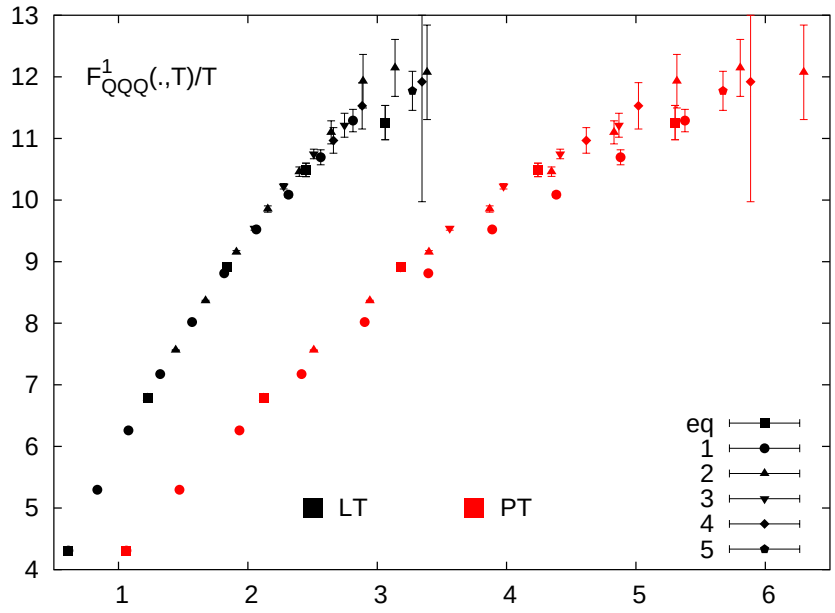

Figure 6.10: $F^1_{QQQ}(.,T)$ at $T/T_c = 0.925$ over the Y-string length L and the perimeter P for equilateral geometries (eq) and geometries with base length $r_b = na\sqrt{2}$, where n is given in the legend.

Hence, $F^1_{QQQ}(P,T)$ can not be expressed in terms of the sum of $F^{\bar{3}}_{QQ}(r_{ij},T)$ except close to the critical temperature. We are left with two possibilities now. First, we could still have a Δ-shaped flux tube, but with a different string tension than that we observe for the QQ-anti-triplet. Since we see $\Delta F(P,T) < 0$, we expect the string tension to be smaller than in the QQ-anti-triplet. In this case the perimeter P would still be the right distance measure for the QQQ-singlet free energy, i. e. F^1_{QQQ} should be a smooth function of P for all geometries a flux tube can form. Or, secondly, the flux tube is Y-shaped and L is the right distance measure. In this case, F^1_{QQQ} should be a smooth function of L for all geometries a flux tube can form.

To elaborate more on the shape of the flux tube, we take a closer look at the QQQ-singlet free energy at a particular temperature below T_c for different geometries as a function of L and P. For equilateral triangles there exist a simple geometrical relation between the length of a Y-shaped flux tube L and the length of a Δ-shaped flux tube P, which is $P = \sqrt{3}L$. Hence for equilateral geometries the QQQ-singlet free energy is a smooth function in both or none ansätze. For more general geometries like the isosceles triangles we have considered here, no simple relation between L and P exists. This may help to clarify the situation more directly. Therefore we plot the QQQ-singlet free energy at $T/T_c = 0.925$ over the Y-string length L and the perimeter P in fig. 6.10 for equilateral geometries and also isosceles geometries up to $n = 5$. We observe that the QQQ-singlet free energy over L is a smooth function for all geometries calculated, whereas in the curve over the perimeter P different branches become visible depending on the geometry, most

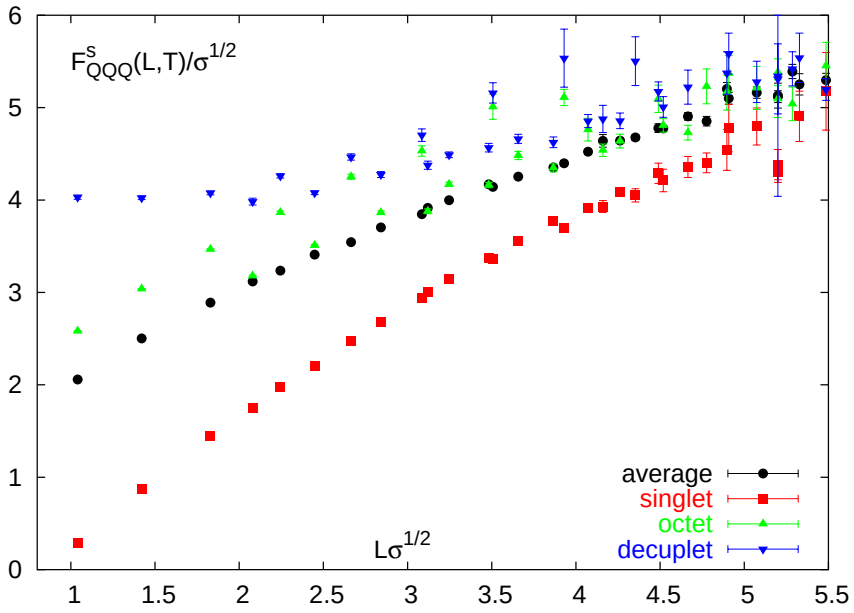

Figure 6.11: Free energies of the colour channels over the Y-string length L at $T/T_c = 0.925$ for all geometries calculated.

prominently for the $n = 1$ triangles. For large L, we see also a branch departing from the main curve for $n = 1$-geometries. This effect is, however, much weaker than for the P case and can be explained by the fact that an oblong geometry reaches its large distance value for comparatively smaller L than those geometries closer to the equilateral shape. Therefore we conclude, that the shape of the flux tube in the QQQ-singlet system is indeed that of the Y-ansatz at least at this temperature and its string length L is the right distance measure for the system.

Having established that, we take a look at the other colour channels below T_c and test whether they display a smooth behaviour as a function of L as well. In fig. 6.11 we show the different colour channels of the QQQ-free energy at $T/T_c = 0.925$ over the Y-string length L. We see again that the singlet is the most attractive channel followed by the average free energy, which is also a smooth function of L. The octet channel is still attractive, but weaker than the average free energy. The decuplet free energy is attractive for large L but becomes flat at smaller L, hinting at a turnover and at a repulsive behaviour at even smaller L. Both the decuplet and the octet channel are not smooth functions over either L and P, but become volatile for $L\sqrt{\sigma} \gtrsim 2$. This suggests that no flux tube may form in these two channels, although the octet free energy shows an attractive behaviour.

Finally, we examine the behaviour of F^1_{QQQ} and especially the string tension with temperature. In fig. 6.12 we show the QQQ-singlet free energy over L for all temperatures below T_c. We observe $F^1_{QQQ}(L,T)$ to nearly coincide at distances $L\sqrt{\sigma} \lesssim 4$ for all temperatures $T/T_c \leq 0.959$. Therefore the Y-shape ansatz for the flux tube is viable

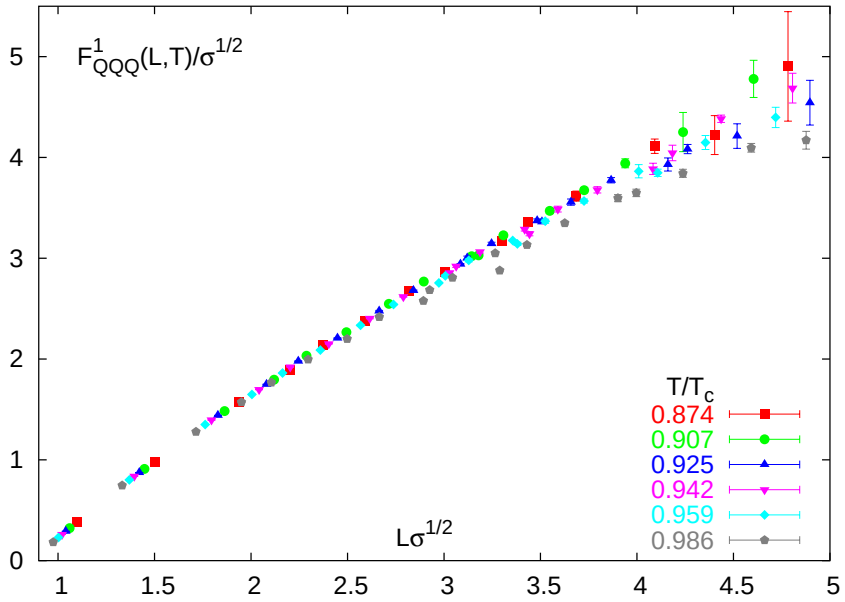

Figure 6.12: $F^1_{QQQ}(L,T)$ below T_c over the Y-string length L for all geometries.

to this temperature as well. We note here, that even for the largest distances analysed here ($L\sqrt{\sigma} \approx 4.5$), we do not observe a significant change with temperature in $\sigma(T)$ for $T/T_c \leq 0.959$. In order to see a dependence of the string tension on temperature for the QQQ-singlet, we will probably have to go to larger L. At $T/T_c = 0.986$ we see that $F^1_{QQQ}(L,T)$ deviates to smaller values for $L\sqrt{\sigma} \gtrsim 3$. As was already seen in fig. 6.9, for this temperature $\Delta F_{QQQ}(P,T) \approx 0$, i. e. a Δ-ansatz for the flux tube shape is possible as well at $T/T_c = 0.986$. This may indicate that the broadening of the flux tube profile with growing temperature has reached the point where the Y-shaped flux tube comprises the entire inner area of the triangular geometry of the QQQ-system and thus becomes indistinguishable from a Δ-shaped flux tube at $T/T_c = 0.986$.

6.4 Results in Full QCD

We now study the baryonic free energies in 2-flavour QCD from a $16^3 \times 4$ lattice using staggered quarks with $m/T = 0.4$. For details see appendices A.1 - A.3 and C. We discuss here our results for equilateral geometries. Since the spatial extension of the lattice is small, we obtain only few data for non-equilateral geometries and hence we do not analyse this data here in more detail. We used the renormalisation procedure outlined in chapter 3.2 for the baryonic free energies.

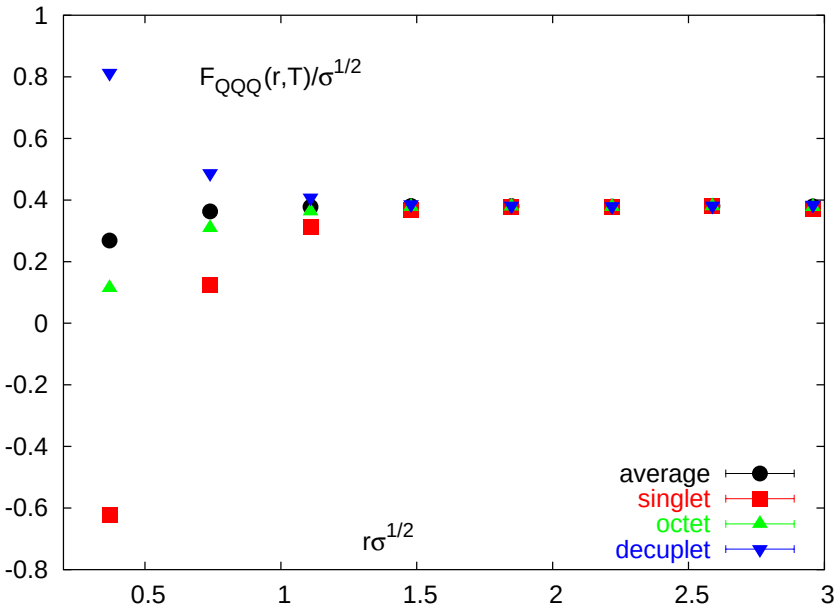

Figure 6.13: Free energies of the colour channels in 2-flavour QCD from a $16^3 \times 4$ lattice at $T/T_c = 1.98$.

6.4.1 Colour Channels

In fig. 6.13 we show the free energies of equilateral geometries of the different colour channels at $T/T_c = 1.98$. Like in the pure gauge case, we observe the singlet to be strongly, the octet weaker attractive and the decuplet to be repulsive. For large distances r the free energies of all colour channels become flat and approach a common value. Again, we obtain similar plots for all $T > T_c$.

6.4.2 Singlet free energy and string breaking

We now compare the free energy of the QQQ-singlet with the free energy of the QQ-anti-triplet for 2-flavour QCD. In fig. 6.14 we plot $F^1_{QQQ}(r,T)$ and $3F^{\overline{3}}_{QQ}(r,T) - 3F_Q(T)$ over the edge length r of the equilateral triangles and QQ-distance respectively. As in pure gauge theory, both curves coincide for all temperatures above T_c. Thus we find the QQQ-singlet free energy of equilateral geometries to be describable as the sum of three QQ-anti-triplet free energies and $F_Q(T)$ as well in 2-flavour QCD above T_c. Moreover, we find the relations of (6.7) to be valid for equilateral geometries in 2-flavour QCD.

Below T_c we expect to see string breaking also in the QQQ-singlet free energy, the breaking mechanism being more involved than in the meson case [69]. Indeed, except at $T/T_c = 0.96$, where both quantities agree, we see deviations for the QQQ-singlet. In fig. 6.15 we compare $F^1_{QQQ}(L,T)$ in 2-flavour QCD (black) ($T/T_c = 0.87, 0.90$) and pure gauge theory (red) ($T/T_c = 0.874, 0.907$) for all geometries calculated, where the pure gauge data stems from the $32^3 \times 4$ lattice. We observe the $N_f = 2$ free energies to

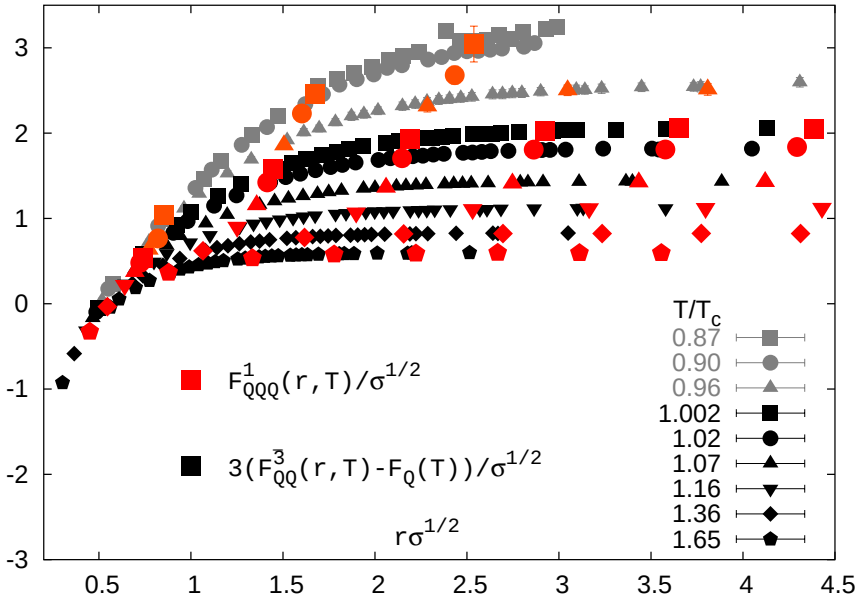

Figure 6.14: $F^1_{QQQ}(r,T)$ and $3(F^{\bar{3}}_{QQ}(r,T) - F_Q(T))$ over r, the edge length of the equilateral triangles and QQ-distance respectively.

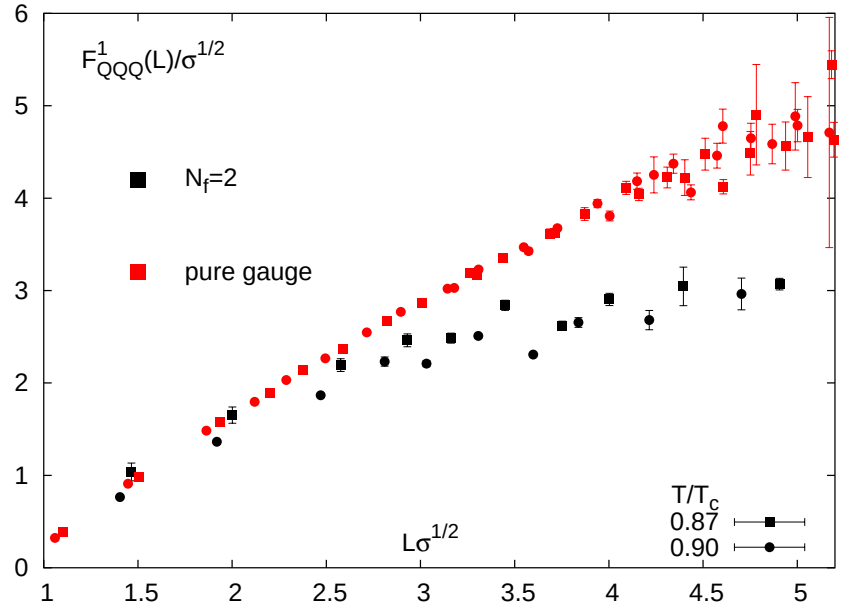

Figure 6.15: Comparison of $F^1_{QQQ}(L,T)$ in 2-flavour QCD (black) and pure gauge theory (red) for two temperatures below T_c. See text.

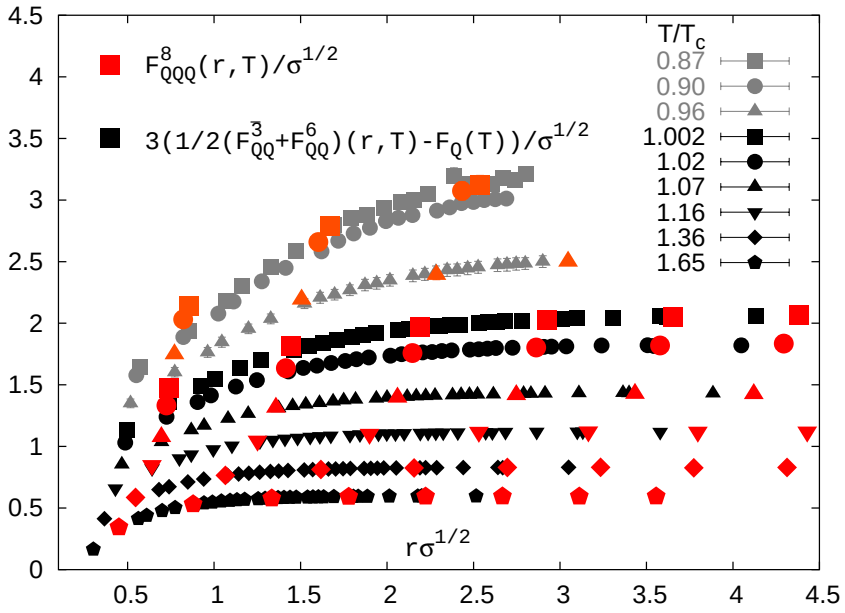

Figure 6.16: $F^8_{QQQ}(r,T)$ and $3(\frac{1}{2}(F^{\bar{3}}_{QQ}+F^6_{QQ})(r,T)-F_Q(T))$ over r, the edge length of the equilateral triangles and QQ-distance respectively.

deviate to smaller values and eventually become flat. Specifying a definite value for the string breaking distance is quite difficult given the present data. Nevertheless we can give a rough estimate for the distance at which the pure gauge free energies assumes the asymptotic value of the 2-flavour free energies, which is $L\sqrt{\sigma} \approx 3$. This value is larger than those found for the $Q\bar{Q}$-system [29], in accordance with the findings in [69]. Since observing a clear string behaviour is prevented by string breaking, we refrain from an analysis of the flux tube shape below T_c in 2-flavour QCD.

6.4.3 Octet and decuplet free energies

Fig. 6.16 shows $F^8_{QQQ}(r,T)$ and $3(\frac{1}{2}(F^{\bar{3}}_{QQ}+F^6_{QQ})(r,T)-F_Q(T))$ for equilateral geometries in 2-flavour QCD. We observe like in the pure gauge case coincidence of both curves for all $T > T_c$ and distances r except for the first data point of $F^8_{QQQ}(r,T)$ at temperatures $T/T_c = 1.002, 1.02, 1.07$, which deviate to slightly larger values. This maybe due to insufficient statistics close to T_c for the QQQ-octet free energy, which has the weakest signal of all colour channels and is therefore prone to noise. Below T_c the two quantities do not agree except for $T/T_c = 0.96$ at large r. Again, we find insufficient statistics to be responsible, which is even more true for $T < T_c$.

For the QQQ-decuplet free energies we plot $F^{10}_{QQQ}(r,T)$ and $3(F^6_{QQ}(r,T)-F_Q(T))$ for equilateral geometries in fig. 6.17. Like in pure gauge theory, we observe both curves to coincide for all temperatures above T_c and distances r. The situation below T_c is analogous to the singlet case. At the temperature closest to T_c both curves coincide for

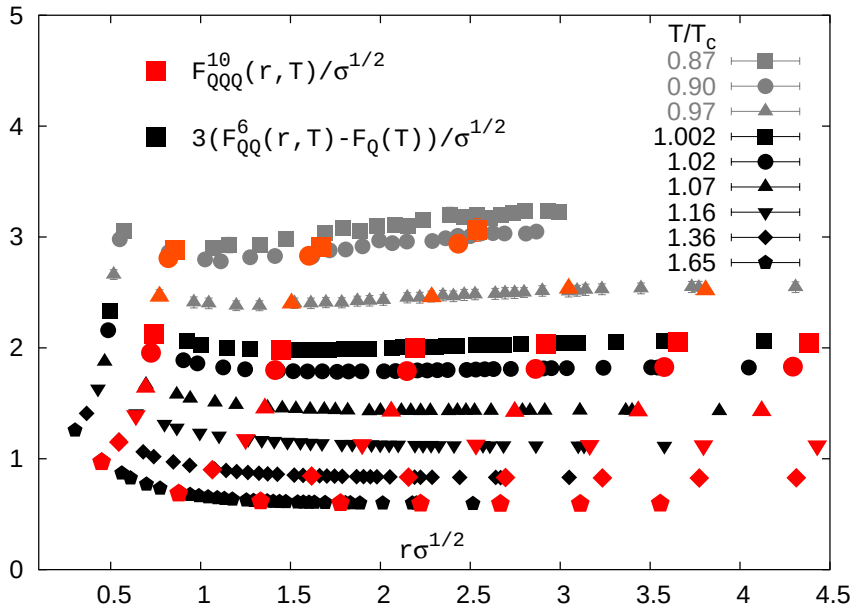

Figure 6.17: $F^{10}_{QQQ}(r,T)$ and $3(F^{6}_{QQ}(r,T) - F_Q(T))$ over r, the edge length of the equilateral triangles and QQ-distance respectively.

all r, at smaller T we observe deviations to smaller values for $F^{10}_{QQQ}(r,T)$.

6.5 Screening mass and diquark and baryonic bound states

The comparison to the quark-anti-quark free energies in chapter 5.3 and 5.4 shows that the diquark anti-triplet free energies are related to those of the $Q\bar{Q}$-singlet system by the ratio of their Casimir factors, i.e. by a factor of two, in good approximation for all temperatures in the deconfined phase at all distances. As (6.5) shows, the corresponding statement is also true for the relation of the free energies of the QQQ-singlet and the QQ-anti-triplet, i. e. a resulting ratio of 3. This applies to both pure gauge theory and 2-flavour QCD. As a consequence, the screening masses extracted from the large distance behaviour of these free energies, employing the relation (2.74),

$$\Delta F^{s}_{n\bar{n}}(r,T) = -\frac{\alpha^{s}_{n\bar{n}}(r,T)}{r}\, e^{-m^{s}_{n\bar{n}D}(T)\, r} \quad rT \gg 1, \tag{6.8}$$

are independent of the colour symmetry state $s = 1, \overline{3}$ as well as the static quark content $(n,\bar{n}) = (1,1);(2,0);(0,2);(3,0);(0,3)$ of the investigated systems. This makes clear, that the screening mass m_D reflects a property of the thermal medium, i. e. its influence on the gluons that mediate the interaction between static quark sources, and not of the particular heavy quark system immersed in it. In [30] the extraction of the screening masses obtained from two and three quark systems is extended to the case of systems at finite chemical potential.

The relation of the various heavy quark systems in terms of the ratios of the corresponding Casimirs extends to the internal energies $U^s_{n\bar{n}}$ as well, as we have shown in (5.14) and (6.7). This justifies the use of this relations in potential models, which utilise inner energies or free energies to solve the Schrödinger equation for the system in question [71]. The diquark is found to be only weakly bound in the deconfined phase and will dissociate quickly. Therefore it is expected that QQ bound states do not play an important rôle for the properties of the Quark Gluon Plasma near T_c, at least for zero baryon densities. Baryonic bound states may be bound more strongly, where their binding energy is greater than the temperature at T_c and comparable up to $1.3\,T_c$. We note, that when the binding energy becomes of the order of the temperature, the bound state may dissociate easily and therefore cease to contribute to the properties of the QGP. Thus baryonic bound states can play some rôle for temperatures near above T_c according to [71]. The findings for heavy mesons suggest that they are most strongly bound systems considered here and dissociate at temperatures clearly larger than T_c. Therefore mesons are expected to contribute significantly to the properties of the QGP not too far from the phase transition temperature. Similar results have been found in other calculations using various potentials to solve the Schrödinger equation [28, 72, 73] and the Maximum Entropy Method (MEM) to extract mesonic spectral functions [74, 75, 76]. In order to avoid the heavy quarks approximation for the diquark, one could apply MEM to finite temperature diquark correlators in the future.

7 Conclusion

We will now summarise our work and give an outlook on possible future directions of research.

We have calculated the Polyakov loop in representations $D = 3, 6, 8, 10, 15, 15', 24, 27$ and diquark and baryonic Polyakov loop correlation functions with fundamental sources in SU(3) pure gauge theory and 2-flavour QCD with staggered quarks and $Q\bar{Q}$-singlet correlation functions with sources in the fundamental and adjoint representation in SU(3) pure gauge theory. For the gauge dependent free energies we fixed to Coulomb gauge employing an overrelaxation algorithm.

We extended the renormalisation procedure for the $Q\bar{Q}$-singlet free energy [24], where the sources are in the fundamental representation, to the case of $Q\bar{Q}$-singlet free energies with adjoint sources. We found it to be sound and could establish that the effective renormalisation constants for both representations agree within errors. Furthermore, we proposed and tested the N_τ-variation method as a new renormalisation procedure for the Polyakov loop. The good agreement of the two renormalisation procedures indicates that the renormalisation constants indeed depend only on the bare coupling rather than on the temperature, i. e. renormalised coupling, as assumed in [56]. The new procedure was applied to Polyakov loops for various representations in SU(3) pure gauge theory. The bare Polyakov loops obey Casimir scaling to a good degree for temperatures down close to T_c. Together with the good agreement with Casimir scaling for the renormalisation constants this behaviour persists for the renormalised Polyakov loops as well for the representations and temperatures analysed.

Below T_c we were able to extend the volume scaling of the random walk model [58] to arbitrary representations and could show, that $\langle |L_D| \rangle \neq 0$ for representations with zero triality in the thermodynamic limit. We determined their actual value for $D = 8$ in SU(3) pure gauge theory. For $D = 10$ and $D = 27$ we were not able to extract $\langle L_D \rangle$ in the thermodynamic limit, but we could derive upper limits, which are $\langle \mathrm{Re}\, L_{10} \rangle < 1.4 \times 10^{-4}$ and $\langle L_{27} \rangle < 4.75 \times 10^{-5}$. After renormalisation, we discussed L_8^R in the vicinity of the phase transition temperature and were able to determine asymptotic values of the adjoint free energy F_∞ and the values for the two alternative definitions for the string breaking distance of the adjoint $Q\bar{Q}$-singlet free energy below T_c. We found F_∞ and $r_{\mathrm{string}}(V_8)$ to decrease to around 80 % of their corresponding vacuum value close to T_c. The string breaking distance $r_{\mathrm{string}}(F_8)$ was found to have a systematically smaller value than $r_{\mathrm{string}}(V_8)$ by about 0.15 fm.

In 2-flavour QCD we have investigated $\langle L_D \rangle$ and we observed Casimir scaling to be realised in the bare Polyakov loop for various representations down close to T_c. Below $1.5\,T_c$ we saw a *violation* of Casimir scaling when entering the transition region which continues to the smallest temperatures calculated. Another interesting and straight-

forward application of the N_τ-variation method might be the renormalisation of the plaquette.

For future investigations the determination of L_{10}^R and L_{27}^R below T_c might be desirable, though this will need spatial lattices sizes far bigger than those accessible today. An extension of the analysis of these observables, i. e. the Polyakov loop in higher representations above T_c and L_8^R below T_c, to non-zero values of the chemical potential is possible. Moreover, the computation of the torelon, i. e. a closed Wilson line in a spatial direction, and its $Q\bar{Q}$-like correlators could provide a new way of calculating the temperature dependence of the spatial string tension.

For static quark-anti-quark free energies in higher representations we showed that Casimir scaling in $F^1_{Q\bar{Q},3}(r,T)$ and $F^1_{Q\bar{Q},8}(r,T)$ is realised to a good degree for all separations r and temperatures $T/T_c \geq 1.682$. For lower temperatures above T_c and for all temperatures below T_c considered here, deviations occur already at small distances at the level of 5-10 %. Moreover, we have shown that Casimir scaling is violated for the colour average $Q\bar{Q}$ free energies in the temperature range 0.9-3 T_c for the fundamental, sextet and adjoint representations.

In SU(3) pure gauge theory we investigated the volume scaling of the anti-triplet diquark free energy below and above T_c with sources in the fundamental representation. Below T_c we found the anti-triplet correlator to vanish in the thermodynamic limit like $\langle L_3 \rangle$. Despite these divergencies the r-dependence of the diquark free energies shows non-trivial behaviour. Above the critical temperature $C^{\overline{3}}_{QQ}$ was found to be constant with V. For the renormalised QQ-free energies we observed screening in the anti-triplet and anti-screening in the colour sextet channel. Both free energies approach a common cluster value, which coincides with that of the $Q\bar{Q}$-system. We were able to show, that in the deconfined phase $F^{\overline{3}}_{QQ}$ is related to $F^1_{Q\bar{Q}}$ by a factor of 2 for the r-dependence with an additional contribution of the free energy of a single static quark. The same results were found in 2-flavour QCD above T_c. Moreover, we observed in 2-flavour QCD string breaking in $F^{\overline{3}}_{QQ}$ below T_c.

Finally, we investigated the free energy of the static baryonic system in its different colour symmetry states. We found that the QQQ-singlet and the QQQ-decuplet free energies can be described in terms of QQ-free energies plus a $F_Q(T)$ contribution for all isosceles geometries and for equilateral geometries for the QQQ-octet free energies except close to T_c in the deconfined phase in SU(3) pure gauge theory. This statement holds for equilateral geometries in the deconfined phase of 2-flavour QCD as well.

Below T_c we were able to show, that the QQQ-system in the colour singlet state has a Y-shaped flux tube and that the string tension $\sigma(T)$ of the system shows no significant dependence on T for $T < 0.959\,T_c$ and the distances investigated in this work. Larger separations would be needed to analyse the temperature dependence of the string tension. Moreover, we demonstrated that most likely no flux tube forms in the QQQ-octet and -decuplet free energies at the distances analysed here in the confined phase and that the QQQ-free energy of the colour average channel has a Y-shaped flux tube as well. In 2-flavour QCD we found string breaking in F^1_{QQQ} below T_c and were able to give a rough estimate for the string breaking distance, which is $L\sqrt{\sigma} \approx 3$.

As a consequence of the relation of the QQ- and QQQ-systems with the ratio of the Casimirs to the $Q\bar{Q}$-system, we were able to make clear, that the screening mass extracted from the large distance behaviour of the corresponding free energies is the same in all three systems and therefore describes the screening properties of the medium. An extension of diquark and baryonic free energies to finite chemical potentials has been done in [30]. Moreover, the demonstration of the relation of the free energies of these three systems by their Casimir ratios suggests that they can be used in potential models for the extraction of bound states temperatures in the QGP [71]. A straightforward application of the Casimir ratio rule found for the diquark and baryonic system in the deconfined phase could be the prediction of tetra- and pentaquark free energies above T_c, which have – to our knowledge – not been calculated at finite temperature and are expected to be difficult to obtain due to weak signals.

A QCD on the Lattice

A.1 Notation, Action, Scale

We regularise the path integral in (2.1) by introducing a spacetime lattice of size $N_\sigma^3 \times N_\tau$ with lattice spacing a, where N_σ is the number of lattice sites in a spatial direction and N_τ the number of points in the Euclidean time direction. The volume V of the system and the temperature T are then obtained by

$$V = (aN_\sigma)^3 \quad \text{and} \quad T = \frac{1}{aN_\tau}. \tag{A.1}$$

As gauge invariance is the central construction principle of quantum field theories and therefore for QCD as well, we introduce *link variables* $U_\mu(x)$, which are the parallel transporter from the lattice point x in direction $\mu = 1, \ldots, 4$ to the point $x + \hat{\mu}a$, where $\hat{\mu}$ is the unit vector in direction μ and $\mu = 4$ is the Euclidean time direction on the lattice. They are defined by

$$U_\mu(x) = \mathcal{P} \exp\left(ig \int_x^{x+\hat{\mu}a} \mathrm{d}x_\mu A_\mu(x) \right), \tag{A.2}$$

where $\mathcal{P}$ denotes path ordering and $x = (\mathbf{x}, x_4)$. The link variables $U_\mu(x)$ are elements of the gauge group SU(3). We will often refer to the lattice coupling β, which is connected to the gauge coupling g in SU(3) by $\beta = \frac{6}{g^2}$. Introductions to lattice gauge field theory and QCD on the lattice can be found in [77, 17, 7].

For our simulations of pure gauge theory, which is in the continuum defined by (2.2), we employed the tree level-Symanzik improved gauge action [78, 79, 80, 81] on the lattice,

$$\begin{aligned} S^{(2,1)} \;=\; & \beta \sum_n \sum_{\mu<\nu} \frac{5}{3} \left(1 - \frac{1}{3}\mathrm{Re\ Tr} \right. \\ & \left. \qquad \right)_{\mu\nu}(n) \\ & -\frac{1}{6} \left(1 - \frac{1}{6}\mathrm{Re\ Tr} \left(\right.\right. \\ & \left.\left. \qquad \right)_{\mu\nu}(n) + \qquad (n) \right) \Bigg), \end{aligned} \tag{A.3}$$

which is $O(a^2)$ improved. Besides this improvement the action (A.3) shows an improved rotational symmetry compared to the standard Wilson gauge action, which is an advantage for calculating the correlation functions used in this work. The simulations in 2-flavour QCD used staggered fermions with a quark mass of $\frac{m}{T} = 0.4$, where for the

fermions the p4-action [82, 65, 66] and for the gauge fields again the tree level-Symanzik improved gauge action were employed. Detailed descriptions for the staggered formulation of the fermionic part of the action can be found in [17, 77]. The scale was set using the string tension following [83]. The critical lattice couplings in pure gauge theory using (A.3) are then for $N_\tau = 4$ obtained to be $\beta_c = 4.073$.For 2-flavour QCD using the p4-action for the fermions we have $\beta_c = 3.649$. We use periodic boundary conditions for the gluon field in all directions. For the dynamical quark fields we employ periodic boundary conditions in the spatial directions and anti-periodic boundary conditions in the Euclidean time direction.

A.2 Update and Error Analysis

In this work we employed a pseudo-heatbath algorithm for SU(3) pure gauge theory [84] and an overrelaxation algorithm [85] to the gauge configurations. In order to thermalize the gauge configurations, we applied 200 heat bath updates. After the gauge configurations were thermalized, we used one heat bath update followed by four overrelaxation updates to obtain a new gauge configuration. In order to generate a new configuration in 2-flavour QCD the R algorithm was used [86] – a Hamiltonian formulation in four spatial dimensions, which was evaluated numerically by the aid of the leapfrog algorithm with finite step size $\delta\tau$. The resulting systematic error is the $\mathcal{O}(\delta\tau^2)$. Additionally, a noisy estimator was used for quantities involving the traces of the fermion determinant and the inversion of the fermion matrix was done by using conjugate gradient algorithms. Due to the introduction of a stochastic term in the equations of motions the R algorithm is not time reversible and can not be made exact using a Metropolis step.

Since a new lattice configuration shows correlations to its parent which can not be neglected, the naïve estimation of the mean and the error of some lattice quantity are usually too small. The *Jackknife*-method eases this problem and gives more reliable estimates. The data set to be analysed is divided into N blocks of equal length. From this partition N different data sets are obtained by grouping $N-1$ blocks together. Let T be the mean of some observable O on the original data set and T_i the mean on the ith new data set, where $i = 1, \ldots, N-1$. We then obtain an improved estimation for the mean and the error of O by

$$\bar{O} \approx \bar{J} = \frac{1}{N}\sum_{i=1}^{N} J_i \tag{A.4}$$

$$\Delta O \approx \sqrt{\frac{\sum_i (J_i - \bar{J})^2}{N(N-1)}}, \tag{A.5}$$

where

$$J_i = NT - (N-1)T_i. \tag{A.6}$$

We use this method for the free energies discussed in this work, where we found $N = 10$ to be a good choice for the correlations present.

A.3 Gauge Fixing on the Lattice

Some of the observables investigated in this work are gauge dependent quantities and therefore a gauge fixing procedure has to be administered to the gauge configuration. For the reasons addressed in chapter 2.2.1 and in [23], we choose to fix to *Coulomb gauge*, which is defined by

$$\partial_i A_i(x) = 0. \tag{A.7}$$

The gauge field $A_\mu(x)$ on the lattice is obtained by

$$A_\mu(x) = \frac{1}{2ig}\left(U_\mu(x) - U_\mu^\dagger(x)\right)\Big|_{\text{traceless}}. \tag{A.8}$$

The derivative on the lattice is defined through

$$\partial_\mu A_\mu(x) = A_\mu(x) - A_\mu(x - \hat{\mu}), \tag{A.9}$$

where no summation over μ is understood and $\hat{\mu}$ is the unit vector in direction μ. Therefore the three divergence in (A.7) on the lattice becomes

$$\Delta(x) = \sum_i A_i(x) - A_i(x - \hat{i}). \tag{A.10}$$

Fixing a gauge configuration to meet the condition (A.7) on the lattice is equivalent to finding a gauge transformation $g(x)$, such that the functional

$$\epsilon(g) = -\sum_x \text{Tr}\left(\sum_i g(x)U_i(x)g^\dagger(x+\hat{i})\right) \tag{A.11}$$

becomes minimal. We use an overrelaxation algorithm [87] with $\tau = 1.4$ for this task. We monitor

$$\theta = \frac{1}{3V}\text{Tr}\left(\sum_x \Delta(x)\Delta^\dagger(x)\right), \tag{A.12}$$

which decreases monotonically towards zero, the better the gauge condition (A.7) is met by the gauge configuration. We stop the overrelaxation algorithm when $\theta < 10^{-7}$.

It is possible that the functional $\epsilon(g)$ has more then one minimum, such that the gauge condition (A.7) does not specify the gauge completely. This minima correspond to different *Gribov copies* [88]. We do not address this issue in greater detail in this work.

B SU(3)

Introductions to group theory offer [31, 32, 33], a compendium of useful relations can be found in chapter 8 of [89]. We will give a short overview of the quantities used in this work and some of their properties.

SU(3) is the group of $N \times N$ unitary matrices, $UU^\dagger = U^\dagger U = 1$, with $\det U = 1$. The generators t^a with $a = 1, \ldots, 8$ are hermitian, traceless matrices which satisfy the commutation relations

$$\left[t^a, t^b\right] = i f^{abc} t^c, \tag{B.1}$$

where the *structure constants* of SU(3) are real and totally anti-symmetric $f^{bac} = f^{acb} = -f^{abc}$. Additionally we have the d^{abc}, which are totally symmetric. The only non-zero components (up to permutations) are

$$\begin{aligned}
&f^{123} = 1, \quad f^{147} = -f^{156} = f^{246} = f^{257} = f^{345} = -f^{367} = \frac{1}{2},\\
&f^{458} = f^{678} = \frac{\sqrt{3}}{2},\\
&d^{146} = d^{157} = -d^{247} = d^{256} = d^{344} = d^{355} = -d^{366} = -d^{377} = \frac{1}{2},\\
&d^{118} = d^{228} = d^{338} = -d^{888} = \frac{1}{\sqrt{3}},\\
&d^{448} = d^{558} = d^{668} = d^{778} = -\frac{1}{2\sqrt{3}}.
\end{aligned} \tag{B.2}$$

Some useful properties are

$$\begin{aligned}
&f^{abe} f^{cde} + f^{ace} f^{dbe} + f^{ade} f^{bce} = 0 \qquad && \textstyle\sum_b d^{abb} = 0\\
&f^{abe} d^{cde} + f^{ace} d^{dbe} + f^{ade} d^{bce} = 0 \qquad && d^{abc} d^{ebc} = \tfrac{8}{3}\delta^{ae}
\end{aligned} \tag{B.3}$$

In table B.1 we give the irreducible representations of SU(3) and some of their properties for $p + q \leq 4$. We follow the custom to name the representation by their dimension D

D	(p,q)	t	$C(D)$	d_D	
3	$(1,0)$	1	4/3	1	fundamental
$\overline{3}$	$(0,1)$	2	4/3	1	
6	$(2,0)$	2	10/3	5/2	
8	$(1,1)$	0	3	9/4	adjoint, real
10	$(3,0)$	0	6	9/2	
15	$(2,1)$	1	16/3	4	
$15'$	$(4,0)$	1	28/3	7	
24	$(3,1)$	2	25/3	25/4	
27	$(2,2)$	0	8	6	real

Table B.1: Triality t, Casimir $C(D)$ and their ratios $d_D = C(D)/C(3)$ for irreducible representations with dimension D for $p+q \leq 4$ of SU(3).

where ambiguities can be ruled out. The dimension of a representation can be determined from their canonical label (p,q) by

$$D = \frac{(p+1)(q+1)(p+q+2)}{2}. \tag{B.4}$$

Throughout this work, we call the eigenvalue $C(D)$ of the quadratic Casimir operator C_D^2 the *Casimir operator* or simply the *Casimir*, which is implicitly defined by

$$C_D^2 = t^a t^a = C(D)\,\mathbb{1}, \quad \text{with} \quad a = 1, \ldots, 8 \tag{B.5}$$

where t^a are the generators of the representation D of SU(3). For the fundamental representation, we have in general for SU(N) $C(F) = \frac{N^2-1}{2N}$ and for the adjoint representation $C(A) = N$. We often use ratios of Casimirs of representations D_1 and D_2, which we define by

$$d(D_2, D_1) = \frac{C(D_2)}{C(D_1)} \quad \text{and} \quad d_D = d(D, 3). \tag{B.6}$$

Another important quantity is the *triality* t of a representation

$$t = (p - q) \bmod 3. \tag{B.7}$$

Representations with $p = q$ are called *real*. In our work, this is the case for $D = 8, 27$. The group $\mathbb{Z}(3)$ is the *center* of SU(3). An element of the center $z \in \mathbb{Z}(3)$ commutes with every element g of SU(3)

$$zg = gz \quad \forall g \in \mathrm{SU}(3). \tag{B.8}$$

B.1 Gell-Mann Matrices

A popular choice for the generators t^a with $a = 1, \ldots, 8$ of SU(3) is the one that uses the *Gell-Mann* matrices λ^a, which are related to the generators by $t^a = \lambda^a/2$. The Gell-Mann matrices are

$$\begin{aligned}
\lambda^1 &= \begin{pmatrix} 0 & 1 & 0 \\ 1 & 0 & 0 \\ 0 & 0 & 0 \end{pmatrix}, \quad \lambda^2 = \begin{pmatrix} 0 & -i & 0 \\ i & 0 & 0 \\ 0 & 0 & 0 \end{pmatrix}, \quad \lambda^3 = \begin{pmatrix} 1 & 0 & 0 \\ 0 & -1 & 0 \\ 0 & 0 & 0 \end{pmatrix} \\
\lambda^4 &= \begin{pmatrix} 0 & 0 & 1 \\ 0 & 0 & 0 \\ 1 & 0 & 0 \end{pmatrix}, \quad \lambda^5 = \begin{pmatrix} 0 & 0 & -i \\ 0 & 0 & 0 \\ i & 0 & 0 \end{pmatrix}, \quad \lambda^6 = \begin{pmatrix} 0 & 0 & 0 \\ 0 & 0 & 1 \\ 0 & 1 & 0 \end{pmatrix} \\
\lambda^7 &= \begin{pmatrix} 0 & 0 & 0 \\ 0 & 0 & -i \\ 0 & i & 0 \end{pmatrix}, \quad \lambda^8 = \frac{1}{\sqrt{3}} \begin{pmatrix} 1 & 0 & 0 \\ 0 & 1 & 0 \\ 0 & 0 & -2 \end{pmatrix}.
\end{aligned} \tag{B.9}$$

For $a, b, c = 1, \ldots, 8$ they have the following properties

$$\begin{aligned}
&\lambda^a = \lambda^{a\dagger}, \quad \text{Tr}\, \lambda^a = 0, \quad \text{Tr}\, \left(\lambda^a \lambda^b\right) = 2\delta^{ab}, \\
&\text{Tr}\, \left(\lambda^a \lambda^b \lambda^c\right) = 2(d^{abc} + i f^{abc}), \\
&\left[\lambda^a, \lambda^b\right] = 2i f^{abc} \lambda^c, \quad \left\{\lambda^a, \lambda^b\right\} = \frac{4}{3}\delta^{ab}\mathbb{1} + 2d^{abc}\lambda^c, \\
&\det \lambda^i = 0 \quad \text{for} \quad i = 1, \ldots, 7 \quad \text{and} \quad \det \lambda^8 = -\frac{2}{3\sqrt{3}}.
\end{aligned} \tag{B.10}$$

The *Fierz-identity* of SU(3) is

$$\lambda^a_{ij} \lambda^a_{kl} = 2\delta^{il}\delta^{kj} - \frac{2}{3}\delta^{ij}\delta^{kl}, \tag{B.11}$$

where $a = 1, \ldots, 8$ and $i, j, k, l = 1, 2, 3$.

B.2 Reduction of Direct Products

For the reduction of direct products we use the following identities, which can be obtained for instance by the aid of young tableaux:

$$
\begin{aligned}
3 \otimes 3 &= 6 \oplus \overline{3} & (1,0) \otimes (1,0) &= (2,0) \oplus (0,1) \\
3 \otimes \overline{3} &= 8 \oplus 1 & (1,0) \otimes (0,1) &= (1,1) \oplus (0,0) \\
6 \otimes 3 &= 10 \oplus 8 & (2,0) \otimes (1,0) &= (3,0) \oplus (1,1) \\
6 \otimes \overline{3} &= 15 \oplus 3 & (2,0) \otimes (0,1) &= (2,1) \oplus (1,0) \\
8 \otimes 3 &= 15 \oplus \overline{6} \oplus 3 & (1,1) \otimes (1,0) &= (2,1) \oplus (0,2) \oplus (1,0) \qquad \text{(B.12)} \\
10 \otimes 3 &= 15' \oplus 15 & (3,0) \otimes (1,0) &= (4,0) \oplus (2,1) \\
10 \otimes \overline{3} &= 24 \oplus 6 & (3,0) \otimes (0,1) &= (3,1) \oplus (2,0) \\
6 \otimes 6 &= 15' \oplus 15 \oplus \overline{6} & (2,0) \otimes (2,0) &= (4,0) \oplus (2,1) \oplus (0,2) \\
6 \otimes \overline{6} &= 27 \oplus 8 \oplus 1 & (2,0) \otimes (0,2) &= (2,2) \oplus (1,1) \oplus (0,0).
\end{aligned}
$$

C Tables

We have combined the statistics of the simulations used in this work and the data of the bare and renormalised Polyakov loops together with the effective renormalisation constants obtained in pure gauge theory in this table work.

The number of configurations evaluated for the Polyakov loop in different representations and free energies in pure gauge theory and 2-flavour QCD is shown in C.1. For the lattice couplings from the $32^3 \times N_\tau$ lattices in pure gauge theory not listed we used 1000 configurations for $N_\tau = 4$, 2000 for $\beta \leq 4.700$ and 1000 otherwise for $N_\tau = 6$ and 3000 for $\beta \leq 4.8661$ and 1000 otherwise for $N_\tau = 8$. For the singlet free energies every tenth configuration was gauge fixed in pure gauge theory, in 2-flavour QCD we applied the gauge fixing procedure to every configuration.

In tab. C.2 - C.6 we show the value of the bare Polyakov loop in representations $D = 3, 6, 8, 10, 15$ obtained from $32^3 \times N_\tau$ lattices with $N_\tau = 4, 6, 8$ in pure gauge theory. Tab. C.7 displays the values of the bare Polyakov loops for the representations $D = 15', 24, 27$ from the $32^3 \times 4$ lattice in pure gauge theory.

In tab. C.8 we show the effective renormalisation constants $Z_D^R(g^2)$ obtained from the renormalisation procedure employing the $Q\bar{Q}$-singlet free energies (see chapter 3.2) in representations $D = 3, 8$ using a $32^3 \times 4$ lattice in pure gauge theory.

Tab. C.9 displays the effective renormalisation constants $Z_3^R(g^2)$ from the N_τ-variation method described in chapter 3.3 in pure gauge theory. The values of Z_D^R for higher representations agree within errors.

In tab. C.10 we show the renormalised fundamental Polyakov loop near above T_c and the renormalised adjoint Polyakov loop in the vicinity of T_c, where the effective renormalisation constants in tab. C.8 have been used.

In tab. C.11 we list the renormalised Polyakov loops for the representations $D = 3, 6, 8, 10, 15$ obtained by the N_τ-variation method in pure gauge theory.

Tab. C.12 shows the bare Polyakov loops in representations $D = 3, 6, 8, 10, 15$ in 2-flavour QCD from a $16^3 \times 4$ lattice. In tab. C.13 we display the renormalised Polyakov loops, where the effective renormalisation constants Z_3^R have been determined in [29, 60]. For the higher representations we assume Casimir scaling $Z_D^R = Z_3^R$. See chapter 4.5 for details.

$N_\tau = 4$ pg		$N_\tau = 8$ pg		$N_\tau = 4$, $N_f = 2$	
β	#	β	#	β	#
4.020	9920	4.4472	9950	3.520	3000
4.030	10066	4.4862	10010	3.550	2243
4.040	10079	4.5000	9950	3.580	3500
4.050	9930	4.5951	10010	3.600	3800
4.060	9480	4.6291	10010	3.630	3000
4.065	10205	4.6619	9583	3.650	4000
4.070	10208	4.8393	9596	3.660	4000
4.080	9490	4.9275	10010	3.680	3600
4.090	9340	5.4261	10010	3.700	2000
4.150	9330			3.720	2000
4.400	9460			3.750	920
4.800	9470			3.800	1000
				3.850	1000
				3.900	1010
				3.950	1001
				4.000	1010
				4.245	1000
				4.430	1610

Table C.1: Number of configurations evaluated for the Polyakov loop in different representations and free energies in pure gauge theory (pg) and 2-flavour QCD ($N_f = 2$). For the lattice couplings not listed, see text.

$N_\tau = 4$			$N_\tau = 6$			$N_\tau = 8$		
β	T/T_c	$\langle\|L_3\|\rangle$	β	T/T_c	$\langle\|L_3\|\rangle$	β	T/T_c	$\langle\|L_3\|\rangle$
4.0760	1.005	0.1125(20)	4.3350	1.021	0.0677(11)	4.5300	1.009	0.0366(14)
4.0800	1.013	0.11690(61)	4.3500	1.044	0.07473(54)	4.5592	1.049	0.0426(12)
4.0900	1.031	0.13189(39)	4.3750	1.083	0.08187(67)	4.5600	1.050	0.04384(40)
4.1000	1.049	0.14289(74)	4.4000	1.123	0.08979(36)	4.5951	1.100	0.04952(28)
4.1270	1.099	0.16209(34)	4.4250	1.163	0.09456(34)	4.6000	1.107	0.04950(39)
4.1500	1.143	0.17350(12)	4.4500	1.205	0.10033(41)	4.6244	1.143	0.05373(33)
4.1540	1.151	0.17536(52)	4.4800	1.256	0.10600(35)	4.6291	1.150	0.05480(17)
4.1790	1.200	0.18525(38)	4.5500	1.382	0.11890(29)	4.6605	1.198	0.05859(35)
4.2000	1.242	0.19339(32)	4.6120	1.500	0.12955(24)	4.6619	1.200	0.05815(16)
4.2290	1.301	0.20244(26)	4.7000	1.680	0.14312(21)	4.6821	1.232	0.06117(33)
4.3210	1.500	0.22819(22)	4.8000	1.905	0.15787(29)	4.6874	1.240	0.06172(26)
4.3430	1.550	0.23323(22)	4.9000	2.154	0.17186(34)	4.7246	1.300	0.06579(26)
4.3650	1.601	0.23859(21)	5.0000	2.430	0.18440(30)	4.8393	1.500	0.07893(18)
4.4000	1.684	0.246301(71)	5.1800	3.007	0.20825(28)	4.8661	1.550	0.08194(21)
4.6000	2.215	0.28593(19)	5.4500	4.112	0.23906(34)	4.8921	1.600	0.08485(33)
4.8000	2.858	0.319424(63)	5.6250	5.024	0.25839(32)	4.9275	1.671	0.08819(13)
4.8390	2.999	0.32588(18)	5.7850	6.030	0.27443(30)	4.9340	1.684	0.08909(29)
5.0750	3.986	0.35925(18)	6.0350	8.010	0.29927(34)	5.0500	1.935	0.10068(42)
5.2683	5.000	0.38350(22)	6.2300	9.993	0.31725(34)	5.2500	2.447	0.12109(34)
5.4261	6.001	0.40180(19)	6.4050	12.186	0.33286(27)	5.4261	3.000	0.13764(14)
5.6773	8.000	0.42839(19)	6.5300	14.042	0.34313(33)	5.6000	3.662	0.15499(37)
5.8733	10.000	0.44838(18)	6.6480	16.054	0.35281(29)	5.8000	4.600	0.17198(38)
6.0434	12.130	0.46337(16)	6.7500	18.025	0.36043(34)	5.9930	5.728	0.18903(33)
6.1698	14.000	0.47410(18)	6.8400	19.965	0.36801(26)	6.0434	6.065	0.19323(39)
6.2876	16.001	0.48418(15)	6.9270	22.039	0.37397(34)	6.2000	7.244	0.20667(43)
6.3919	18.009	0.49235(16)				6.3910	8.996	0.22177(51)
6.4843	19.999	0.49968(17)				6.5937	11.321	0.23815(36)
6.5683	21.999	0.50607(14)				6.6450	12.000	0.24165(38)
6.6450	23.999	0.51160(16)						

Table C.2: Bare Polyakov loop in the fundamental representation from $32^3 \times N_\tau$ lattices with $N_\tau = 4, 6, 8$ in pure gauge theory.

$N_\tau = 4$			$N_\tau = 6$			$N_\tau = 8$		
β	T/T_c	$\langle\|L_6\|\rangle$	β	T/T_c	$\langle\|L_6\|\rangle$	β	T/T_c	$\langle\|L_6\|\rangle$
4.0760	1.005	0.00555(18)	4.3350	1.021	0.001376(27)	4.5300	1.009	0.000324(18)
4.0800	1.013	0.005950(56)	4.3500	1.044	0.001718(29)	4.5592	1.049	0.000424(23)
4.0900	1.031	0.007501(44)	4.3750	1.083	0.002106(44)	4.5600	1.050	0.000466(17)
4.1000	1.049	0.008842(87)	4.4000	1.123	0.002578(28)	4.5951	1.100	0.000580(10)
4.1270	1.099	0.011518(58)	4.4250	1.163	0.002900(28)	4.6000	1.107	0.000595(18)
4.1500	1.143	0.013429(23)	4.4500	1.205	0.003328(34)	4.6244	1.143	0.000701(17)
4.1540	1.151	0.013761(72)	4.4800	1.256	0.003801(31)	4.6291	1.150	0.000740(10)
4.1790	1.200	0.015601(79)	4.5500	1.382	0.005027(39)	4.6605	1.198	0.000870(18)
4.2000	1.242	0.017250(69)	4.6120	1.500	0.006184(35)	4.6619	1.200	0.000851(10)
4.2290	1.301	0.019223(66)	4.7000	1.680	0.007892(35)	4.6874	1.240	0.001007(18)
4.3210	1.500	0.025518(69)	4.8000	1.905	0.010077(51)	4.7246	1.300	0.001176(18)
4.3430	1.550	0.026910(66)	4.9000	2.154	0.012378(71)	4.8393	1.500	0.001789(12)
4.3650	1.601	0.028416(67)	5.0000	2.430	0.014762(64)	4.8661	1.550	0.001961(18)
4.4000	1.684	0.030712(25)	5.1800	3.007	0.019890(72)	4.8921	1.600	0.002140(32)
4.6000	2.215	0.044226(74)	5.4500	4.112	0.028088(98)	4.9275	1.671	0.002358(13)
4.8000	2.858	0.058137(31)	5.6250	5.024	0.03407(11)	4.9340	1.684	0.002415(30)
4.8390	2.999	0.061095(88)	5.7850	6.030	0.03958(12)	5.0500	1.935	0.003268(49)
5.0750	3.986	0.077762(99)	6.0350	8.010	0.04908(14)	5.2500	2.447	0.005162(42)
5.2683	5.000	0.09142(13)	6.2300	9.993	0.05681(16)	5.4261	3.000	0.007084(21)
5.4261	6.001	0.10264(12)	6.4050	12.186	0.06403(14)	5.6000	3.662	0.009524(64)
5.6773	8.000	0.12038(14)	6.5300	14.042	0.06907(17)	5.8000	4.600	0.012310(66)
5.8733	10.000	0.13489(14)	6.6480	16.054	0.07404(16)	5.9930	5.728	0.015603(70)
6.0434	12.130	0.14641(13)	6.7500	18.025	0.07809(19)	6.0434	6.065	0.016461(93)
6.1698	14.000	0.15494(15)	6.8400	19.965	0.08222(15)	6.2000	7.244	0.01948(11)
6.2876	16.001	0.16333(13)	6.9270	22.039	0.08562(19)	6.3910	8.996	0.02320(13)
6.3919	18.009	0.17026(14)				6.5937	11.321	0.02775(10)
6.4843	19.999	0.17665(15)				6.6450	12.000	0.02875(13)
6.5683	21.999	0.18236(13)						
6.6450	23.999	0.18738(15)						

Table C.3: Bare Polyakov loop in the sextet representation from $32^3 \times N_\tau$ lattices with $N_\tau = 4, 6, 8$ in pure gauge theory.

$N_\tau = 4$			$N_\tau = 6$			$N_\tau = 8$		
β	T/T_c	$\langle L_8 \rangle$	β	T/T_c	$\langle L_8 \rangle$	β	T/T_c	$\langle L_8 \rangle$
4.0760	1.005	0.00905(27)	4.3350	1.021	0.002658(65)	4.5300	1.009	0.000684(34)
4.0800	1.013	0.009647(82)	4.3500	1.044	0.003166(49)	4.5592	1.049	0.000924(30)
4.0900	1.031	0.011959(64)	4.3750	1.083	0.003830(70)	4.5600	1.050	0.000941(19)
4.1000	1.049	0.01389(13)	4.4000	1.123	0.004621(43)	4.5951	1.100	0.001221(13)
4.1270	1.099	0.017799(79)	4.4250	1.163	0.005167(44)	4.6000	1.107	0.001241(23)
4.1500	1.143	0.020474(31)	4.4500	1.205	0.005877(42)	4.6244	1.143	0.001446(26)
4.1540	1.151	0.020939(99)	4.4800	1.256	0.006614(49)	4.6291	1.150	0.001528(14)
4.1790	1.200	0.02346(11)	4.5500	1.382	0.008486(50)	4.6605	1.198	0.001755(24)
4.2000	1.242	0.025685(90)	4.6120	1.500	0.010259(46)	4.6619	1.200	0.001723(13)
4.2290	1.301	0.028325(84)	4.7000	1.680	0.012788(47)	4.6874	1.240	0.001963(25)
4.3210	1.500	0.036709(86)	4.8000	1.905	0.015894(72)	4.7246	1.300	0.002248(24)
4.3430	1.550	0.038497(85)	4.9000	2.154	0.019164(90)	4.8393	1.500	0.003370(18)
4.3650	1.601	0.040453(84)	5.0000	2.430	0.022480(83)	4.8661	1.550	0.003693(25)
4.4000	1.684	0.043385(32)	5.1800	3.007	0.029418(95)	4.8921	1.600	0.003969(48)
4.6000	2.215	0.060310(92)	5.4500	4.112	0.04011(13)	4.9275	1.671	0.004295(17)
4.8000	2.858	0.077168(36)	5.6250	5.024	0.04775(14)	4.9340	1.684	0.004433(42)
4.8390	2.999	0.08071(10)	5.7850	6.030	0.05464(14)	5.0500	1.935	0.005786(65)
5.0750	3.986	0.10030(12)	6.0350	8.010	0.06634(17)	5.2500	2.447	0.008723(65)
5.2683	5.000	0.11607(14)	6.2300	9.993	0.07567(19)	5.4261	3.000	0.011609(28)
5.4261	6.001	0.12882(14)	6.4050	12.186	0.08425(16)	5.6000	3.662	0.015129(90)
5.6773	8.000	0.14871(15)	6.5300	14.042	0.09020(19)	5.8000	4.600	0.019124(92)
5.8733	10.000	0.16476(15)	6.6480	16.054	0.096041(18)	5.9930	5.728	0.023634(99)
6.0434	12.130	0.17737(14)	6.7500	18.025	0.10076(22)	6.0434	6.065	0.02481(12)
6.1698	14.000	0.18667(16)	6.8400	19.965	0.10556(17)	6.2000	7.244	0.02886(14)
6.2876	16.001	0.19574(14)	6.9270	22.039	0.10944(22)	6.3910	8.996	0.03382(17)
6.3919	18.009	0.20321(15)				6.5937	11.321	0.03967(14)
6.4843	19.999	0.21006(16)				6.6450	12.000	0.04099(13)
6.5683	21.999	0.21616(14)						
6.6450	23.999	0.22151(16)						

Table C.4: Bare Polyakov loop in the adjoint representation from $32^3 \times N_\tau$ lattices with $N_\tau = 4, 6, 8$ in pure gauge theory.

$N_\tau = 4$			$N_\tau = 6$			$N_\tau = 8$		
β	T/T_c	$\langle L_{10} \rangle$	β	T/T_c	$\langle L_{10} \rangle$	β	T/T_c	$\langle L_{10} \rangle$
4.0760	1.005	0.000121(18)						
4.0800	1.013	0.0001388(59)						
4.0900	1.031	0.0001950(60)						
4.1000	1.049	0.000257(18)						
4.1270	1.099	0.000360(19)						
4.1500	1.143	0.0004825(62)						
4.1540	1.151	0.000508(19)						
4.1790	1.200	0.000639(20)						
4.2000	1.242	0.000736(19)						
4.2290	1.301	0.000913(20)						
4.3210	1.500	0.001433(21)						
4.3430	1.550	0.001556(20)						
4.3650	1.601	0.001716(22)						
4.4000	1.684	0.0019763(74)						
4.6000	2.215	0.003748(24)	4.8000	1.905	0.000271(19)			
4.8000	2.858	0.0060871(88)	4.9000	2.154	0.000392(20)			
4.8390	2.999	0.006641(30)	5.0000	2.430	0.000508(19)			
5.0750	3.986	0.010214(33)	5.1800	3.007	0.000879(20)			
5.2683	5.000	0.013600(43)	5.4500	4.112	0.001626(23)	5.0500	1.935	0.0000237(189)
5.4261	6.001	0.016716(42)	5.6250	5.024	0.002302(23)	5.2500	2.447	0.0000856(182)
5.6773	8.000	0.022246(52)	5.7850	6.030	0.003032(25)	5.4261	3.000	0.0001426(61)
5.8733	10.000	0.027284(53)	6.0350	8.010	0.004429(28)	5.6000	3.662	0.0002311(187)
6.0434	12.130	0.031616(55)	6.2300	9.993	0.005756(36)	5.8000	4.600	0.0003707(189)
6.1698	14.000	0.034938(65)	6.4050	12.186	0.007141(38)	5.9930	5.728	0.0005673(200)
6.2876	16.001	0.038446(64)	6.5300	14.042	0.008183(36)	6.0434	6.065	0.0006282(191)
6.3919	18.009	0.041404(69)	6.6480	16.054	0.009256(43)	6.2000	7.244	0.0008501(198)
6.4843	19.999	0.044236(68)	6.7500	18.025	0.010196(48)	6.3910	8.996	0.0011376(207)
6.5683	21.999	0.046846(61)	6.8400	19.965	0.011138(45)	6.5937	11.321	0.0016010(219)
6.6450	23.999	0.049194(75)	6.9270	22.039	0.012021(51)	6.6450	12.000	0.0016896(216)

Table C.5: Bare Polyakov loop in the $D = 10$ representation from $32^3 \times N_\tau$ lattices with $N_\tau = 4, 6, 8$ in pure gauge theory.

$N_\tau = 4$			$N_\tau = 6$			$N_\tau = 8$		
β	T/T_c	$\langle L_{15} \rangle$	β	T/T_c	$\langle L_{15} \rangle$	β	T/T_c	$\langle L_{15} \rangle$
4.0760	1.005	0.000317(15)						
4.0800	1.013	0.0003465(54)						
4.0900	1.031	0.0004792(52)						
4.1000	1.049	0.000593(17)						
4.1270	1.099	0.000863(17)						
4.1500	1.143	0.0011073(61)						
4.1540	1.151	0.001148(17)						
4.1790	1.200	0.001386(17)						
4.2000	1.242	0.001604(19)						
4.2290	1.301	0.001909(18)						
4.3210	1.500	0.002938(22)						
4.3430	1.550	0.003182(20)						
4.3650	1.601	0.003457(23)						
4.4000	1.684	0.0039105(80)						
4.6000	2.215	0.006922(27)	4.8000	1.905	0.000643(17)			
4.8000	2.858	0.010676(11)	4.9000	2.154	0.000901(16)			
4.8390	2.999	0.011562(34)	5.0000	2.430	0.001203(17)			
5.0750	3.986	0.016928(43)	5.1800	3.007	0.001902(19)			
5.2683	5.000	0.021888(55)	5.4500	4.112	0.003311(25)	5.0500	1.935	0.0000936(144)
5.4261	6.001	0.026307(58)	5.6250	5.024	0.004514(31)	5.2500	2.447	0.0002220(145)
5.6773	8.000	0.033918(65)	5.7850	6.030	0.005739(34)	5.4261	3.000	0.0003652(49)
5.8733	10.000	0.040672(71)	6.0350	8.010	0.008074(44)	5.6000	3.662	0.0005860(166)
6.0434	12.130	0.046360(69)	6.2300	9.993	0.010207(50)	5.8000	4.600	0.0009092(178)
6.1698	14.000	0.050694(82)	6.4050	12.186	0.012330(50)	5.9930	5.728	0.0012804(183)
6.2876	16.001	0.055176(76)	6.5300	14.042	0.013931(52)	6.0434	6.065	0.0014135(213)
6.3919	18.009	0.058949(82)	6.6480	16.054	0.015557(55)	6.2000	7.244	0.0018581(223)
6.4843	19.999	0.062521(86)	6.7500	18.025	0.016947(74)	6.3910	8.996	0.0024362(211)
6.5683	21.999	0.065787(74)	6.8400	19.965	0.018388(59)	6.5937	11.321	0.0032386(251)
6.6450	23.999	0.068710(91)	6.9270	22.039	0.019610(74)	6.6450	12.000	0.0034142(267)

Table C.6: Bare Polyakov loop in the $D = 15$ representation from $32^3 \times N_\tau$ lattices with $N_\tau = 4, 6, 8$ in pure gauge theory.

β	T/T_c	$\langle L_{15'} \rangle$	$\langle L_{24} \rangle$	$\langle L_{27} \rangle$
4.1270	1.099	0.000017(13)	0.0000145(86)	0.000022(10)
4.1500	1.143	0.0000040(41)	0.0000266(29)	0.0000427(35)
4.1540	1.151	0.000013(13)	0.0000276(87)	0.000046(11)
4.1790	1.200	0.000015(13)	0.0000436(89)	0.000059(11)
4.2000	1.242	−0.000002(13)	0.0000494(86)	0.000068(10)
4.2290	1.301	0.000034(13)	0.0000678(90)	0.000086(11)
4.3210	1.500	0.000045(14)	0.000117(10)	0.000161(12)
4.3430	1.550	0.000039(13)	0.000131(10)	0.000197(12)
4.3650	1.601	0.000048(14)	0.000151(11)	0.000205(13)
4.4000	1.684	0.0000640(44)	0.0001811(33)	0.0002563(39)
4.6000	2.215	0.000193(15)	0.000438(12)	0.000590(14)
4.8000	2.858	0.0003788(49)	0.0008562(42)	0.0011284(48)
4.8390	2.999	0.000421(15)	0.000964(14)	0.001269(15)
5.0750	3.986	0.000834(17)	0.001744(15)	0.002235(18)
5.2683	5.000	0.001258(18)	0.002577(18)	0.003266(20)
5.4261	6.001	0.001739(18)	0.003431(17)	0.004302(23)
5.6773	8.000	0.002709(20)	0.005100(21)	0.006295(23)
5.8733	10.000	0.003719(20)	0.006760(24)	0.008250(27)
6.0434	12.130	0.004682(22)	0.008298(26)	0.010041(29)
6.1698	14.000	0.005435(22)	0.009503(27)	0.011448(31)
6.2876	16.001	0.006333(27)	0.010868(31)	0.013012(34)
6.3919	18.009	0.007092(27)	0.012035(33)	0.014356(36)
6.4843	19.999	0.007859(26)	0.013193(33)	0.015680(37)
6.5683	21.999	0.008591(25)	0.014285(30)	0.016924(33)
6.6450	23.999	0.009275(29)	0.015292(36)	0.018067(40)

Table C.7: Bare Polyakov loop in the $D = 15', 24, 27$ representation from $32^3 \times 4$ lattice in pure gauge theory.

g^2	$Z_3^R(g^2)$	g^2	$Z_8^R(g^2)$
1.47059	1.3677(50)	1.49254	1.393(25)
1.46699	1.3670(51)	1.48148	1.398(27)
1.46341	1.3675(55)	1.47783	1.399(22)
1.45384	1.3682(50)	1.47059	1.388(20)
1.44439	1.3676(48)	1.46699	1.388(19)
1.43575	1.3686(44)	1.44578	1.391(20)
1.42857	1.3686(41)	1.36364	1.387(19)
1.41878	1.3691(38)	1.25000	1.335(20)
1.38857	1.3674(28)		
1.38153	1.3664(23)		
1.37457	1.3660(22)		
1.36364	1.3644(19)		
1.30435	1.34929(68)		
1.23993	1.32936(82)		

Table C.8: Effective renormalisation constants $Z_3^R(g^2)$ from the fundamental singlet $Q\bar{Q}$-free energy and $Z_8^R(g^2)$ from the adjoint singlet $Q\bar{Q}$-free energy. See chapter 3.2.

g^2	$Z_3^R(g^2)$	g^2	$Z_3^R(g^2)$
0.903	1.20926(21)	1.216	1.3279(22)
0.939	1.22209(18)	1.226	1.3310(41)
0.954	1.22790(41)	1.229	1.3271(15)
0.978	1.23640(72)	1.240	1.3342(24)
1.012	1.24983(62)	1.251	1.3431(22)
1.020	1.25287(88)	1.265	1.3426(32)
1.038	1.26033(34)	1.276	1.3486(24)
1.057	1.26718(39)	1.287	1.3511(59)
1.065	1.2703(13)	1.290	1.3454(19)
1.076	1.27378(88)	1.301	1.3523(34)
1.085	1.27907(65)	1.312	1.3625(43)
1.106	1.28741(68)	1.315	1.3375(89)
1.115	1.2907(22)	1.326	1.3597(54)
1.127	1.29355(76)	1.338	1.3650(31)
1.137	1.2990(12)	1.349	1.3642(69)
1.149	1.30048(68)	1.352	1.3687(69)
1.159	1.3074(11)	1.363	1.3604(65)
1.169	1.3114(30)	1.377	1.3588(29)
1.182	1.3150(15)	1.463	1.3534(52)

Table C.9: Effective renormalisation constants $Z_3^R(g^2)$ from the N_τ-variation method in chapter 3.3. The values for higher representations agree within errors.

T/T_c	L_3^R	L_8^R
0.907		0.0087(16)
0.924		0.0099(17)
0.942		0.0116(17)
0.959		0.0143(19)
0.977		0.0168(23)
0.986		0.0198(53)
0.995		0.0219(48)
1.005	0.396(21)	0.154(37)
1.013	0.4107(65)	0.163(11)
1.031	0.4621(42)	0.2008(86)
1.049	0.5126(79)	0.246(19)
1.144	0.6089(12)	0.3451(42)
1.242	0.6874(35)	0.446(13)

Table C.10: Renormalised Polyakov loop for $D = 3, 8$ in pure gauge theory obtained with the Z_D^R from the renormalisation procedure employing the $Q\bar{Q}$-singlet free energy.

T/T_c	L_3^R	L_6^R	L_8^R	L_{10}^R	L_{15}^R
1.053	0.4888(64)	0.1791(57)	0.2090(58)		
1.068	0.647(73)	0.371(83)	0.292(54)		
1.125	0.577(16)	0.267(21)	0.298(18)		
1.185	0.647(19)	0.344(27)	0.385(22)		
1.201	0.649(22)	0.356(28)	0.388(30)		
1.266	0.6976(78)	0.457(23)	0.476(18)		
1.333	0.726(19)	0.438(20)	0.489(29)		
1.424	0.792(15)	0.553(22)	0.590(29)		
1.500	0.798(12)	0.571(23)	0.602(20)		
1.580	0.8115(70)	0.591(12)	0.625(12)		
1.602	0.842(22)	0.667(41)	0.685(41)		
1.688	0.8695(96)	0.719(21)	0.737(18)		
1.778	0.882(12)	0.725(22)	0.777(25)		
1.898	0.9294(81)	0.839(25)	0.864(23)		
2.000	0.9272(95)	0.829(24)	0.840(20)		
2.136	0.955(18)	0.905(42)	0.901(38)	0.77(47)	0.94(18)
2.250	0.9722(91)	0.941(24)	0.935(20)	0.90(33)	0.969(85)
2.370	0.9713(53)	0.925(12)	0.933(11)	0.870(29)	0.877(21)
2.531	1.0098(73)	1.031(20)	1.029(19)	1.20(17)	1.095(80)
2.667	1.0100(62)	1.022(14)	1.025(14)	1.15(10)	1.023(49)
2.848	1.032(13)	1.085(40)	1.080(33)	1.22(17)	1.189(87)
3.000	1.0424(45)	1.108(12)	1.098(11)	1.241(79)	1.192(33)
3.375	1.0624(49)	1.163(13)	1.145(12)	1.334(90)	1.310(33)
3.556	1.0597(47)	1.150(12)	1.135(11)	1.294(19)	1.240(24)
3.797	1.0739(95)	1.197(29)	1.177(25)	1.37(12)	1.377(67)
4.000	1.0797(33)	1.2087(85)	1.1863(83)	1.396(43)	1.367(27)
4.500	1.0874(35)	1.231(10)	1.2074(90)	1.464(54)	1.431(24)
5.062	1.0909(65)	1.243(20)	1.219(17)	1.485(60)	1.453(55)
5.333	1.0946(24)	1.2516(68)	1.2246(60)	1.501(15)	1.432(13)
6.000	1.1002(18)	1.2691(58)	1.2391(50)	1.550(31)	1.465(17)
6.750	1.1012(47)	1.272(14)	1.243(12)	1.546(72)	1.492(41)
8.000	1.1060(15)	1.2855(44)	1.2539(38)	1.5704(96)	1.4935(80)
9.000	1.1049(30)	1.2823(90)	1.2521(77)	1.547(37)	1.492(22)
12.000	1.106*	1.286*	1.254*	1.574*	1.496*

Table C.11: Renormalised Polyakov loop in the $D = 3, 6, 8, 10, 15$ in pure gauge theory obtained with the N_τ-variation method (see chapter 3.3). *: seed value.

β	T/T_c	$\langle L_3 \rangle$	$\langle L_6 \rangle$	$\langle L_8 \rangle$	$\langle L_{10} \rangle$	$\langle L_{15} \rangle$
3.520	0.76	0.03744(53)	0.01377(18)	0.01230(24)		
3.550	0.81	0.04818(81)	0.01407(22)	0.01257(29)		
3.580	0.87	0.06550(87)	0.01400(18)	0.01306(24)		
3.600	0.90	0.0821(12)	0.01431(17)	0.01329(24)		
3.630	0.96	0.1364(20)	0.01514(21)	0.01790(38)		
3.650	1.002	0.2037(32)	0.01823(28)	0.02875(72)		
3.660	1.02	0.2448(34)	0.02180(35)	0.0390(10)		
3.680	1.07	0.3380(28)	0.03410(48)	0.0698(10)		
3.700	1.11	0.3905(23)	0.04469(63)	0.0919(11)		
3.720	1.16	0.4334(17)	0.05415(56)	0.1116(10)		
3.750	1.23	0.4817(20)	0.06726(85)	0.1373(14)	0.01462(38)	
3.800	1.36	0.5376(18)	0.08652(82)	0.1733(14)	0.01526(37)	0.02173(54)
3.850	1.50	0.5837(14)	0.10523(77)	0.2073(14)	0.01641(39)	0.02741(62)
3.900	1.65	0.6229(13)	0.12283(80)	0.2390(13)	0.01775(42)	0.03309(71)
3.950	1.81	0.6603(16)	0.14094(90)	0.2707(15)	0.01941(46)	0.04034(85)
4.000	1.98	0.6951(14)	0.15869(94)	0.3025(15)	0.02104(47)	0.04722(82)
4.245	3.00	0.8347(13)	0.2480(11)	0.4529(17)	0.03633(61)	0.09283(104)
4.430	4.01	0.9273(10)	0.32161(96)	0.5734(14)	0.05442(55)	0.14091(94)

Table C.12: Bare Polyakov loop in the $D = 3, 6, 8, 10, 15$ representation from $16^3 \times 4$ lattice in 2-flavour QCD.

T/T_c	L_3^R	L_6^R	L_8^R	L_{10}^R	L_{15}^R
0.76	0.03477(62)	0.00139(80)	0.00170(66)		
0.81	0.04950(95)	0.0025(11)	0.00361(85)		
0.87	0.0720(10)	0.00342(99)	0.00719(79)		
0.90	0.0934(14)	0.00758(99)	0.01160(75)		
0.96	0.1599(24)	0.0219(12)	0.0302(11)		
1.002	0.2399(38)	0.0474(16)	0.0595(18)	0.0045(73)	0.0107(30)
1.02	0.2880(41)	0.0673(18)	0.0828(23)	0.0161(76)	0.0216(30)
1.07	0.3949(33)	0.1219(21)	0.1469(22)	0.0309(78)	0.0418(33)
1.11	0.4582(27)	0.1668(26)	0.1952(24)	0.056(10)	0.0728(46)
1.16	0.5118(20)	0.2082(23)	0.2405(21)	0.070(11)	0.0916(48)
1.23	0.5757(24)	0.2690(35)	0.3039(31)	0.102(17)	0.1240(79)
1.36	0.6565(22)	0.3667(36)	0.4024(33)	0.161(19)	0.2037(85)
1.50	0.7227(18)	0.4636(35)	0.4966(33)	0.277(20)	0.3115(92)
1.65	0.7795(16)	0.5564(37)	0.5862(32)	0.376(21)	0.407(11)
1.81	0.8305(21)	0.6471(43)	0.6717(38)	0.502(23)	0.525(12)
1.98	0.8759(18)	0.7327(45)	0.7538(38)	0.585(23)	0.625(12)
3.00	1.0290(19)	1.0861(52)	1.0739(45)	1.212(24)	1.152(14)
4.01	1.1074(13)	1.3013(44)	1.2658(37)	1.636(18)	1.544(11)

Table C.13: Renormalised Polyakov loop in the $D = 3, 6, 8, 10, 15$ representation from $16^3 \times 4$ lattice in 2-flavour QCD. Casimir scaling in Z_D^R is assumed. See chapter 4.5 for details.

Bibliography

[1] M. Gyulassy and L. McLerran, "New forms of qcd matter discovered at rhic", *Nucl. Phys.* **A750** (2005) 30–63, `nucl-th/0405013`.

[2] E. V. Shuryak and I. Zahed, "Rethinking the properties of the quark gluon plasma at t approx. t(c)", *Phys. Rev.* **C70** (2004) 021901, `hep-ph/0307267`.

[3] S. Ejiri, F. Karsch, and K. Redlich, "Hadronic fluctuations at the qcd phase transition", *Phys. Lett.* **B633** (2006) 275–282, `hep-ph/0509051`.

[4] G. S. Bali, "Casimir scaling of su(3) static potentials", *Phys. Rev.* **D62** (2000) 114503, `hep-lat/0006022`.

[5] Y. Schroder, "The static potential in QCD to two loops", *Phys. Lett.* **B447** (1999) 321–326, `hep-ph/9812205`.

[6] **Particle Data Group** Collaboration, S. Eidelman *et al.*, "Review of particle physics", *Phys. Lett.* **B592** (2004) 1.

[7] F. Karsch and E. Laermann, "Thermodynamics and in-medium hadron properties from lattice qcd", `hep-lat/0305025`.

[8] M. Le Bellac, *Thermal Field Theory*. Cambridge Univ. Press, 1996.

[9] J. I. Kapusta, *Finite Temperature Field Theory*. Cambridge Univ. Press, 2000.

[10] K. Holland and U.-J. Wiese, "The center symmetry and its spontaneous breakdown at high temperatures", `hep-ph/0011193`.

[11] R. D. Pisarski, "Notes on the deconfining phase transition", `hep-ph/0203271`.

[12] G. 't Hooft, "On the phase transition towards permanent quark confinement", *Nucl. Phys.* **B138** (1978) 1.

[13] G. 't Hooft, "A property of electric and magnetic flux in nonabelian gauge theories", *Nucl. Phys.* **B153** (1979) 141.

[14] A. M. Polyakov, "Thermal properties of gauge fields and quark liberation", *Phys. Lett.* **B72** (1978) 477–480.

[15] L. Susskind, "Lattice models of quark confinement at high temperature", *Phys. Rev.* **D20** (1979) 2610–2618.

[16] L. D. McLerran and B. Svetitsky, "Quark liberation at high temperature: A monte carlo study of su(2) gauge theory", *Phys. Rev.* **D24** (1981) 450.

[17] I. Montvay and G. Munster, *Quantum fields on a lattice*. Cambridge University Press, 1997.

[18] G. Boyd *et al.*, "Thermodynamics of su(3) lattice gauge theory", *Nucl. Phys.* **B469** (1996) 419–444, `hep-lat/9602007`.

[19] M. Cheng *et al.*, "The transition temperature in qcd", `hep-lat/0608013`.

[20] S. Nadkarni, "Nonabelian debye screening. 1. the color averaged potential", *Phys. Rev.* **D33** (1986) 3738.

[21] S. Nadkarni, "Nonabelian debye screening. 2. the singlet potential", *Phys. Rev.* **D34** (1986) 3904.

[22] K. Huebner, "Freie energien schwerer quarks in su(3)-reiner eichtheorie", *Diploma thesis* (2003).

[23] O. Philipsen, "Non-perturbative formulation of the static color octet potential", *Phys. Lett.* **B535** (2002) 138–144, `hep-lat/0203018`.

[24] O. Kaczmarek, F. Karsch, P. Petreczky, and F. Zantow, "Heavy quark anti-quark free energy and the renormalized polyakov loop", *Phys. Lett.* **B543** (2002) 41–47, `hep-lat/0207002`.

[25] K. Hubner, O. Kaczmarek, and O. Vogt, "Heavy two- and three-quark free energies at finite t", *PoS* **LAT2005** (2006) 194, `hep-lat/0509110`.

[26] S. Necco and R. Sommer, "The n(f) = 0 heavy quark potential from short to intermediate distances", *Nucl. Phys.* **B622** (2002) 328–346, `hep-lat/0108008`.

[27] O. Kaczmarek, F. Karsch, E. Laermann, and M. Lutgemeier, "Heavy quark potentials in quenched qcd at high temperature", *Phys. Rev.* **D62** (2000) 034021, `hep-lat/9908010`.

[28] S. Digal, P. Petreczky, and H. Satz, "String breaking and quarkonium dissociation at finite temperatures", *Phys. Lett.* **B514** (2001) 57–62, `hep-ph/0105234`.

[29] O. Kaczmarek and F. Zantow, "Static quark anti-quark interactions in zero and finite temperature qcd. i: Heavy quark free energies, running coupling and quarkonium binding", *Phys. Rev.* **D71** (2005) 114510, `hep-lat/0503017`.

[30] M. Doering, "Screening of heavy quarks and hadrons at finite temperature and density", *PhD thesis* (2006).

[31] H. Georgi, "Lie algebras in particle physics. from isospin to unified theories", *Front. Phys.* **54** (1982) 1–255.

[32] W. K. Tung, "Group theory in physics",. Singapore, Singapore: World Scientific (1985) 344p.

[33] M. Laine, *Symmetrien in der Physik*. Lecture, Bielefeld, SoSe 2005. `www.physik.uni-bielefeld.de/~laine/symmetrien/cover.html`.

[34] V. I. Shevchenko and Y. A. Simonov, "On casimir scaling in qcd", `hep-ph/0104135`.

[35] C. Michael, "Glueballs, hybrid and exotic mesons and string breaking", `hep-ph/0009115`.

[36] G. S. Bali, "Qcd forces and heavy quark bound states", *Phys. Rept.* **343** (2001) 1–136, `hep-ph/0001312`.

[37] F. Karsch and M. Lutgemeier, "Deconfinement and chiral symmetry restoration in an su(3) gauge theory with adjoint fermions", *Nucl. Phys.* **B550** (1999) 449–464, `hep-lat/9812023`.

[38] G. S. Bali and P. Boyle, "Perturbative wilson loops with massive sea quarks on the lattice", `hep-lat/0210033`.

[39] P. H. Damgaard, "The free energy of higher representation sources in lattice gauge theories", *Phys. Lett.* **B194** (1987) 107.

[40] V. I. Shevchenko and Y. A. Simonov, "Casimir scaling as a test of qcd vacuum", *Phys. Rev. Lett.* **85** (2000) 1811–1814, `hep-ph/0001299`.

[41] M. Faber, J. Greensite, and S. Olejnik, "Casimir scaling from center vortices: Towards an understanding of the adjoint string tension", *Phys. Rev.* **D57** (1998) 2603–2609, `hep-lat/9710039`.

[42] G. S. Bali, "Casimir scaling or flux counting?", *Nucl. Phys. Proc. Suppl.* **83** (2000) 422–424, `hep-lat/9908021`.

[43] C. Michael, "Adiabatic surfaces from the lattice: Excited gluonic potentials", `hep-ph/9809211`.

[44] G. S. Bali, C. Schlichter, and K. Schilling, "Probing the qcd vacuum with static sources in maximal abelian projection", *Prog. Theor. Phys. Suppl.* **131** (1998) 645–656, `hep-lat/9802005`.

[45] G. S. Bali, "The mechanism of quark confinement", `hep-ph/9809351`.

[46] M. R. Douglas and S. H. Shenker, "Dynamics of su(n) supersymmetric gauge theory", *Nucl. Phys.* **B447** (1995) 271–296, `hep-th/9503163`.

[47] A. Hanany, M. J. Strassler, and A. Zaffaroni, "Confinement and strings in mQCD", *Nucl. Phys.* **B513** (1998) 87–118, `hep-th/9707244`.

[48] S. Ohta, M. Fukugita, and A. Ukawa, "Forces between quark clusters", *Phys. Lett.* **B173** (1986) 15.

[49] H. Markum and M. E. Faber, "Quark multiplets and their interactions", *Phys. Lett.* **B200** (1988) 343–347.

[50] W. Buerger, M. Faber, H. Markum, and M. Muller, "Chiral condensates and potentials for quark - multiplet sources", *Phys. Rev.* **D47** (1993) 3034–3040.

[51] A. M. Polyakov, "Gauge fields as rings of glue", *Nucl. Phys.* **B164** (1980) 171–188.

[52] V. S. Dotsenko and S. N. Vergeles, "Renormalizability of phase factors in the nonabelian gauge theory", *Nucl. Phys.* **B169** (1980) 527.

[53] R. A. Brandt, F. Neri, and M.-a. Sato, "Renormalization of loop functions for all loops", *Phys. Rev.* **D24** (1981) 879.

[54] E. Gava and R. Jengo, "Perturbative evaluation of the thermal wilson loop", *Phys. Lett.* **B105** (1981) 285.

[55] M. Peter, "The static quark-antiquark potential in qcd to three loops", *Phys. Rev. Lett.* **78** (1997) 602–605, `hep-ph/9610209`.

[56] A. Dumitru, Y. Hatta, J. Lenaghan, K. Orginos, and R. D. Pisarski, "Deconfining phase transition as a matrix model of renormalized polyakov loops", *Phys. Rev.* **D70** (2004) 034511, `hep-th/0311223`.

[57] C. Wozar, T. Kaestner, A. Wipf, T. Heinzl, and B. Pozsgay, "Phase structure of z(3) polyakov loop models", *arXiv:hep-lat/0605012*.

[58] J. Engels and T. Scheideler, "The pseudospecific heat in su(2) gauge theory: Finite size dependence and finite temperature effects", *Phys. Lett.* **B394** (1997) 147–151, `hep-lat/9610019`.

[59] Y. A. Simonov, "Gluelump spectrum in the qcd string model", *Nucl. Phys.* **B592** (2001) 350–368, `hep-ph/0003114`.

[60] O. Kaczmarek and F. Zantow, "Static quark anti-quark interactions at zero and finite temperature qcd. ii: Quark anti-quark internal energy and entropy", `hep-lat/0506019`.

[61] Z. Fodor, C. Hoelbling, M. Mechtel, and K. Szabo, "Nonperturbative investigation of the diquark potential", *PoS* **LAT2005** (2006) 310, `hep-lat/0511032`.

[62] A. Nakamura and T. Saito, "Qcd color interactions between two quarks", *Phys. Lett.* **B621** (2005) 171–175, `hep-lat/0512043`.

[63] O. Kaczmarek, F. Karsch, F. Zantow, and P. Petreczky, "Static quark anti-quark free energy and the running coupling at finite temperature", *Phys. Rev.* **D70** (2004) 074505, `hep-lat/0406036`.

[64] A. Armoni and B. Lucini, "Universality of k-string tensions from holography and the lattice", *JHEP* **06** (2006) 036, `hep-th/0604055`.

[65] C. R. Allton *et al.*, "The qcd thermal phase transition in the presence of a small chemical potential", *Phys. Rev.* **D66** (2002) 074507, `hep-lat/0204010`.

[66] C. R. Allton *et al.*, "The equation of state for two flavor qcd at non-zero chemical potential", *Phys. Rev.* **D68** (2003) 014507, `hep-lat/0305007`.

[67] T. T. Takahashi, H. Suganuma, Y. Nemoto, and H. Matsufuru, "Detailed analysis of the three quark potential in su(3) lattice qcd", *Phys. Rev.* **D65** (2002) 114509, `hep-lat/0204011`.

[68] **DIK** Collaboration, V. G. Bornyakov *et al.*, "Baryonic flux in quenched and two-flavor dynamical qcd", *Phys. Rev.* **D70** (2004) 054506, `hep-lat/0401026`.

[69] V. G. Bornyakov *et al.*, "Profiles of the broken string in two-flavor qcd below and above the finite temperature transition", *Prog. Theor. Phys.* **112** (2004) 307–324, `hep-lat/0401027`.

[70] J. M. Cornwall, "The baryon wilson loop area law in QCD", *Phys. Rev.* **D54** (1996) 6527–6536, `hep-th/9605116`.

[71] J. Liao and E. V. Shuryak, "Polymer chains and baryons in a strongly coupled quark- gluon plasma", *Nucl. Phys.* **A775** (2006) 224–234, `hep-ph/0508035`.

[72] C.-Y. Wong, "Heavy quarkonia in quark gluon plasma", *Phys. Rev.* **C72** (2005) 034906, `hep-ph/0408020`.

[73] W. M. Alberico, A. Beraudo, A. De Pace, and A. Molinari, "Heavy quark bound states above t(c)", *Phys. Rev.* **D72** (2005) 114011, `hep-ph/0507084`.

[74] M. Asakawa and T. Hatsuda, "J/psi and eta/c in the deconfined plasma from lattice qcd", *Phys. Rev. Lett.* **92** (2004) 012001, `hep-lat/0308034`.

[75] S. Datta, F. Karsch, P. Petreczky, and I. Wetzorke, "Behavior of charmonium systems after deconfinement", *Phys. Rev.* **D69** (2004) 094507, `hep-lat/0312037`.

[76] G. Aarts *et al.*, "Charmonium spectral functions in two-flavour qcd", `hep-lat/0608009`.

[77] H. J. Rothe, *Lattice gauge theories: an introduction*. World Scientific Publishing, 2005.

[78] P. Weisz, "Continuum limit improved lattice action for pure yang-mills theory. 1", *Nucl. Phys.* **B212** (1983) 1.

[79] P. Weisz and R. Wohlert, "Continuum limit improved lattice action for pure yang-mills theory. 2", *Nucl. Phys.* **B236** (1984) 397.

[80] K. Symanzik, "Continuum limit and improved action in lattice theories. 1. principles and phi**4 theory", *Nucl. Phys.* **B226** (1983) 187.

[81] K. Symanzik, "Continuum limit and improved action in lattice theories. 2. o(n) nonlinear sigma model in perturbation theory", *Nucl. Phys.* **B226** (1983) 205.

[82] F. Karsch, E. Laermann, and A. Peikert, "Quark mass and flavor dependence of the qcd phase transition", *Nucl. Phys.* **B605** (2001) 579–599, `hep-lat/0012023`.

[83] B. Beinlich, F. Karsch, E. Laermann, and A. Peikert, "String tension and thermodynamics with tree level and tadpole improved actions", *Eur. Phys. J.* **C6** (1999) 133–140, `hep-lat/9707023`.

[84] N. Cabibbo and E. Marinari, "A new method for updating su(n) matrices in computer simulations of gauge theories", *Phys. Lett.* **B119** (1982) 387–390.

[85] M. Creutz, "Overrelaxation and monte carlo simulation", *Phys. Rev.* **D36** (1987) 515.

[86] S. A. Gottlieb, W. Liu, D. Toussaint, R. L. Renken, and R. L. Sugar, "Hybrid molecular dynamics algorithms for the numerical simulation of quantum chromodynamics", *Phys. Rev.* **D35** (1987) 2531–2542.

[87] J. E. Mandula and M. Ogilvie, "Efficient gauge fixing via overrelaxation", *Phys. Lett.* **B248** (1990) 156–158.

[88] V. N. Gribov, "Quantization of non-abelian gauge theories", *Nucl. Phys.* **B139** (1978) 1.

[89] V. I. Borodulin, R. N. Rogalev, and S. R. Slabospitsky, "Core: Compendium of relations: Version 2.1", `hep-ph/9507456`.

Acknowledgement

I am deeply indebted to Prof. Dr. Frithjof Karsch for supervising my PhD thesis and providing me the opportunity to collaborate with him and his group. He was always open for my questions, provided many fruitful discussions and made it possible that I could participate in many conferences and research visits abroad.
It is a pleasure to thank Prof. Dr. Jürgen Engels for co-supervising my thesis and for inspiring discussions.
I am extraordinary grateful to AkadR Dr. Olaf Kaczmarek, with whom I have worked with for four years now and who I benefited immensely from during my entire time as a Diploma and PhD student. Due to his continuous willingness to discuss my questions and to support me, he provided invaluable help to bring this thesis to a successful conclusion.
In addition I would like to thank Prof. Sourendu Gupta for the opportunity to collaborate with him and for many fruitful and enlightening discussions.
I am grateful to Prof. Dr. Olivier Péne for kindly hosting me in Orsay, Paris and for the inspiring time I could spend with him and his group.
I also like to thank Oliver Vogt for being there quite often to have many illuminating discussions as well on scientific and other issues in and out of our office and during our time as undergraduate students. Many thanks go to Matthias Döring for the great time I spent with him in various places around the world.
Last but not least I would like to thank all other members of the particle physics group for their friendship, valuable discussions and the great time we spent together. Special thanks go to Gudrun Eickmeyer and Susi von Reder for all the support and help I received from them.

Kay Hübner
Bielefeld, September 2006